PARAMETRIC DESIGN OF TIMBER SHELL STRUCTURES

by

Alexandra Adelle Hinkel Cheng

B.A., B.S., The University of Colorado Denver, 2012

A THESIS SUBMITTED IN PARTIAL FULFILLMENT OF

THE REQUIREMENTS FOR THE DEGREE OF

MASTER OF APPLIED SCIENCE

in

THE FACULTY OF GRADUATE AND POSTDOCTORAL STUDIES

(Civil Engineering)

THE UNIVERSITY OF BRITISH COLUMBIA

(Vancouver)

October 2015

Abstract

Increasingly complex architectural geometries present new challenges for structural engineers. Collaborative, digital workflows which integrate 3D parametric architectural models with Finite Element Modelling software grant structural engineers a higher degree of geometric versatility and influence during the preliminary design phase. Through integrated parametric design models – also labelled "co-rationalized" – structural engineers may not only easily respond to rapid model variations and unusual assemblies, but also inform the building design from inception.

This thesis presents an example of a project executed in a co-rationalized manner through architectural and structural collaboration, using both digitally-integrated and analog models, for the design and construction of solid timber shells structures using Cross-Laminated Timber (CLT) panels. By exploring a co-rationalized design process, timber engineering details are identified and integrated into the architectural model, and the role of structural engineer takes an active rather than reactionary role in the preliminary design stages.

The result of this process using integrated parametric models was the design, fabrication, and assembly of a folded plate wall prototype and three CLT panels with double curvature. This research demonstrates how collaboration and integrated modeling enables the realization of the architectural versatility that mass-timber has to offer, and the efficacy which co-rationalized design and integrated models can bring to orthodox and unusual structures alike. As a

consequence, this research serves as a precedent for structural detailing-based generative architecture and collaborative work in the future.

Preface

This thesis describes my structural engineering research made in part in service of a larger, collaborative research project “Shell Structure in Wood” in partnership with the School of Architecture and Landscape Architecture and the Centre for Advanced Wood Processing at the University of British Columbia. Support was provided by Forest Innovations Investment through the Wood First Act (Government of British Columbia 2009) . The project was carried out by myself in collaboration with graduate architecture students under the supervision of Prof. Tannert, Prof Meyboom, and Prof. Neumann. Owing to the interdisciplinary nature of the project, roles of each researcher in the team can be broadly sketched as follows:

Primary Masters Student researchers from SALA:

- Thomas Gaudin: Primary Parametric Modelling, Diagrams, Architectural Conceptualization
- Jessica Hunter: Wood Fabrication, Architectural Conceptualization
- Roy Cloutier: Wood Fabrication, Parametric Modelling, Diagrams, Renderings, Architectural Conceptualization

Supporting Masters Student researchers from SALA:

- Sarah Maria: Photographic Documentation
- Nicole Tischler: Photographic Documentation, Fabrication

Masters Student researcher from Civil Engineering:

- Myself: Integration with FEM, Structural Parametric Modelling, Structural Research, Design, Definition of Constraints, Fabrication, Diagrams, Architectural Conceptualization

In addition, parts of this research have been published in collaboration with the aforementioned as follows:

- Neumann O, Hunter J, Cheng A, Gaudin T, Tannert T, Meyboom AL (2015) TimberShell: Large Scale Timber Shell Structure Prototypes. Association for Computer-Aided Design in Architecture (ACADIA) Computational Ecologies: Design in the Anthropocene, October19-25, Cincinnati, USA.
- Hunter J, Cheng A, Tannert T, Neumann O, Meyboom AL (2015) Extending the Perception of Wood: Research in Large Scale Surface Structures in Wood. Association for education and research in computer aided architectural design in Europe (eCAADe) 33rd Annual Conference, September 16-18, Vienna, Austria.
- Cheng A, Tannert T (2015) Comparative Study on Timber-based Hybrid Systems for High-rise Construction. ASCE Structures Congress, April 23-25, Portland, USA.
- Cheng A, Meyboom AL, Gaudin T, Neumann O, Tannert T (2015) Large Scale Wood Surface Structures. International Conference on Architecture and Civil Engineering (ACE 2015), April 13-14, Singapore, Singapore.

Table of Contents

List of Tables

List of Figures

Acknowledgements

First and foremost, I would like to express my special appreciation and thanks to my advisor Professor Dr. Thomas Tannert, for his excellent mentorship, continually positive support, guidance, patience, and good humour throughout my masters, and his willingness to take part in an unorthodox project such as this. I would also like to thank the project lead investigator, Professor AnnaLisa Meyboom, as well as Professor Oliver Neumann, for not only initiating this research, but also encouraging me to push my own conceptions of the possible in architecture and engineering. Thanks also go to Vincent Leung, whose invaluable work and facilities were essential to bringing the project to fruition. In addition, a thank you also goes to Professor Dr. Sheryl Staub-French, for her helpful input and comments as the second reader for this thesis. Much gratitude also goes to Forest Innovations Investment, by whose generosity this project was made possible through a grant to the Centre for Advanced Wood Processing. Your support is much appreciated.

I especially want to thank my project cohorts: fundamental to the success of this research was Thomas Gaudin, whose talent with Grasshopper and imagination for the possibilities of material computation are outstanding; also to Jessica Hunter, for her leadership, skill, and practicality, and to Roy Cloutier for his support and assistance. We've spent long hours together in the studio and the fabrication workshop, and I thank them all sharing their insight and knowledge with me,

and for being dedicated team-mates and friends. Many thanks also to Dr. Tannert's Timber Engineering Research Group, for their edifying technical discussions and comradery.

Deep appreciation goes to my past and present friends at Green College. Words cannot express how grateful I am to have had them in my life and been a part of the Green community, more home than home. I owe much of my present happiness to their support, spirit, and friendship.

Lastly, I thank my parents for their love and all of the sacrifices that they've made on my behalf.

Dedication

For my friends and family.

Chapter 1: Introduction

1.1 Overview of Project

This thesis documents the author's structural contribution performed in the context of a larger research project, "Shell Structures in Wood - Technical Research & Testing". Its objective was the investigation and execution of the technical understanding and tools necessary to realize mass-timber shell structures.

This project, funded by Forest Innovation Investment (FII), was pursued through collaboration between the UBC School of Architecture and Landscape Architecture (SALA), the Department of Civil Engineering, and the Centre for Advanced Wood Processing (CAWP). From March 2014 until March 2015, graduate students from SALA formed a collaborative team with the author and undertook the design, fabrication, and documentation of the process thereof, for two prototypical solid timber wall elements: 1) double-curvature CLT panels and 2) folded timber panel walls.

The resulting elements were accomplished through an interdisciplinary investigation of i) Integrated Design practice and processes ii) procedures for integrating parametric architecture models with Finite-Element-Method (FEM) structural analysis software, and iii) timber engineering design requirements and analytical material models to embed as constraints within the models, and iv) timber shell design precedents.

1.2 Architectural Demand

The proliferation of contemporary parametric architecture with complex geometry attests to the geometric versatility of computational design and 3D parametric architectural modelling software (Pottmann et al. 2007; Ramage et al. 2009). Manifesting these geometries requires structural engineering solutions which current design guidelines do not directly address (Taylor 2013; Jeska & Pascha 2014). This obstacle is twofold. One, with respect to timber in particular, timber engineering design codes lack guidance for composite members in atypical orientations with unusual load configurations. Two, parametric architecture modelling software is versatile but abstracted from material characteristics for fabrication considerations, while stand-alone FEM software used for structural analysis is ill-equipped for rapid geometric changes. Addressing these challenges offers the opportunity to expand the vocabulary of structural design capabilities.

Contemporary architecture has seen the rise of a design philosophy termed variously as "emergent design", "material computation", or "morphogenetic", characterized by exploration of the relationships between material, form, and structure. This rise has been fueled by 3D parametric architectural software which provides the ability to associate and manipulate data with geometric consequences (Hensel et al. 2010; Menges & Ahlquist 2011; Menges 2012; Wien & York 2014; Weinstock 2010; Ramage et al. 2009; Rippmann et al. 2012)

Though unorthodox from an engineering perspective in their methods and execution, morphogenetic design concepts and critiques revolve around questions of material properties, deflection, bracing, and other considerations for structural mechanics and their relationship to the

global geometry (Hensel & Menges 2006). As such, practitioners are interested in embedding physical principles into their design schemas which presents a valuable opportunity for structural engineering to introduce itself early in the design process. This method of digital and conceptual collaboration is also termed Integrated Design (Deutsch 2011).

1.3 Renaissance of Structural use of Timber

Coinciding with the inception of morphogenetic architecture is increasing global demand for sustainable construction, and thus a renewed interest in timber construction. Changes in international building legislation have relaxed outdated height restrictions on timber constructions as well as government edicts encouraging wood-based mid-rise and high-rise construction, for example by allowing six-story wood frame construction in Canada (BCBC 2009)

In British Columbia, Canada, the Wood First Act (Parliament of British Columbia 2009) requires new, provincially-funded building projects to consider wood as the primary building material. Similarly the US Tall Wood Building Competition (McKalip 2014) is intended to demonstrate the use of timber as a safe and successful material for large-scale structures. Meanwhile, technological advancements in high-strength connections, digital fabrication, as well as the introduction of CLT provide the means to use timber in ways which were previously unheard of. As such there exists a potential market for shell structures constructed from solid mass-timber panels such as CLT. Timber shell structures, whose form and function are inseparable, are prime candidates for demonstrating the benefits of both Integrated Design and mass-timber.

1.4 Historical Context

Advances in technology satisfy old design challenges while presenting new ones, as designers push the boundaries of new tools and mediums. For instance, a loose architectural lineage of shell structures can be sketched from Roman arches (pozzolanic concrete), the Pantheon (essentially a revolved concrete arch), the Hagia Sophia (of similar diameter to the Pantheon, but fashioned from brick, and whose equatorial windows mitigate the hoop stresses and thereby avoid the longitudinal cracks that creep up the sides of the Pantheon dome), to the High Gothic masonry vaults (funicular rather than spherical masonry) (Mark 1990). Remarkably these shells were built by following geometric rules of proportion (Mark 1990; Heyman 1995).

Prior to the Scientific Revolution of the 18th century, quantitative methods for understanding force and material strength were not known (Heyman 1995). The success of proportional geometric rules can be attributed to the materials used and the methods of communication and construction. Masonry shells are dependent on compression from self-weight for stability, which is considerable if using stone. Since masonry effectively has no tensile strength, geometric rules for building with masonry evolved to favour purely compressive forms for stability, which scale linearly, hence their success (Williams 2014). Medieval timber construction in both Europe and Asia also adhered to geometric laws of proportion (Zhong 2002; Zwerger 2012). To a contemporary eye, with the line of thrust contained in the elements by the proper proportion and arrangement of forms, these geometric rules resemble a reversed application of graphic statics. In their time, these geometric rules constituted the whole of building design knowledge, and were given the same degree of seriousness and dedication as design codes today. Without a supporting

scientific theory, however, these rules became matters of dogma or were simply never written down and forgotten (Zwerger 2012), and were progressively less well understood, resulting in building failures (Heyman 1995).

The Renaissance saw complex High Gothic rules truncated and simplified. Doing so made for heavier buildings, but ensured their stability; it also made building design accessible outside of Masonic Lodges and craft guilds societies and began the removal of the designer, as well as aesthetics, from the construction process. This shift marks the beginning of the division of the master builder into artist-architect and technician-engineer (Mark 1990). The gap was widened yet further during the Scientific Revolution, which introduced material science (Heyman 1995) and cemented in the Industrial Revolution. The introduction of mass production, mechanized fabrication, and expansion of knowledge made technical specialization a necessity, at which point building design clearly split into two professions, focusing on the fine arts at the Ecole des Beaux-Arts and the sciences at the Ecole Polytechnique (Hauschild & Karzel 2011).

Industrialization also had a severe effect on timber construction practices. Standardized members and mechanical fasteners could be assembled quickly and cheaply; hand-fabricated joinery fell out of favour (Jeska & Pascha 2014). The invention of the computer and Computer Numerically Controlled (CNC) fabrication machines has had a similarly revolutionary effect which is still ongoing. To utilize these fabrication tools to the fullest extent of their geometric capacity, the 1950s automotive and aerospace manufacturing industries developed higher-order polynomials called Non-Uniform Rationalized B-Spline (NURBS) curves (Pottmann et al. 2007), which could communicate free-form surface geometries as Cartesian coordinates for interpretation by CNC

machines. Later manufacturing programs associated NURBS algorithms with design information (Boeykens 2012) for parametric manipulation and rapid production. In contrast, Computer Aided Design (CAD) software for the construction industry evolved out of the intention of mimicking construction drawings; as such, drawings produced in 2D CAD are vector, rather than algorithm based, and representative rather than associative (Pottmann et al. 2007).

The latest advancement in CNC robotic fabrication machines and free-form NURBS architectural models bring together the capabilities of the manufacturing sector to the building design industry. As a consequence, 2D CAD drawings are no longer adequate. Parametric 3D NURBS models grant building designers the ability to engage in "Mass-Customization", in which individually unique curved and angled members can be modeled in succession quickly (Jeska & Pascha 2014; Scheurer 2012). In combination with advances in mass-timber and proprietary timber connection systems, freeform timber structures with custom members and complicated carpentry joinery are possible on an unprecedented scale.

1.5 3D Parametric Building Design

1.5.1 Parametric Modeling Concepts

Consider that a drawing is a visual representation of an idea, whereas an algorithm is a set of rules which define that idea (Figure 1). A drawing has explicit dimensions, but the design decision processes by which those dimensions were determined —the algorithms— are left implicit. Parametric modeling makes the design decisions explicit as algorithms and allows the

model dimension to become implicit. The definition of systems of rules which produce a model, rather than an explicit set of dimensions, becomes the main focus of a design.

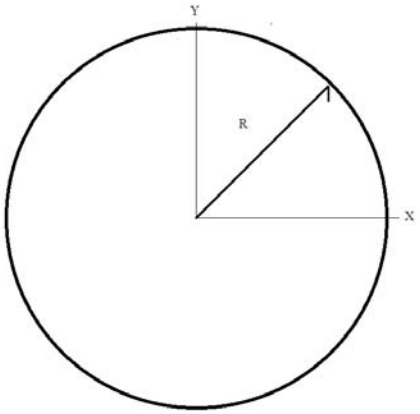

$$X^2 + Y^2 = R^2$$

Figure 1: Two incarnations of a circle. Drawing (left), algorithm (right).

Many of the fundamental concepts of parametric modelling derive from mathematics and programming (Woodbury 2010), and like a program, rules in a parametric model must not only be explicit in their operation but also applicable to all possible scenarios within the bounds of the problem (Scheurer 2012). Thus the designer's task consist of defining rules their systematic application, and a parametric model does not produce one solution but describes a collection of potential solutions. Madkour and Neumann (2009) give a useful generalised outline for applying parametric design to a building design problem, shown in Figure 2.

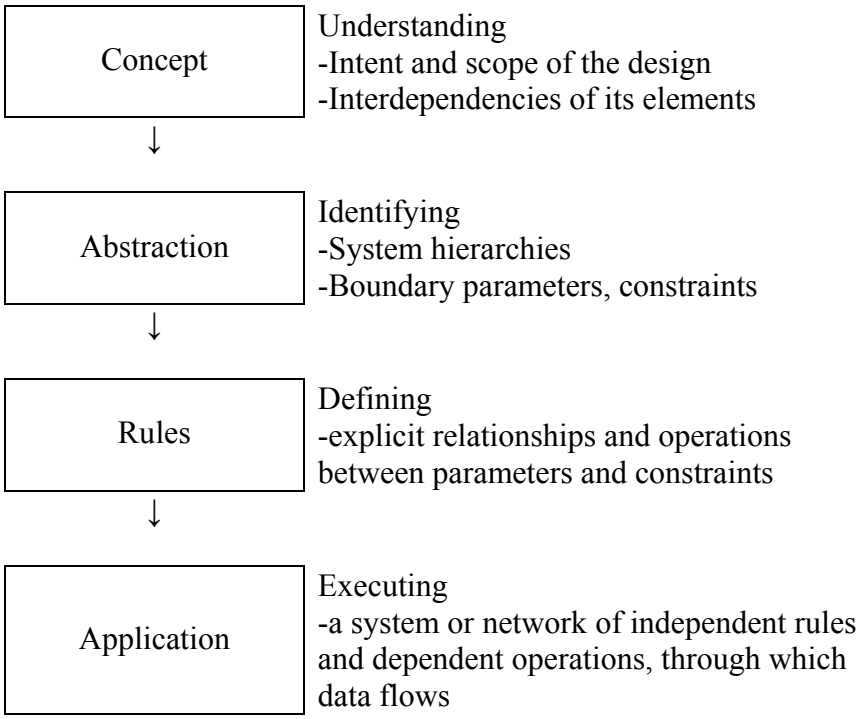

Figure 2: Conceptual process of parametric design

Still-life sketching provides a good metaphor for the general principles of parametric design. The manner in which problems are framed and addressed is the same. Subjects are first broadly blocked-in as linear geometries. These are refined with increasing detail, and always in relation the whole. For example, drawing an apple follows the same steps of Concept, Abstraction, Rules, and then Execution (Figure 3). Concept: it is impossible to draw an actual apple, but easy to draw a 2D representation of an apple. This general description of the intended outcome situates the design within geometric space. Abstraction: 2D geometry can be described in 2D space. A very basic frame of reference is constructed (Figure 3a), here a two-dimensional plane for orientation, with corners, midpoints, and centre denoted. Rules: All points and lines within this space can be described in relation to the plane and its boundary (Figure 3b). Broad outlines of any subject can be drawn between points which freely slide along the frame (Figure 3c). Further

refinements are made in relation to the previous outlines in a recursive manner until the geometry satisfies the design criteria of a more specific objective (Figure 3d and e), and then details can be filled-in to complete the model (Figure 3f). Execution: a systematic representation of how the apple drawing would look like as a symbolic model (Woodbury 2010) is shown in Figure 4.

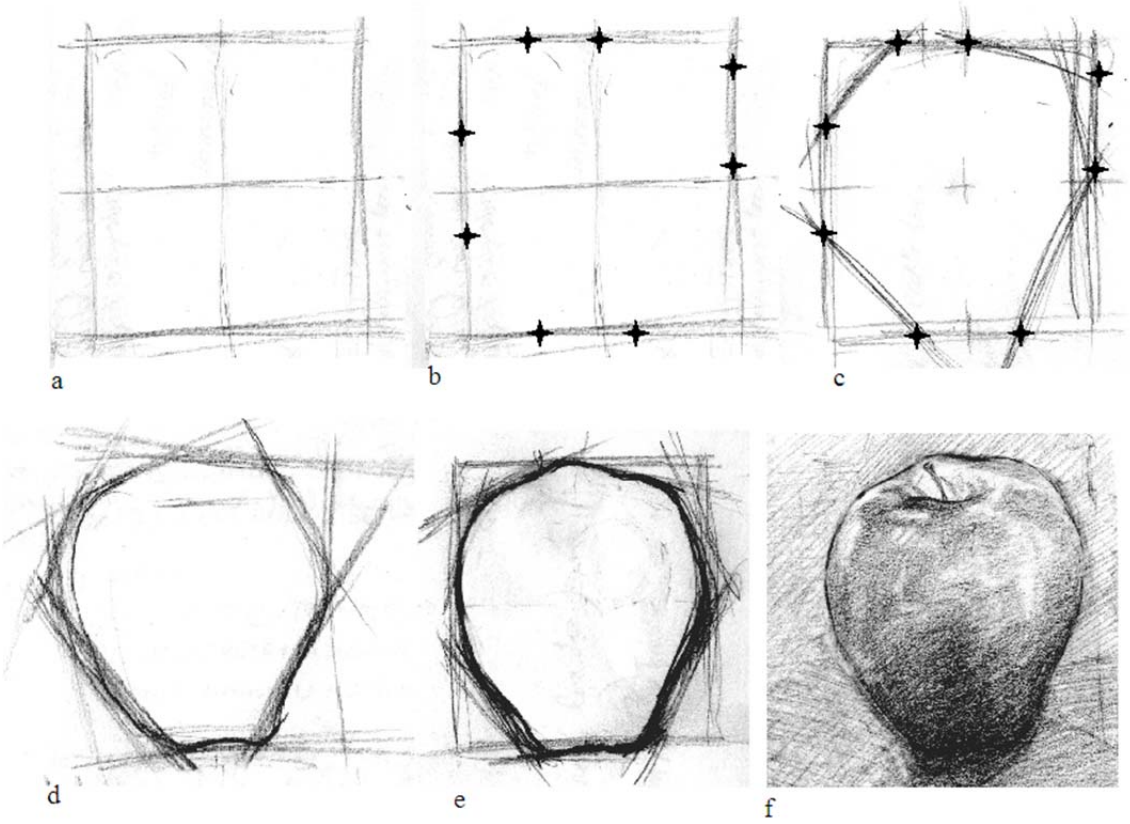

Figure 3 Parametric drawing. Top, left to right: 2a) Reference plane, 2b) Points 2c) Lines. Bottom left to right: 2d-2e) Refining associations, 2f) Resultant form

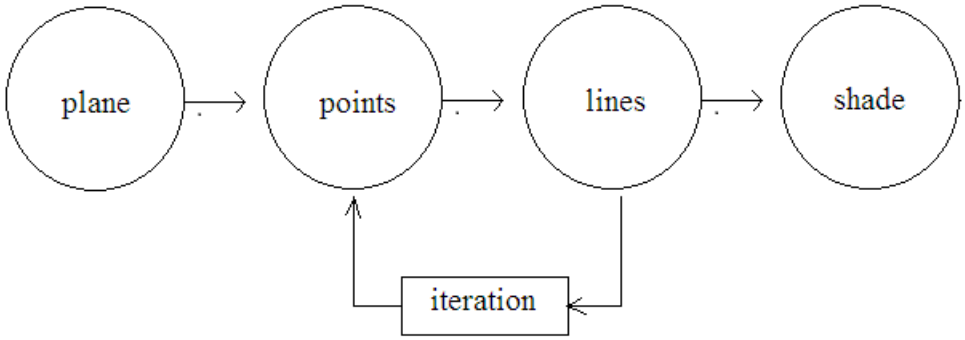

Figure 4: Symbolic model showing the process of drawing as a parametric system

Far from being a purely automatic process, within the designer's discretion is the conceptual and algorithmic essence of what is being modeled, i.e. i) the intent of the model, ii) judging what is and isn't essential, and iii) implementing hierarchies at different levels of abstraction (Scheurer 2012). The apple could be rendered from any perspective by altering the positions of the reference points, or abstracted further as a collection of dark and light tones rather than linear outlines which are later filled-in.

In principle, FEM software is already parametric, since it associates geometric dimensions with material definitions, design criteria, and conduct various analysis procedures. The FEM user-interface prevents the engineer from engaging directly with the underlying parametric system. With respect to building design, the terms "parametric modelling" or "parametric design" from here on refer to digital modelling software whose interfaces provide the means to define and manipulate systems of algorithms and definitions themselves, not simply the parameters. Parametric software enables complex architectural designs (Jeska & Pascha 2014) and can be equally useful for engineering design. Furthermore, a shared parametric model can be used to correlate geometry between the two fields.

1.6 Approaches to Structural Design of Parametric Architecture

1.6.1 Overview

To understand the tools and methods of predecessors, a conceptual frame needed to be applied which would relate prior work to the objectives of this research. Structural design of complex geometries varies depending on the role which the engineer is allowed to take, and these approaches have been categorized in the past on different rationales. Kloft (2003) differentiates on the spatial boundaries dictated by the architect in which the engineer may operate, Manglesdorf (2010) on geometric types and their implications for the structural designer. To embed structural design into the form finding practise, rather than focusing on final forms and spaces, architectural-structural relationships can be placed in a 4-tiered system to reflect how early the structural engineer is brought into the design process:

1) Architect->Concept->Algorithm->Geometry->Structural Design

2) Architect->Concept, physics-based geometry acknowledges action of structure->Algorithm->Geometry->Structural Design

3) Architect->Concept->Algorithms->Geometry->Consults engineer and manufacturer on Materials, Fabrication Process->Optimization of Shape->Structural Design

4) Architect-> Concept->designs with engineer and manufacturer on physical behaviour, materials, fabrication->Algorithms->Preliminary Structural Design->Optimization/Trade-offs->Geometry->Final Structural Design.

Precedent parametric structural designs have largely fallen under tier 3, wherein the architect authors the final form, but the structural engineer can use the versatility of parametric tools to realize the form.

1.6.2 Precedents, Methods, and Tools

Examples of precedent parametric structures illustrate how architects and engineers have used parametric models for their own ends, their tools, what aspects of the design they were applied to, and to what extent collaboration was carried out in tandem with these tools. This information was used to frame the methods and tools with which the structural portion of the project was carried out. The majority of preliminary structures designed with parametric models have been steel and concrete whose material homogeneity permit freeform geometries without penalty to their characteristic properties. Timber is considered orthotropic, see Chapter 2, with consequences for the machining, connection detailing, and final form.

The concept of "digital workflows" refers to a seamless transfer of information from one modelling platform to the next and from concept to fabrication and construction. Complex building design requires collaboration between numerous specialized professions (Scheurer 2012; Kara 2008; Olsen & Mac Namara 2014; Jeska & Pascha 2014). Lack of interoperability between platforms obstructs collaborative design process, since each specialized profession has its own discipline-specific software: there are more than 20 architecture platforms, nearly 50 structural programs, and at least 10 Computer Aided Machining (CAM) software packages

specific to wood machining, and over 100 types of file formats (Hauschild & Karzel 2011; Kahaner 2014; Larsen 2007).

Adoption of shared 3D models encourages collaboration and allows more design conflicts to be identified before construction (Staub-French & Khanzode 2007). Building Information Modeling (BIM) is the most popular means of transcending digital boundaries by sharing information between disparate models. Complex architectural geometry produces interdependent systems, requiring higher levels of collaboration as well as non-standard elements (Scheurer 2012). To understand how the proposed timber shell systems should be defined in order to make our own self-defined model, requires initial geometric abstraction for investigation. Hence, data exchange between architectural and engineering design platforms without loss of investigative flexibility therefore remains a hurdle.

As competing software makers are reluctant to provide interoperability with rival platforms, some large design firms with a history of collaboration have opted to create their own custom programs for interoperability. Schwitter & Keough (2012) give an example to such a modelling approach where structural engineers at Buro Happold were commissioned to design a 145 ft long net sculpture by artist Janet Echelman. Engineers were to determine the cable material and net weave pattern while preserving the original form of the 3D model provided by the artist. The net would be produced on mechanical looms, only capable of certain weaving patterns. Cables would have to be stiff enough to resist sagging or excessive wind deformation but be flexible enough for weaving.

Figure 5: Janet Echelman's *Her Secret Is Patience*, Phoenix AZ (Wikipedia Commons 2009)

Using parametric models, regular points were projected onto the reference model and then adjusted though dynamic relaxation using custom software. The gradient changes to the point locations were used to map the size and spacing of weave pattern cells, thereby preserving the original curves of the reference geometry. Similar methodologies have been followed at numerous other projects by other firms, (Maher & Burry 2006; Thornton Tomasetti 2014). With regard to timber structures specifically, this includes the Crystal Bridges Art Museum in Bentonville, Arkansas (Schwitter & Keough 2012), the Center Pompidou in Metz, France, the Nine Bridges Golf Course in Yeoju-gun, South Korea (Scheurer 2012; Jeska & Pascha 2014), as well as the Elefantenhaus in Zurich, Switzerland (Kuebler 2013; Kuebler 2014; Jeska & Pascha 2014).

The recurring role of the engineer within these examples of parametric design is one who enables realization of abstract geometry. In all given case studies the engineers follow a framework (Figure 6) that is similar to the conceptual parametric process. Granted, a conventional structural design follows a similar sequence, but the conceptual basis is accentuated with a parametric model.

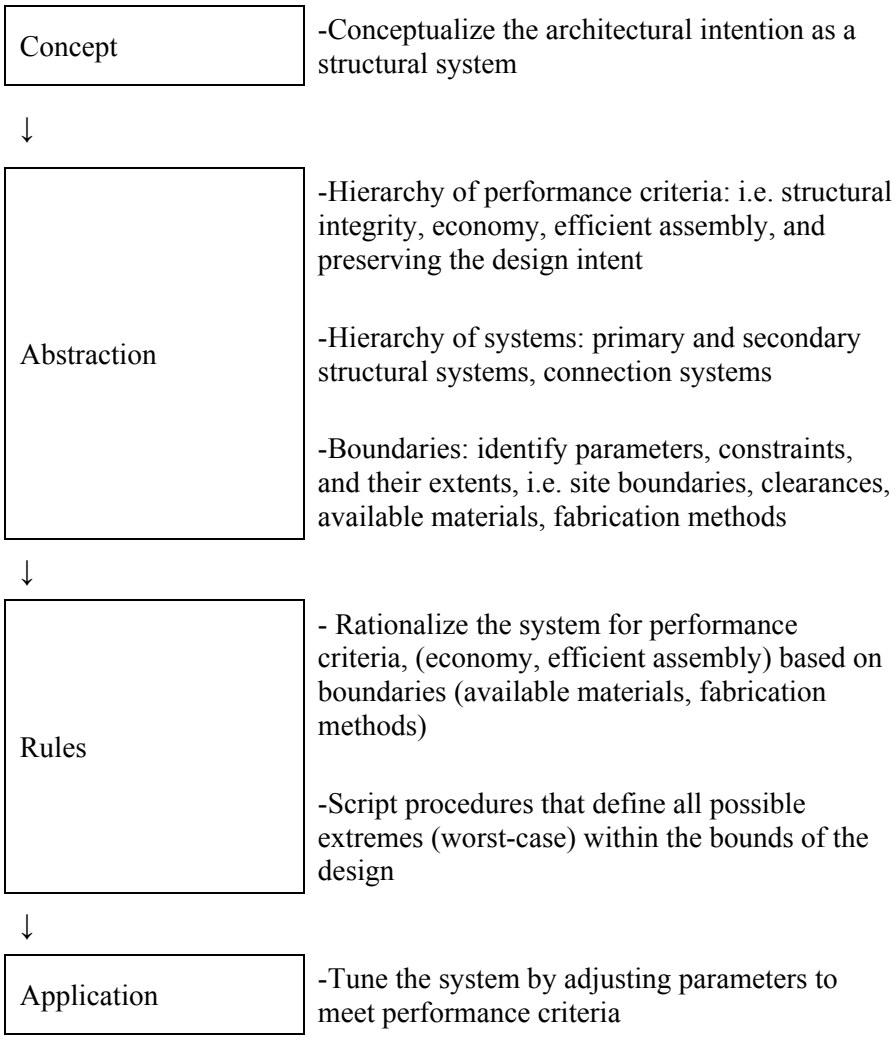

Figure 6: Flowchart showing the conceptual framework for applying structural design to parametric architectural models

This framework also highlights the importance of structural concepts in the design process. Parametric models are merely mathematic facsimiles, only as accurate as their designers are at identifying all potential constraints. Though advanced modelling software provides the means to model novel forms, unfamiliarity with structural mechanics or the nuances of material properties

requires working closely with an engineer. Physical prototypes are a necessary means by which to evaluate the accuracy of the designer's assumptions (Williams 2014).

The general benefits of collaboration using interoperable parametric models are higher speed and more transparent communication. Any changes in the architectural reference geometry automatically update (Mirtschin 2011) the structural model, and subsequently those structural dependents which reference it (Schwitter & Keough 2012). Additionally, by engaging in unusual projects and parametric models, engineers develop powerful and versatile tools with the ability to sustain innovations and challenges. Engaging architects directly with engineering also helps engender wider confidence in novel forms and systems.

1.6.3 Co-Rationalized Structural Engineering

Within this parametric modeling framework, the architectural geometry serves as the reference geometry and is assumed as an absolute design boundary to which the parametrically modeled structural system is applied. While this reference geometry could be augmented gently at the recommendation of the engineer, the geometric concept is still conceived independently of structural criteria and the structural design is still determined after the fact. In architecture, this is referred to as post-rationalization. In alignment with morphogenetic design philosophy, some architects and engineers have proposed using structural concepts as primary generative rules for the form (Tessmann 2013; Wieser 2012). Using an approach to design could help reconcile structural necessity with architectural intent. Design relationships in which the role of "architect" or "engineer" blurred have been termed "co-rationalized"(Maher & Burry 2006).

The decision to approach structural engineering in this manner has the following three implications for the engineer. One: The main revelation of collaborative design studios with architecture and engineering students was that success correlated with the level to which usual discipline divisions were resisted (Maher & Burry 2006; Kara & Georgoulias 2012; Olsen & Mac Namara 2014; Tessmann 2013). Two: While interoperable models are sufficient to facilitate a collaborative design relationship, integrated models, in which the parametric model is linked live to the FEM software, are needed to facilitate co-rationalized design relationships (Mirtschin 2011; Mirtschin 2014; CORE studio 2014; Maher & Burry 2006). The former allows the structural engineer to respond quickly to design changes, but the latter grants the engineer geometric agility and influence, and embed structural constraints in the formal design logic itself. Three: If the roles of both architect and engineer are re-arranged to share authorship of form, then the integrated model paradigm which depends on a-priori reference geometry is no longer valid, and the engineering process dissolves into concepts and variables for which there are few precedents and no detailed design framework for guidance (Olsen & Mac Namara 2014).

1.7 Research Objectives

In keeping with the project brief, this research focuses on some of the structural challenges for the design and fabrication of folded CLT panel walls and CLT panels with double curvature. Given the co-rationalized premise of this project, the structural design task was to size members and connections for a CLT shell without the use of reference geometry. The scope of this thesis therefore focuses on identifying the engineering design challenges presented by two common

shell structure typologies constructed from CLT, namely the parametric structural design boundaries for i) folded CLT panel structures and ii) double-curvature CLT panels.

This research addresses these hurdles by:

1) Identifying parameters and structural design constraints;
2) Conceptualizing structural systems with generative potential for architectural expression;
3) Implementing a computational design process that integrates 3D parametric architectural models with structural analysis software; and
4) Exhibiting the process through the execution of several design projects.

The procedure and tools used in this research are described more fully in the following methodology section. Chapter 2 discusses the state-of-the-art on CLT fabrication, use, and analytical models followed by a discussion of Self-Tapping Screws (STS) commonly used for CLT construction. Then the structural behaviour of two common shell structure typologies, namely folded plates and gridshells, and discusses precedent applications of timber to these systems is described. Chapter 3 discusses the software architecture, scripting, geometry, and the operation and intent of both architectural and structural FEM software applied in this research. Chapters 4 and 5 contain the design, modeling, analysis, and fabrication of folded CLT panel walls and doubly-curved CLT panels, respectively, followed by discussions of the results.

1.8 Methodology

1.8.1 Overview

Part of the research was carried out in service to the project supported by Forest Innovations Investment through the Wood First Act (Government of British Columbia 2009) . The grant was awarded to CAWP, a centre that is administered by the Department of Wood Science for the promotion and continued development of Canada's value-added wood products manufacturing sector, with supporting technical and testing facilities. The project was carried out by myself in collaboration with students from the SALA under the supervision of Prof. Tannert, Prof Meyboom, and Prof. Neumann. From March 2014 until March 2015, our team undertook the design, fabrication, and documentation of the process thereof, for two prototypical solid timber wall elements: double-curvature CLT panels and folded timber panel walls.

Since material properties, form, and performance are inseparable in the case of shell structure design, structural behaviour was made an integral part of the parametric geometric model definitions. The underlying conceptual framework and assumptions of these models could then be verified through physical measurement of the resulting prototypes. As the structural engineer in the project, my role was to identify, define, and integrate relevant structural properties into the parametric model. Hence the structural research and investigation was a 9-step procedure:

1) Develop a structural concept aligned with the architectural concept. (Chapter 2.4-2.5)
    a. Folded plates (Chapter 2.6), and
    b. Doubly-curved shells (Chapter 2.7)

2) Develop analytical models which describe
    a. CLT material properties (Chapter 2.1), and
    b. Connection design detailing. (Chapter 2.2, 2.3)
3) Integrate the parametric model with FEM software via third-party plugins, then characterizing forms by assigning joint, linear, or shell element identities to nodes, curves, and surfaces. (Chapter 3)
4) Modify/Rationalize the parametric model to respond to geometric changes associated with key structural parameters and procedures.
    a. For folded timber plates (Chapter 4.1)
    b. For doubly-curved timber shells (Chapter 5.1)
5) Materialize forms: translate analytical material models into parametric definitions for material properties and assigning materials to elements.
    a. For folded timber plates (Chapter 4.2; 4.4)
    b. For doubly-curved timber shells (Chapter 5.2)
6) Constrain forms: Relate fabrication and connection detailing characteristics to geometric consequences at a panel level and to the whole; translate these relationships into parametric script definitions within the modeling software.
    a. For folded timber plates (Chapter 4.5)
    b. For doubly-curved timber shells (Chapter 5.3)
7) Compare FEM output with analytical predictions.
    a. For folded timber plates (Chapter 4.2.3, 4.4.2)
    b. For doubly-curved timber shells (Chapter 5.3)

8) Fabricate physical prototypes.
    a. For folded timber plates (Chapter 4.6)
    b. For doubly-curved timber shells (Chapter 5.4)
9) Evaluate prototype behaviour against FEM and analytical predictions. Geometrically: scaled prototypes serve to validate the material and fabrication assumptions made in the script definitions. Structurally: deflection and stiffness behaviour of the prototypes are explored further through measurement and load tests.
    a. For folded timber plates (Chapter 4.7)
    b. For doubly-curved timber shells (Chapter 5.5, 5.6)

1.8.2 Project Team

The roles of each researcher in the team can be broadly sketched as follows.

Primary Masters Student researchers from SALA:

- Thomas Gaudin: Primary Parametric Modelling, Diagrams, Architectural Conceptualization
- Jessica Hunter: Wood Fabrication, Architectural Conceptualization
- Roy Cloutier: Wood Fabrication, Parametric Modelling, Diagrams, Renderings, Architectural Conceptualization

Supporting Masters Student researchers from SALA:

- Sarah Maria: Photographic Documentation
- Nicole Tischler: Photographic Documentation, Fabrication

Masters Student researcher from Civil Engineering:

- Myself: Integration with FEM, Structural Parametric Modelling, Structural Research, Design, Definition of Constraints, Fabrication, Diagrams, Architectural Conceptualization

Supervisory Roles

- AnnaLisa Meyboom and Oliver Neumann from SALA provided design advice.
- Thomas Tannert, Associate Chair of Wood Building Design and Construction and the author's supervisor, provided technical/engineering design advice.
- Iain Macdonald from CAWP coordinated technical support from CAWP in the form of Vincent Leung.

1.8.3 Tools

This research took special note of the aforementioned parametric stadium designs executed by CORE Studio at Thornton Tomasetti, whose demonstration videos demonstrated a combination of integrated architectural (McNeel's Rhinoceros3D and Grasshopper) and structural models (Computers and Structures' SAP2000) with genetic optimization algorithms (CORE studio 2014). Other firms have used Bentley's GenerativeComponents in combination with MicroStation (Woodbury 2010) and Autodesk's Dynamo in combination with SAP2000 (CORE studio 2014): these latter pairings were not considered in this research. Neither GenerativeComponents nor Dynamo possess the range of third-party tools available with Rhinoceros; both require structural analysis software which were not available without high cost.

Furthermore, the architecture students and myself were already in possession of and familiar with Rhinoceros and Grasshopper and could begin using them immediately.

Rather than integrating with SAP2000 as CORE Studio had done, Autodesk's Robot was selected as the structural analysis software, as it could be integrated through the same plugin (GeometryGym) as SAP2000 and was freely accessible for students. In addition it also provided an orthotropic material definition. The homogeneity of steel and concrete material properties allows them to take on freeform geometries without penalty to their characteristic strength; timber is orthotropic and therefore the ability to model this material through a parametric interface was of great importance. A fuller description of the software and plugins used in this research and the manner in which they were integrated is detailed in Chapter 3.

Chapter 2: Design of Shell Structures using Mass-Timber

2.1 Cross-Laminated Timber

2.1.1 Laminated Wood Composites

Composites of timber laths, veneers, strands, or fibers bonded with adhesive and pressed into beams, columns, and panels are collectively referred to as Engineered Wood Products (EWPs), with the larger structural members belonging to the mass-timber category. The composite process effectively redistributes natural flaws inherent in wood to minimize their effect, and the size of a member is restricted only by the spatial limitations of available means of production and transportation. The end product is more uniform, more reliable, and performs better in a fire than sawn lumber (Gagnon & Pirvu 2011). Plywood is probably the most commonly recognized laminated wood composite, consisting of thin veneers layered orthogonally across each other and cut into panels. Glue-Laminated Timber (GLT) was the first laminated mass-timber product, while CLT panels, commonly used in Europe, are gaining popularity in North America, resemble a cross between plywood and GLT. Both CLT and GLT consist of wood laths assembled into laminations and stacked, in parallel in the case of GLT (Figure 7 right), and orthogonally across each other in the case of CLT (Brandner 2013), resulting in slab-like, rectangular panels (Figure 7 left). Design of CLT systems takes concepts from both GLT and plywood design.

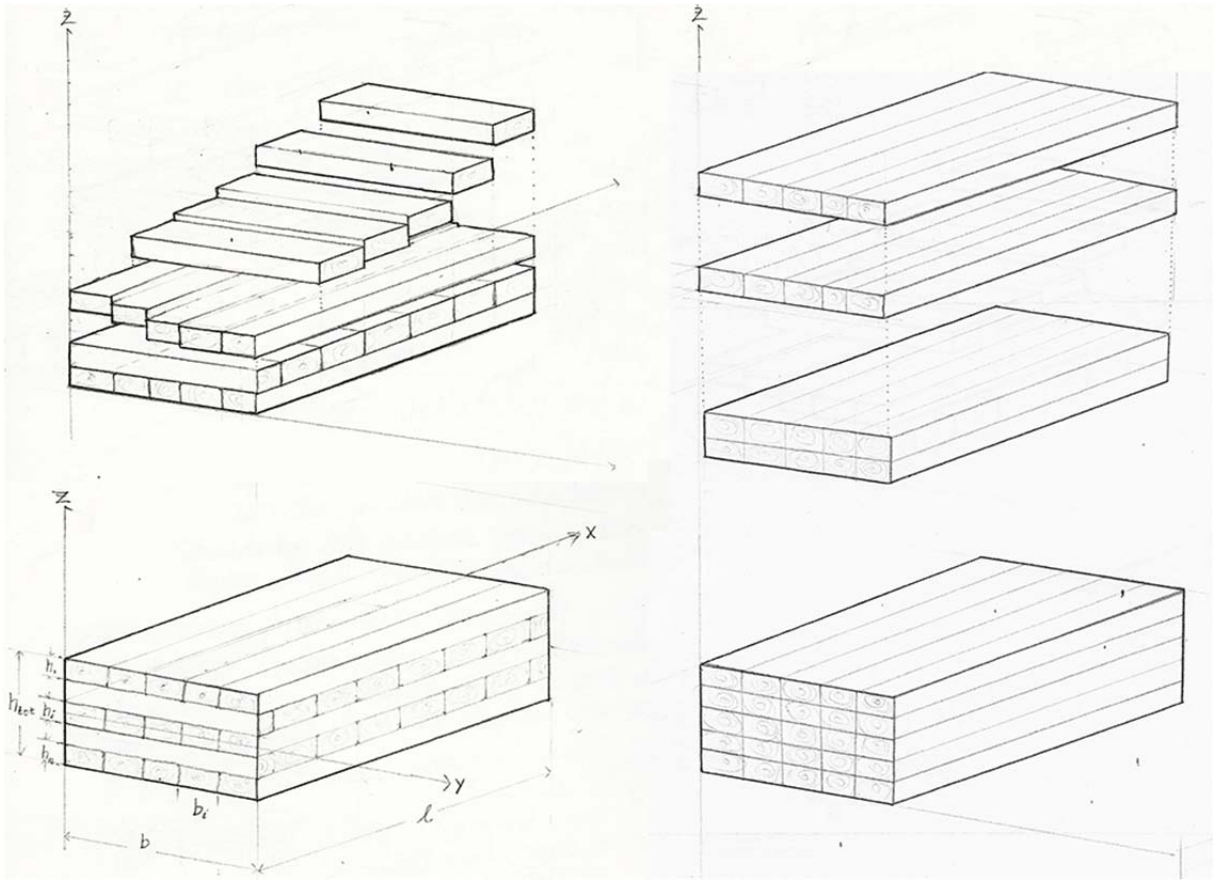

Figure 7: Left: CLT, Right: GLT

The thickness, number, and pattern of alternating longitudinal and transverse layers of CLT can be custom-specified depending on the intended function of the panel, but usually the outermost layers are parallel to the span. The alternating layer directions of CLT provide better dimensional stability and shear capacity compared to sawn timber, making CLT panels excellent for use as floor plates and shear walls (Mestek & Kreuzinger 2008; Jöbstl et al. 2008). This bi-directional in-plane strength is similar to precast concrete slabs, with potentially similar applications. The feasibility of constructing a shell structure using discrete CLT elements is a primary focus of this investigation. To properly inform a parametric model, the material properties and the constraints

imposed by connections, fabrication, and assembly requirements for CLT must be identified and defined in order to explore their geometric consequences.

2.1.2 Mechanical Properties of CLT

Unique among main-stream structural materials as the only one of biological origin, timber structural members are non-homogeneous and anisotropic, with distinct and independent mechanical properties (elastic and shear moduli, *E* and *G*) along three mutually orthogonal orthotropic axes (L,R,T) (Figure 8), identified as the Longitudinal, Radial, and Tangential orientation of wood grain.

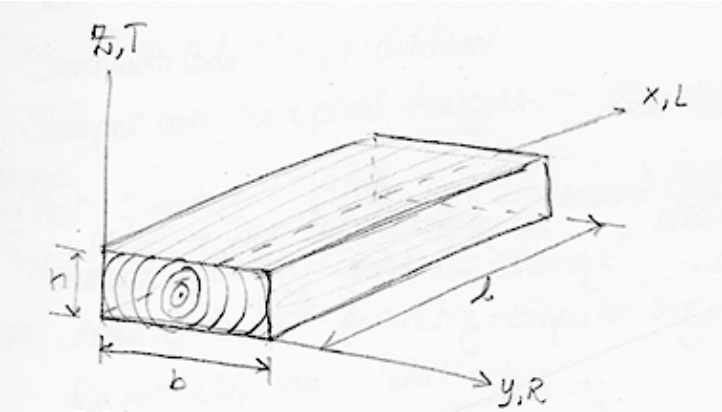

Figure 8: Geometry of a sawn timber lath

Poisson's ratio, the ratio of the strains in any two orthogonal axes, can be used to correlate the shear or elastic modulus in any one orthotropic plane (LR, LT, RT) to another. Empirical studies indicate that the moduli for softwood timber species can be safely expressed by orthotropic material ratios (Gagnon & Pirvu 2011; Mestek & Kreuzinger 2008):

$$E_R = E_0/30;\ \ G_0 = E_0/16;\ G_R = G_0/10 = E_0/160 \quad (1)$$

Sawn lumber is normally cut into longitudinal members parallel to the natural grain direction to prioritize the stronger longitudinal properties of timber under bending and axial loads: that is, the geometric axis (X,Y,Z), is aligned with the orthotropic axis (L,R,T). However, timber is often loaded at an angle to the grain and will exhibit a combination of these orthotropic properties.

As a natural product, it is also not uncommon for the geometric and orthotropic axes to be out of alignment, a condition called *cross-grain* (Bodig & Jayne 1982), and illustrated in Figure 9. The angle resulting from rotation of the orthotropic LR-plane in the XY-plane is herein referred to as cross-grain angle, α, though it properly describes the rotation of any orthotropic plane. For the purposes of clarity, as this research is concerned with linear and planar elements, if $\alpha = 0°$ then the L and X axes are parallel; if $\alpha = 90°$ then X is perpendicular to the grain.

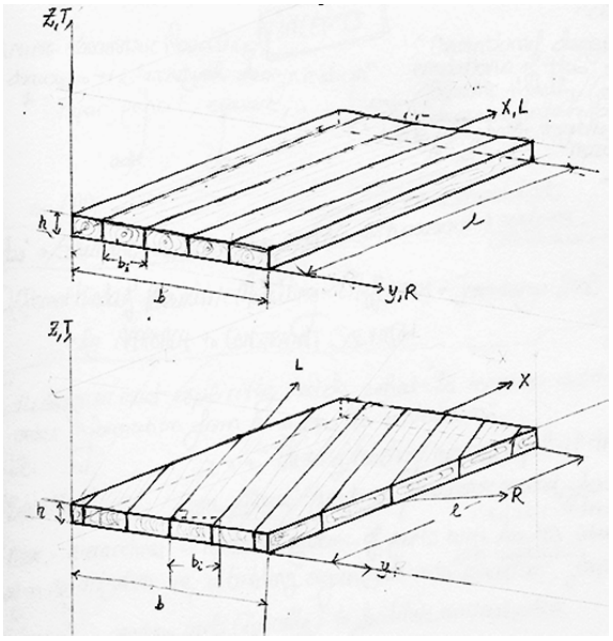

Figure 9: Top: aligned timber lamina Bottom: cross grain misalignment

EWPs, such as plywood, GLT, and CLT, consist of multiple layers of laminations. The alternating lamination orientations that characterize plywood and CLT panels express non-uniform bending stress and strain profiles as illustrated in Figure 10, which compares the stress diagram of a CLT section with no cross-grain angle to that of a uniform beam made of solid timber or GLT. Laminations running parallel to the grain exhibit both individual and group flexural response, while perpendicular layers are subject to rolling shear (Gagnon & Pirvu 2011).

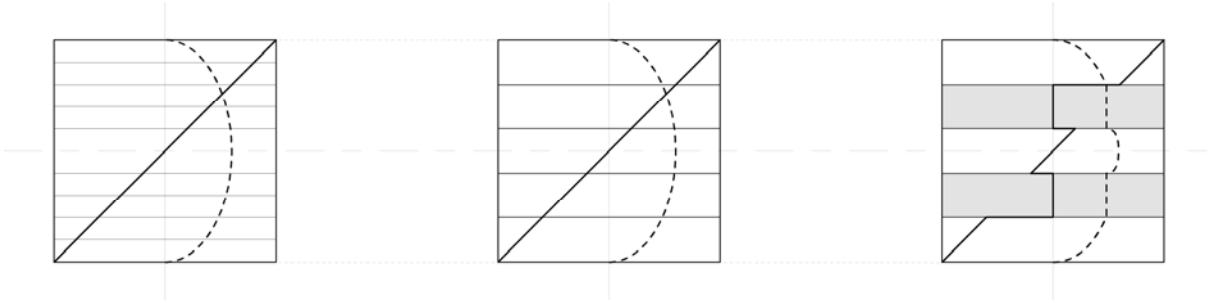

Figure 10: Stress distribution in left: sawn timber, middle: GLT, right: CLT

Shear in timber is the result of interaction between tensile and compressive stresses, resulting in perpendicular-to-grain stresses between wood fibres, producing fissures which propagate through the member. In linear members under bending loads, shear is expressed as diagonal splitting in the longitudinal direction and separation outward from the axis. Confined between axial laminates, transverse CLT layers cannot move out of the plane of principle action and, subjected to contradictory shear directions, begin to deform by rolling in relation to one another. This action influences the stress distribution and the effective bending stiffness of the panel (Blass & Fellmoser 2004). For this reason, determination of both elastic and shear properties are central to structural design with CLT.

A parallel array of identical laths constitutes a lamination. If the cross-grain angle of a laminate is $0° < \alpha < 90°$ a complex system of shear coupling occurs: between shear stresses and normal strains, and normal stresses and shear strains. Quantifying the elastic response of a cross-grained laminate requires the transformation of elastic properties from the orthotropic coordinates to the geometric using matrix operations in combination with Poisson's ratios and trigonometry: however, a general theory for predicting effective strength of anisotropic asymmetric laminates under combined loading has not been found. In such cases the empirical relation given by Hankinson's Equation (1921) (Eq. (2) can be used to determine elastic or shear moduli (and strength properties), *X*, properties at cross-grain angles between $0° < \alpha < 90°$ so long as 0° and 90° properties are known (Bodig & Jayne 1982) and thenceforward be applied as necessary.

$$X_\alpha = \frac{X_0 X_{90}}{X_0 sin^{\mathrm{n}}\alpha + X_{90} cos^{\mathrm{n}}\alpha} \qquad (2)$$

The cross-grain angle should not be confused with the lamina angle of rotation, β, which measures the angle between lamina rotated with respect to one another (Figure 11 left), nor the angle of rotational symmetry, γ, which means that the cross grain angle of laminates within a composite are mirrored about the same geometric axis (Figure 11 right), (Bodig & Jayne 1982). Timber members with laminates layered parallel to one another, such as glulam, are by definition $\beta = 0°$; each laminate in a plywood or CLT panel is $\beta = 90°$ relative to its adjacent layers. If CLT is characterized by a constant lamina rotation angle of $\beta = 90°$, then to describe a CLT panel with a cross-grain angle, α will refer to the cross-grain angle of the face lamination and alternate layers can always be assumed to have a cross-grain angle rotated 90° ($\alpha + \beta$). Hence, if a CLT panel has $\alpha = 45°$ then cross-grain angle of alternating laminations is also 45° and the panel also has a rotational symmetry of $\gamma = 45°$.

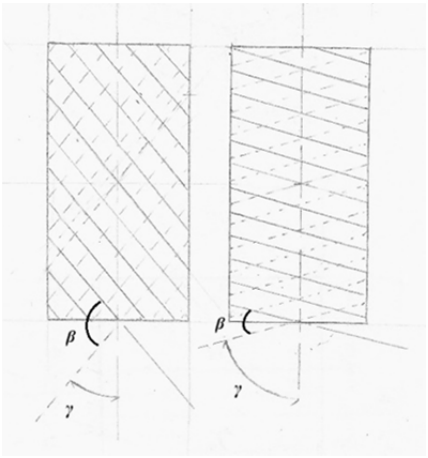

Figure 11: Lamina angle of rotation. Left: cross grain $\beta = 90°$, rotational symmetry $\gamma = 45°$. Right: cross grain $\beta = 30°$, rotational symmetry $\gamma = 60°$

2.1.3 Analytical Methods for Modeling CLT Bending Stiffness

2.1.3.1 Overview

The flexural properties of a CLT panel vary with panel layup and loading direction (Gagnon and Mohammad 2011). As panel size, geometry, and cross-grain orientation are unknown in this research, empirical tests are unfeasible, whereas analytical procedures readily adapt to changes in their parameters and combine well with Grasshopper's algorithm-based operations. The Canadian edition of the CLT Handbook (Gagnon & Pirvu 2011) lists three analytical methods for calculating the flexural properties of CLT, distinguished from one another by the manner in which the shear deformation of the laminates perpendicular to the load is modeled. This research considers two of them on the basis of their geometric versatility for application to CLT with complex geometry: 1) the γ-method which permits easy comparison between mechanically and adhesively bonded laminate assemblies, and 2) the Shear Analogy method which can accommodate variable laminate cross-grain angles.

2.1.3.2 Mechanically-Jointed Beams Theory ("γ-method")

This method was originally developed by Moehler (1955) for composite I and T beams formed with mechanical connectors. For each shear plane, *i*, in-plane shear stiffness is described by the rigidity of the connection γ_i (Eq (3)). Fully rigid (ie, adhesive) connections are $\gamma = 1$; no connection is $\gamma = 0$.

$$\gamma_i = \left[1 + \frac{\pi^2 E_i A_i}{l^2} - k\right] \quad (3)$$

Where:

- A_i is the area of each section which defines shear plane *i*
- E_i is the corresponding elastic modulus of that section
- l is the length of the member, and
- k represents the influence of the fasteners. Mechanical fasteners are modeled by the ratio of their spacing s to the slip, K_s of each fastener:

$$k = \frac{s}{K_s}, \text{ in which } K_s = n{\rho_k}^{0.5} {d_s}^{1.7} n_s \quad (4)$$

Where:

- n – composite factor
- ρ_k – wood dry density
- d_s –fastener diameter
- n_s – number of fasteners in a connection

To model a CLT panel the γ-method is augmented by assuming i) only longitudinal layers carry the load, and ii) deformation due to rolling shear is captured by modeling the transverse layers as mechanical fasteners with equivalent stiffness. Hence, the s/K ratio is replaced with the "slip" between longitudinal layers caused by rolling shear deformation in transverse layers.

$$k = \frac{s}{K_i} = \frac{\sum h_\perp}{G_R b} \quad (5)$$

Where:

- $h_{\perp}$ is the thickness of each transverse layer
- G_R is the rolling shear modulus ($G_R = E_0/160$), and
- b is the panel width, usually taken as a unit value of 1000 mm.

Determination of EI_{eff} (6) combines the bending stiffness of individual lamina, with the stiffness of layers on either side of the neutral axis modified by the γ rigidity value for rolling shear deformation (Figure 12).

$$(EI)_{eff} = \sum (E_i I_i + \gamma_i E_i A_i a_i^2) \quad (6)$$

Where:

- a_i is the distance between the centroid of a load-bearing lamina to the panel neutral axis.

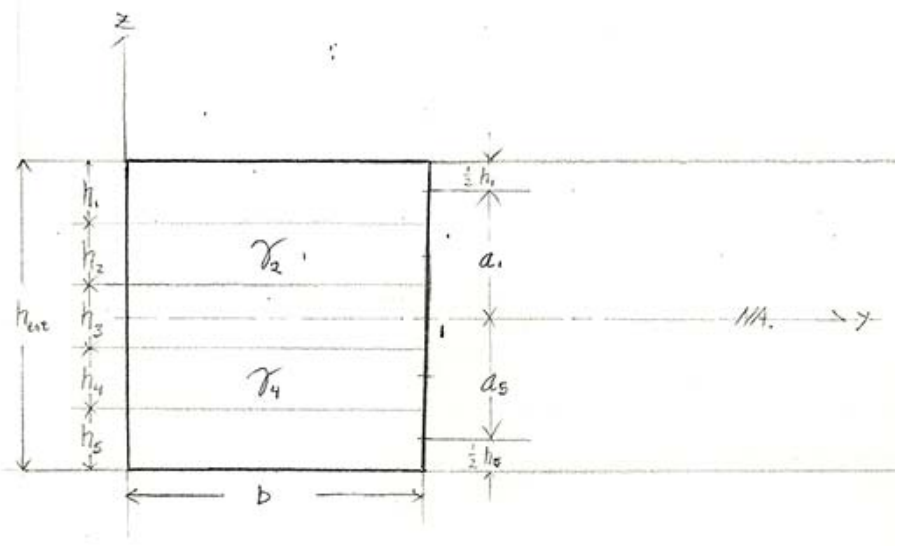

Figure 12: Diagram of gamma method

2.1.3.3 Shear Analogy Method

Kreuzinger's (1999) shear analogy method provides the most precise values for effective bending stiffness $(EI)_{\text{eff}}$ and effective shear stiffness $(GA)_{\text{eff}}$ of a CLT panel (Blass & Fellmoser 2004). This procedure evaluates a CLT panel as two virtual beams (Beams A and B) joined by infinitely rigid webs, see Figure 13. Beam A represents the flexural strength of individual plies along their neutral axes. Beam B combines the flexural shear strength of the panel as a whole with the flexural strength of the "Steiner" points ($E_iA_iZ_i^2$) and the flexibility of the connections (the adhesive). Both beams experience the same deflection due to the web. The procedure provides the. The flexural and shear stiffness properties, $(EI)_{eff}$ (7) and $(GA)_{eff}$ (8) respectively, can be used to determine flexural deflection response Δ_{max}(9).

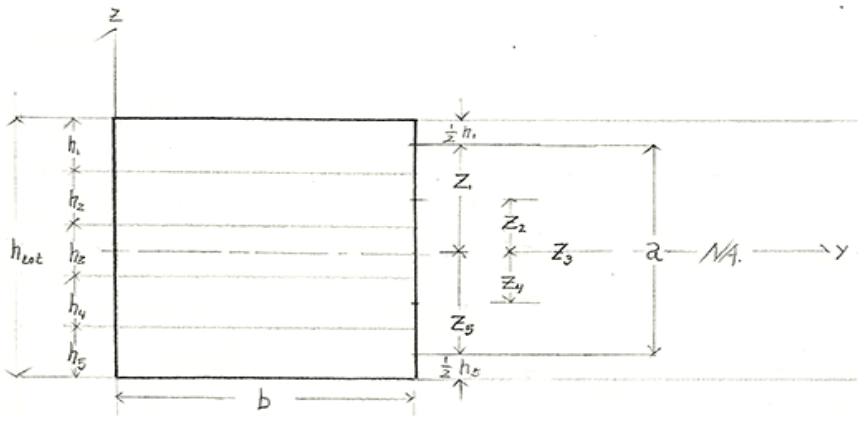

Figure 13: Diagram of Shear Analogy method

$$(EI)_{eff} = \sum \left[E_i b \frac{h_i^3}{12} \right] + \sum [E_i A_i Z_i^2] \qquad (7)$$

Where:

- h_i is the thickness of layer *i*, and

- Z_i is the distance from the centroid of layer *i* to the neutral axis *N.A.*

$$(GA)_{eff} = a^2 \left[\left(\frac{h_i}{2G_i b} \right) + \left(\sum_{i=2}^{n-1} \frac{h_i}{G_i b_i} \right) + \left(\frac{h_n}{2G_n b} \right) \right]^{-1} \quad (8)$$

Where:

- a is the distance between the centroids of the outermost layers *i* and *n*, and
- G_i or G_n is the rolling shear modulus for layers *i* to *n*

$$\Delta_{max} = \frac{5\omega L^4}{384(EI)_{eff}} + \left[1 + \frac{48\omega L^2 1.2}{5(GA)_{eff}} \right] \quad (9)$$

Where:

- ω is the uniformly distributed demand load, and
- L is the panel span

2.1.4 Cross-Grain CLT Properties

By inspection, the analytical methods assume purely orthogonal arrangements of rectangular panels. No guidelines for CLT are given for non-standard shapes or configurations, whose cross-grain angle α results in an asymmetric anisotropic laminate composite (Figure 14). The material behaviour of cross-grain CLT has received little investigation; only on in-plane properties and no research has yet been done on out-of-plane flexural behaviour. Nevertheless, this behaviour is needed for this research in order to develop folded-plane structures with CLT.

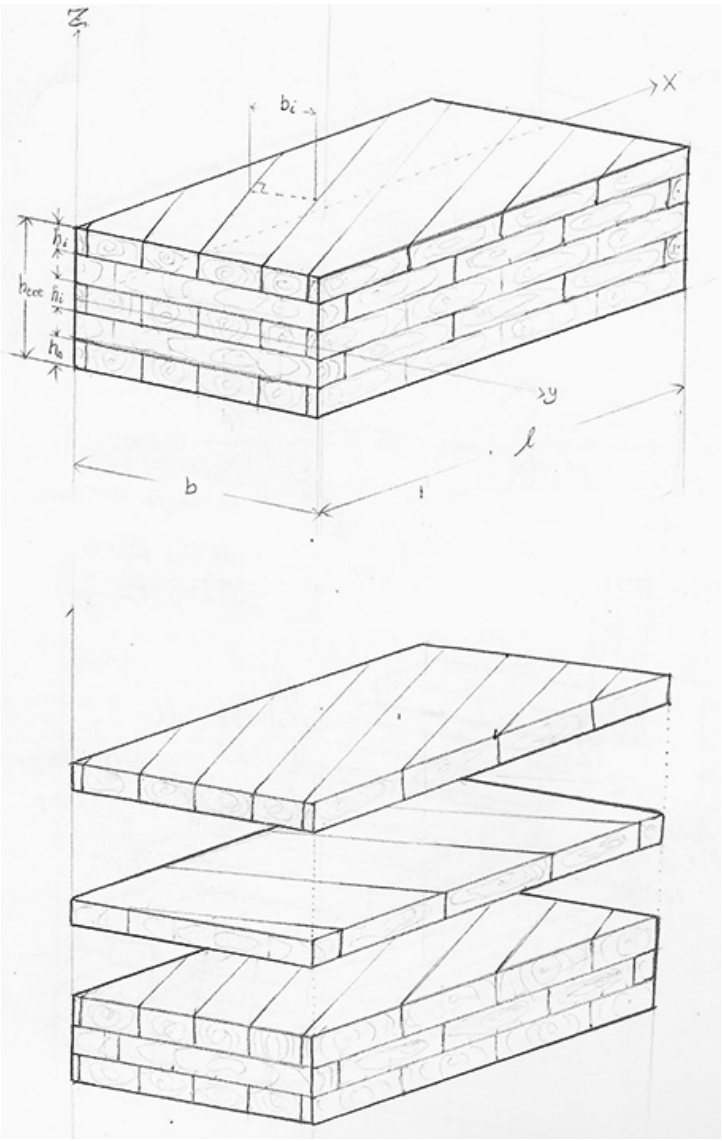

Figure 14: CLT with cross-grain angle, an asymmetric anisotropic laminate

The studies which considered in-plane stiffness are valuable because they reveal how other researchers have approached the problem of expressing the effect of cross grain on the panel behaviour as a whole. Pearson et al. (2012) investigated the behavior of 3-ply CLT panels with polygonal geometries (Figure 15), and measured the strains of CLT panels loaded in

compression in-plane at 0˚, 30 ˚, 45 ˚, 60 ˚, and 90 ˚ with respect to the face grain orientation of the outer laminations.

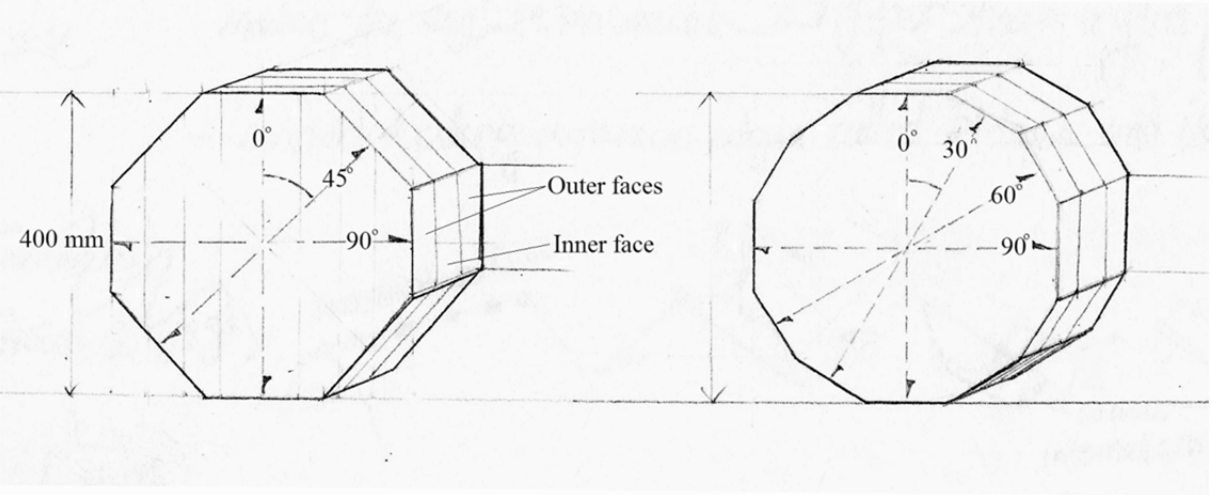

Figure 15: Cross-grain CLT test sample used by Pearson et al. (2012).

Predictions were based upon manufacturer values for longitudinal and transverse in-plane elasticity moduli and calculated using: i) Hankinson's Equation (Eq. (2), and ii) a simplified proportional approach based on Classical Lamination Theory (1959) (10).

$$E_{\alpha_{face}} = E_0 \left[\frac{2}{3}cos^4\alpha_{face} + \frac{1}{3}cos^4\alpha_{inner}\right] \quad (10)$$

Both models proved to be non-conservative by at least a third when compared to the experimental results. The cause of this discrepancy was attributed to the small size of the testing panels (400 mm in breadth), resulting in a deep beam condition. However, test data and predictions took on bell-curve profiles.

Research by Nakashima et al. (2012) on the effect of cross grain on CLT embedment capacity used test samples shown in Figure 16 and proposed applying Hankinson's equation to each grain

direction and then proportioning these values according to the number of panel layers (11). This approach ,too, produced bell-curve profiles which had good correlation with test results.

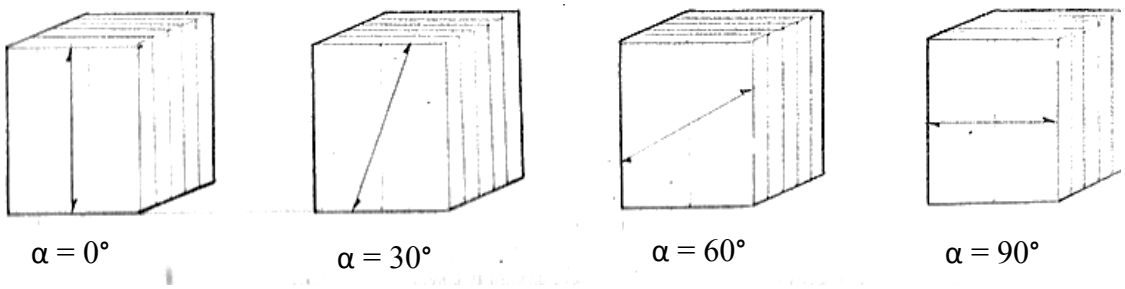

Figure 16: CLT test samples used by Nakashima et al. (2012).

$$E_{\alpha CLT} = \frac{(n+1)E_{\alpha} + (n-1)E_{\alpha-90}}{2n} \quad (11)$$

Though concerned with in-plane properties, these tests by Pearson et al. (2012) and Nakashima et al. (2012), their models also assume no perpendicular stiffness and hence cannot account for the contribution of rolling shear deformation to the material strain measurements. Nevertheless, their work provides valuable insight. Both CLT manufacturers' guides and the analytical design processes described in the CLT Handbook assume that panels are weakest at a 90° orientation, perpendicular to the exterior laminations. This would be true if the panels layers were parallel rather than cross-laminated, yet the studies presented here illustrate the bell-curve effect of cross-grain over a composite laminate and suggest that an interim angle may produce a more critical response than 90°. Determining this critical cross-grain angle would help inform a design composed of CLT panels with non-standard geometry.

This research proposes a novel approach to predicting the bending stiffness of cross-grain CLT panels. Given that the Shear Analogy requires two elastic moduli orthogonal to one another as input parameters, the input E_0 and E_{90} terms are replaced with cross-grain angled moduli values E_α and $E_{\alpha\text{-}90}$ calculated using Hankinson's Equation. The same action is performed on shear moduli G values, thereby modifying the Shear Analogy to suit any cross-grain angle α.

2.2 Timber Panel Joinery

As a panelized system, CLT edges are easily modified with CNC machinery and connection geometries often reference woodworking joinery, which are illustrated in Figure 17 based on the edge profile geometries from which the joint types are derived. Simple types, such as butted, half-lapped and spliced joints, in combination with mechanical fasteners are common structural practice (Gagnon & Pirvu 2011), whereas more complex interlocking furniture-type joints, though long used during the fabrication process of mass-timber products (Jokerst 1982), have only been explored as a generative parameters on a building-scale level in recent architectural research (La Magna et al. 2013; Robeller 2015; Tas 2013).

Complex forms often require CLT assemblies with advanced joint geometries, for which 3D modeling and digital fabrication is essential. These may also require proprietary connectors which are not covered by the Canadian timber design standard (CSA-O86 2009). The National Building Code of Canada (NBCC 2010), however, permits "Alternative Solutions", using innovative materials, products, and systems, so long as code-specified performance objective criteria are satisfied. Part of the structural engineer's role in collaborative design is not only to

ensure structural performance, but to identify to the architects the structural characteristics can be exploited to generate geometric morphologies valuable to the architectural intent. Connection design controls how and where loads are transferred from one structural element to another. Choice of joint type also has implications on the visual aesthetic, the overall form, the fabrication and assembly process, and which connection systems may be employed. Weighing these interconnected design criteria of structure, form, and fabrication is part of the designer's task. Several connection system types were considered in this study, available in Appendix A, but owing to their economy, versatility, and rapid installation, STS were selected in this research.

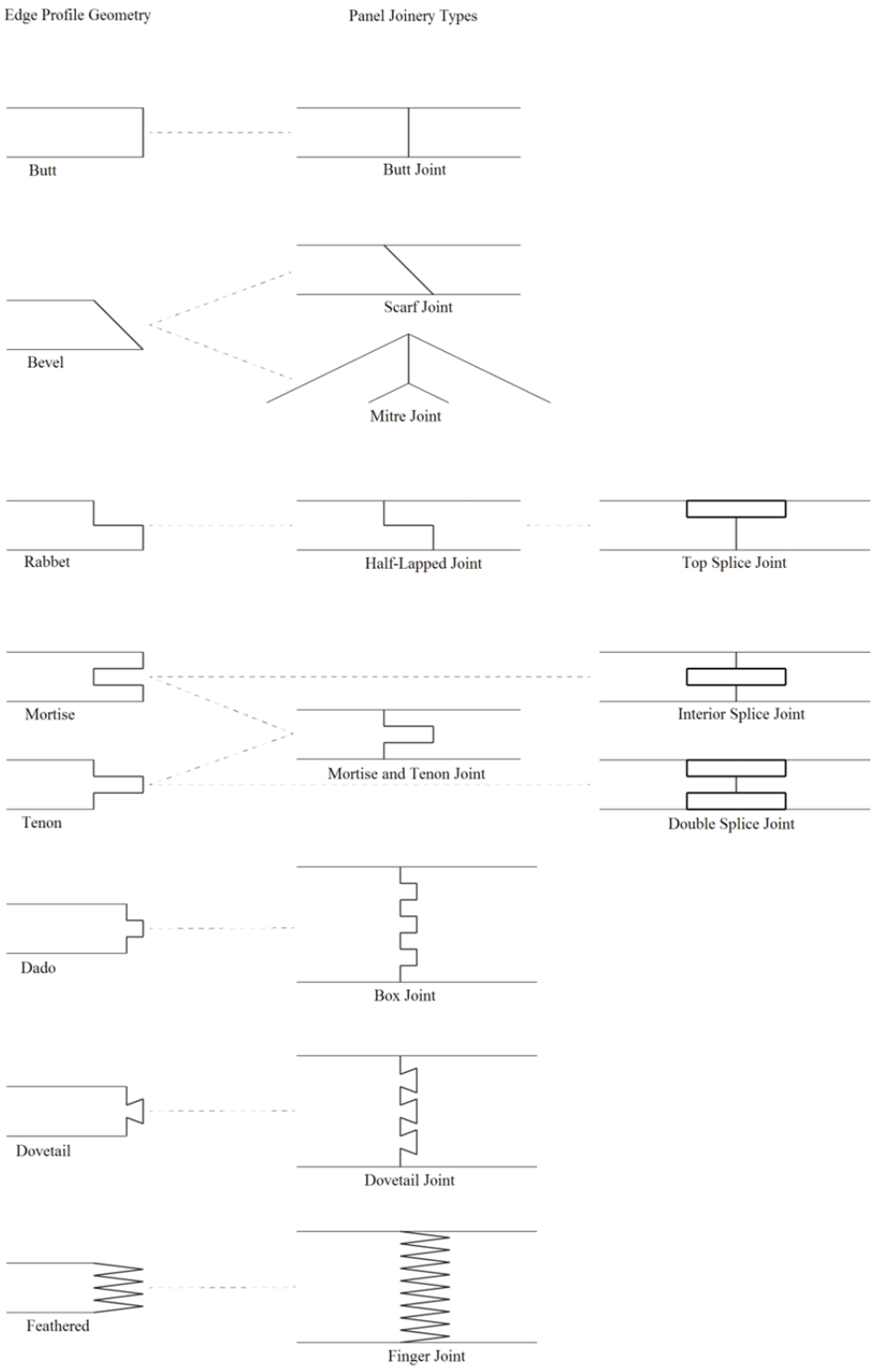

Figure 17: Panel edge profile geometry and joinery types

2.3 Self-Tapping Screws

STS are the industry standard connector in Europe for CLT panel assemblies (Mohammad 2010). Unlike conventional wood screws, STS are made from high capacity steel, have wider threads, and a cutting tip (Closen 2012). Properly designed STS connections are therefore stronger than conventional screws, need no pre-drilling, and easy to hide by countersinking screw heads into the panels and filling the holes with wood inserts. Only the threaded section embedded in the main member, termed the effective length (l_{ef}), provides withdrawal resistance for the connection. These connections function best when screws are loaded in withdrawal and inserted at an angle to the grain direction of the outer layer to maximize l_{ef}, though 90° insertions may be favourable for ease of assembly.

The Canadian Approval CCMC 13677-R (Canadian Construction Materials Centre 2014) provides technical specifications for SWG ASSY STS in accordance with the NBCC 2010 provisions for alternative solutions. According to this approval, the screw's factored withdrawal resistance, $P_{\mathrm{rw},\alpha}$, can be calculated using Eq. (12. Though this equation is directed at sawn lumber or Glulamassemblies, given that the CLT Handbook advises using glulam design procedures for CLT designs, this research assumes that Eq. (12 is also applicable to CLT.

$$P_{rw,\alpha} = \phi \cdot \frac{0.8 \cdot \delta \cdot (b \cdot 0.84 \cdot \rho)^2 \cdot d \cdot l_{ef} \cdot 10^{-6}}{sin^2\alpha + \frac{4}{3}cos^2\alpha} K_D K_{SF} \ [N] \qquad (12)$$

Where:

- ϕ is the withdrawal resistance factor (0.8 for standard-term loading)
- δ is the wood density adjustment factor ($\delta = 82$ for $\rho \geq 440 kg/m^3$, $\delta = 85$ for $\rho \geq$

$440kg/m^3$

- b is the material adjustment factor (0.75 for Parallam; else 1.0; herein 1.0 is taken for CLT)
- ρ is the mean oven-dry relative density (value from Table A.10.1 CSA O86 (2009) times 10^3)
- d is the screw outer diameter including the threads
- l_{eff} effective screw embedment length (thread length, l_{th}, minus tip length = d)
- α is the screw angle relative to grain direction
- K_{D} is the load duration factor
- K_{SF} is the service condition factor

CCMC 13677-R advises that the lateral capacity of a single screw, $P_{rw,\alpha,\beta}$, in the direction of the shear plane be designed according to the lag screw design procedure for lateral resistance in CSA O86-09, Section 10.6.6. The head pull-through resistance, R_{PT} (13) is based on the characteristic pull-through strength

$$R_{PT} = \phi r_{PT} K_d K_{SF} \quad (13)$$

Where:

- ϕ is 0.6 for shear loading
- r_{PT} is the characteristic pull-through strength, adjusted to Standard Term loading (kN), given in CCMC 13677-R according to STS diameter, mean oven-dry wood density, and STS type.

Having calculated the withdrawal, lateral, and head pull-through resistances, the demand load may be divided by the screw unit capacity to determine the required number of fasteners. For STS spacing requirements CCMC 13677-R advises referring to the original specifications given in their European Technical Approval (ETA-11/0190) (European Organisation for Technical

Approvals 2013). These are summarized in Figure 18 and are valid for load *F* at any angle to the grain, φ_p in the plane of the panel face, or φ_e in the plane of the panel edge.

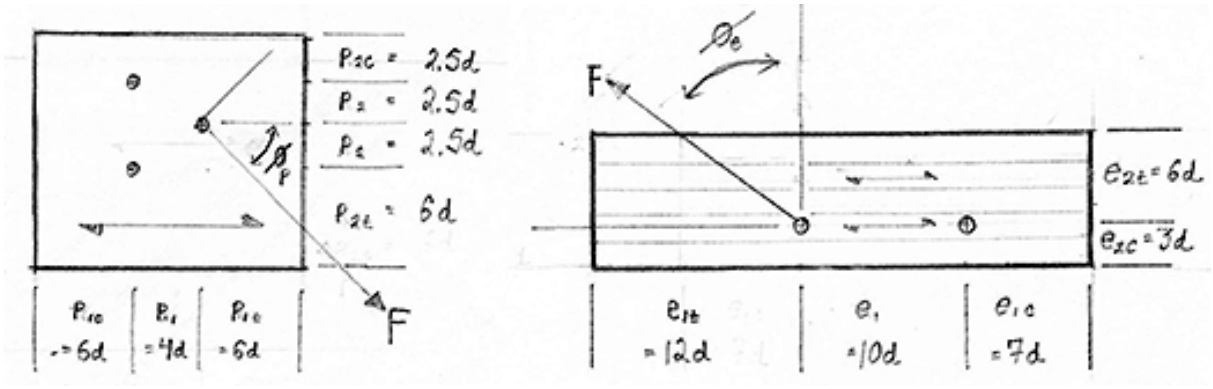

Figure 18: Minimum STS spacing for the panel face, p, (left) and the panel edge, e, (right) in units of screw diameter, d

2.4 Defining Plates and Shells

Breaking down structural element types based on their dominant geometric traits—one-dimensional (linear) frames, and two-dimensional (surface) shells and plates—is useful to differentiate the manner in which these elements carry loads (Williams 2014). Using this geometric hierarchy, a frame member can be defined as a linear load path with a cross-section which provides primarily axial and bending resistance. Similarly, a plate or shell can be defined as a surface load path, whose cross section provides resistance primarily through membrane action. The general theory of shells describes equilibrium for a differential shell or plate element in terms of normal and in-plane shears, normal forces, and bending and torsional moments (Farnsworth Jr 1999). Plates being strictly planar provide resistance primarily through in-plane bending and shear, whereas shells provide out-of-plane resistance through curvature in addition to in-plane sectional bending stiffness (Timoshenko & Woinowsky-Krieger 1987).

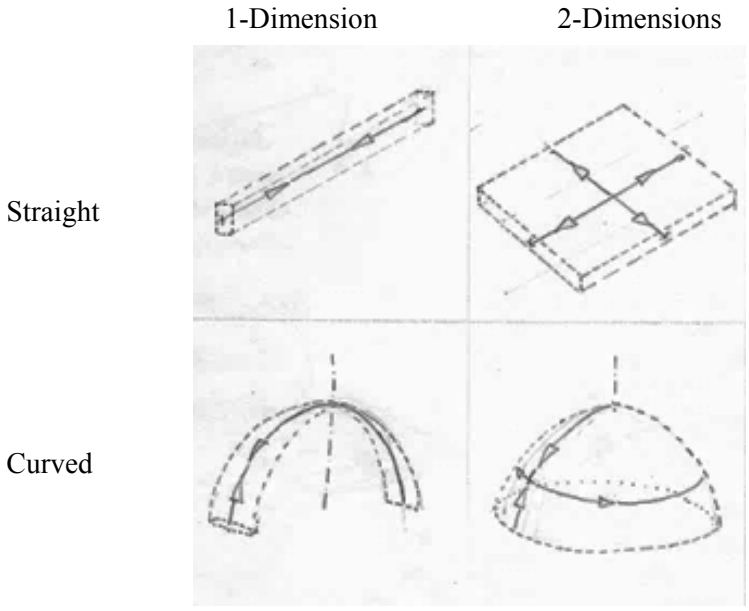

Figure 19: Typology of structural elements based on geometric dominance and curvature

Analytical methods for shell analysis establish relationships between material properties (usually assumed to be isotropic and homogeneous) and deflections to ensure compatibility with the strains of adjacent elements. This results in a system of 11 equations with 11 unknowns which can be simplified to a single eighth-order partial differential equation with 1 unknown that is still "extraordinarily difficult to solve" (Farnsworth Jr 1999). Hence most analytical methods make assumptions in order apply concepts from beam theory, with the addition of "corrective" forces: As the movement of each element is restricted by its adjacent plates or shells, the internal forces must be corrected and redistributed, in order to ensure compatibility between adjacent elements (Farnsworth Jr 1999; Williams 2014; Farshad 1992).

2.5 Approximating Plate and Shell Behaviour with Frame Elements

As an anisotropic, linear, and discontinuous material, an individual timber member inherently cannot exhibit genuine membrane behaviour (Harris 2011). Timber gridshell systems approximate shell forms using a system of linear elements (Happold & Liddell 1975), where connections, diagonal bracing, and members have been designed properly to favour axial load distribution and provide sufficient supplementary coupling at junctions between adjacent plates or shells. The following discussion relates conceptual mechanics of shell structures in timber to the more-familiar timber frame typologies.

Frame, plate, and shell structures can be extrapolated from grids of linear elements. Consider that two columns supporting a beam can be used as a basic unit within a more complex form. Planar repetition of the unit will form a frame system. Heavy timber Post-and-Beam structures repeat this frame unit both horizontally and vertically. Balloon frames have uninterrupted vertical members: floors are supported by beams which hang between continuous exterior and interior columns (or walls). Light-frame timber platform construction stacks frames of one story onto the floor below it. (Herzog et al. 2004). The structural engineer correlates the grid geometry with material properties and design criteria to size members and design connections.

Projecting this grid onto a reference surface provides the basis for a surface structure (Woodbury 2010; Harris 2011; Scheurer 2012). For instance, if the material of a continuous surface is condensed into the linear elements of the projected grid, the result is a lattice (Happold & Liddell 1975). Inversely, if the surface material is divided along the gridlines, the result is a panelized structure. These concepts are illustrated in Figure 20 with a grid projected onto a flat surface.

The dotted lines denote the direction which in-plane stiffness needs to be applied in order to achieve shell or plate action with discrete elements.

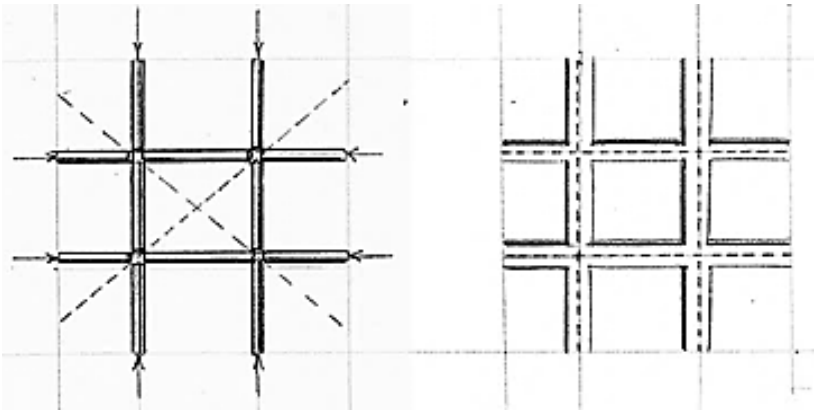

Figure 20: Grid-based structures. Left: lath lattice for gridshells. Right: rectangular panels for folded plates

2.6 Folded Plates

Folded geometries begin as regular grids on a planar surface. Ridge or valley folds run along the gridlines or diagonally between nodes. Folds may be translated/repeated linearly or radially, or mirrored and reversed; producing non-prismatic folds (see Figure 21) composed of trapezoidal or triangular panels (Jackson 2011; Buri 2011). Shifting simple V-fold patterns along gridlines, results in X-folds, whereas Y-folds occur when three ridge or three valley folds converge at a node. Stretching or skewing fold lengths result in more extreme tapering of panel elements. Prismatic structures consist of only rectangular panel elements.

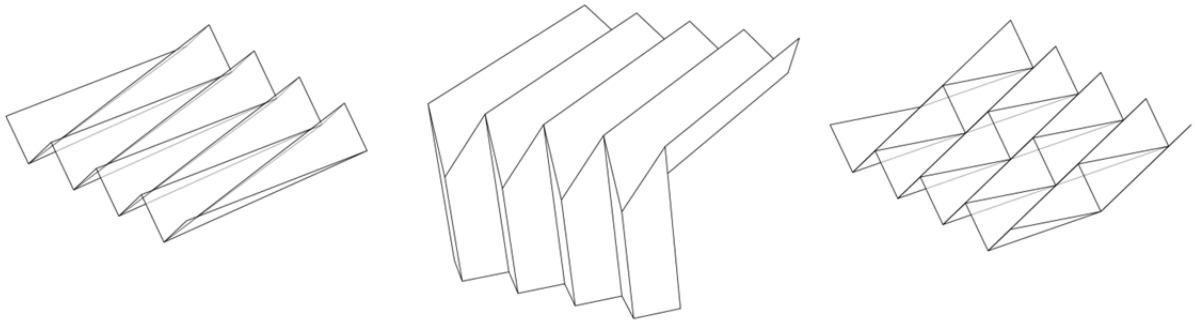

Figure 21: Non-prismatic fold variants: from left to right: V-folds, Y-fold, X-folds

The panelized structure derived from a projected grid can produce a wide variety of folded plate systems across reference geometry by modifying the underlining gridline logic. The final folded structure shape depends upon the pattern of ridges and valleys, which can be grouped into a tessellated unit and tiled over the surface.

A qualitative discussion of the structural behaviour of a prismatic folded plate roof (Figure 22) is useful for its application in CLT. The rationale for folded plate systems is that inclined (folded) plates are stiffer than flat plates by virtue of locating material further from the axis of flexure and thereby creating a larger section moment of inertia (Adriaenssens, Brown, et al. 2014). Additionally, as a continuous system, folded plates do not occupy as much vertical depth as a system of deep beams with equivalent stiffness.

Applied loads are carried by two-part structural action (Farshad 1992), as shown in Figure 23. The roof is divided into transverse unit strips which i) act as a continuous folded beam, simply supported at the plate junctions. The reactions at the junctions are resolved as linearly-distributed loads in the planes of the adjacent plates which then ii) act as simply supported deep beams. This

loading produces bending moments in the plane of each plate, resulting in attendant bending stresses at the extreme fibre, located at junctions between adjacent plates. These are usually unequal and must be balanced through edge shear coupling in the junctions (Figure 24). Therefore, with respect to discrete plates, structural efficiency is influenced by the rigidity of the junction connections.

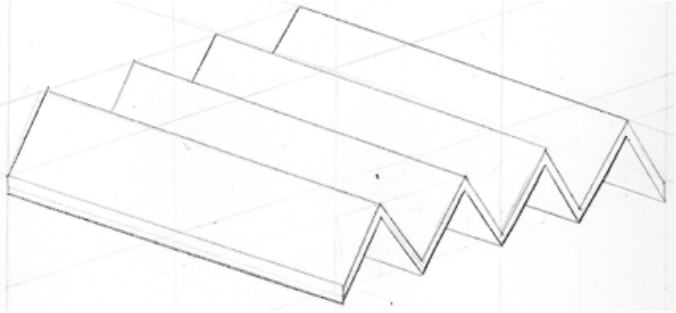

Figure 22: Prismatic folded plate

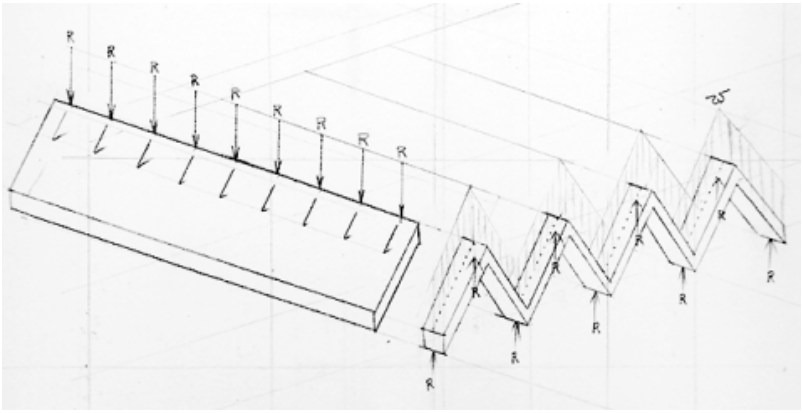

Figure 23: Right: transverse slabs acting s continuous folded beam. Left: longitudinal plates acting as simply supported deep beams

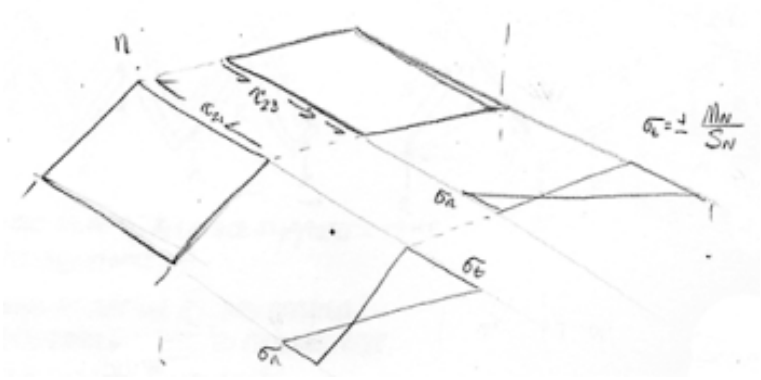

Figure 24: Shear coupling at panel junctions to equalize unbalanced bending stresses

2.6.1 Precedent Folded Timber Panel Structures

The first folded plate systems were proposed in 1924 (Ehlers 1930) and developed further following World War II. The 1963 ASCE "Task Committee Report on Folded Plate Construction" summarized methods of analysis and indicated the popularity of folded plates in modernist architectural aesthetic. Concrete has historically been the material of choice for these structures, given that it can be cast in place, forming rigid connections at the edges of each plate, and exhibits isotropic properties. Design guides for folded plate structures reflect this, and for this reason, most precedent folded timber panel structures are not solid constructions but either timber trusses or beam-and-purlin configurations with plywood sheathing or board cladding (Herzog et al. 2004).

Recent construction provides a two exceptions: one is the Musikprobensaal in Thannhausen, Germany (Figure 25 left), a single-room accordion fold building 20 m deep, with folded 100 mm thick glulam plates spanning its 10 m width (Hensel et al. 2006; Schineis 2004). Folded pairs were prefabricated with mitered and glued edges, and then assembled on site with screws and

additional adhesive and bolted connections at the base (Robeller et al. 2014). The overall geometry of the building allows the plates to act as a series of one-way frame members. The other is the Chapel of St. Loup, Switzerland (Figure 25 right), (Buri & Weinand 2011), of similar size and variation in the fold staggering, whose connections consisted of angled steel strips fastened along joining edges. Architectural research has explored more complex folding timber geometries and methods of assembly, in particular at the University of Stuttgart (IDTKE) (La Magna et al. 2013), and the Ecole Polytechnique Federale de Lausanne (IBOIS) (Weinand 2009; Buri & Weinand 2010; Buri et al. 2011; Robeller et al. 2014; Robeller 2015).

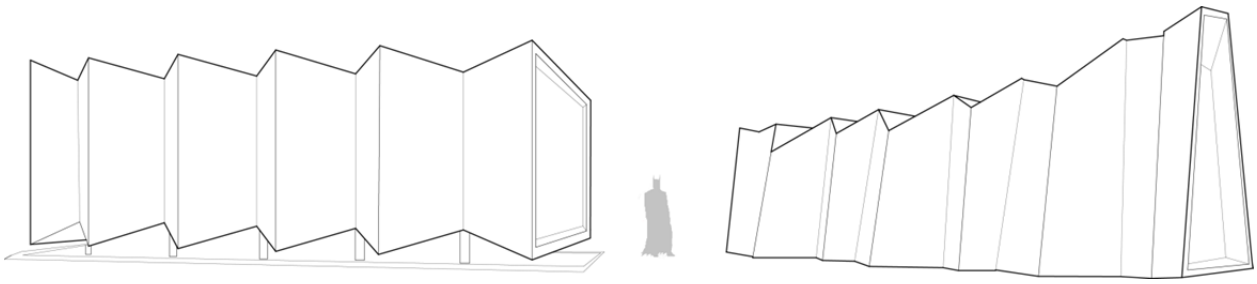

Figure 25: Left: Musikprobensaal. Right: Chapel of St. Loup.

Though non-structural, these pavilions, detailed in Table 1, were designed with a structural mindset and given preliminary structural tests, and therefore provide insight for the design of a larger folded CLT panel structures. This brief survey identifies common strategies and highlights where fabrication and assembly considerations could be addressed further. From a structural perspective these pavilions can be characterized by i) their approach to conceptualizing formal logic in conjunction with structural behaviour, and ii) their approach to connections at panel junctions. In all cases the approach to connection design can be broken into two components. First, how panel edges are milled into mating surfaces—for instance, butted or dovetail-edged.

Secondly, how individual panels are secured, either with mechanical fasteners or adhesively-bonded glued-in plates.

Table 1 Overview of folded timber panel pavilions

Year	Institution	Project	Form	Panels Edges	Connection Method
2002	hiendl_schineis architekten	Thannhausen Musikprobensaal	Prismatic Accordion Fold	Mitered	STS and Polyurethane adhesive
2008	IBOIS, EFPL Lausanne	Origami Folded CLT	Non-Prismatic Fold	Mitred	STS
2009	IBOIS, EFPL Lausanne	Temporary Folded Chapel St. Loup	Non-Prismatic Accordion Fold	Mitred	Steel nail plates
2011	IDTKE, Stuttgart	Biomimetic Pavilion	Cellular Dome	Box Joint	STS to connect Modular Cells
2013	IBOIS, EFPL Lausanne	Curve-Folded CLT	Concave Arched Frame	Box Joint	STS
2014	IDTKE, Stuttgart	Landesgartenschau Exhibition Hall	Hourglass Dome	Box Joint	STS
2015	IBOIS, EFPL Lausanne	Interlocking Folded Timber Plates	Non-Prismatic Fold	Box Joint	Snap-Fit Integral Mechanical Attachment

In agreement with aforementioned folded plate mechanics, studies which considered structural performance conclude that for free-form geometries, fully rigid connections between panels are not necessary but highly influential. Rigid connections at panel edges redistribute bending and load demands, minimize deflections and allow for greater spans and thinner panel sections. (Haasis & Weinand 2014; Tas 2013; Schimek et al. 2012; Buri 2010). In some cases, unglued dovetail joints were used transfer in-plane loads and resist movement through in-plane shear. However, relying solely on geometric configuration to provide pure plate action (La Magna et al.

2013) restricts the global form to Y-fold typologies. Additional STS were still required to provide partial transfer of bending moment between panel elements in free-form arrangements (Krieg & Correa 2014) .

2.7 Doubly-Curved Timber Shells

Conceptually, a gridshell structure effectively introduces regular apertures into continuous thin shells and condenses the shell into a lattice network: the depth required of the resulting linear members increases with the size of the apertures (Harris et al. 2003). Though an individual lath of timber is inherently not a shell, its flexural character allows it to be bent into a curve. Subsequently, a curved timber gridshell may be accomplished by utilizing this material characteristic.

The construction of traditional timber gridshells (Happold & Liddell 1975; Naicu et al. 2014; D'Amico et al. 2014), consists of continuous laths initially laid flat in a loose lattice and then actively bent to provide resistance and achieve the double-curvature form and are thus termed "strained" shells (Adriaenssens, Barnes, et al. 2014). Connections at the nodes must allow the laths to rotate freely in relation to one another during the force-forming process. However, the same rotational freedom necessary for achieving the form becomes a structural disadvantage once the desired curvature has been achieved, as the lattice is unable to transfer diagonal in-plane loads directly. Erection therefore consists of lifting the flat lattice network from internal points with scaffolding and pushing-in from the edges. Then additional diagonal bracing is applied afterwards to provide rigidity against unwanted translation during service. The terminus edge of

the active-bend gridshell is also secured with a tension ring to contain outward hoop thrust. Each lath can be modeled as a beam-column under combined axial and out of plane loading (Figure 26). In this state, deflections and the critical buckling load are controlling factors.

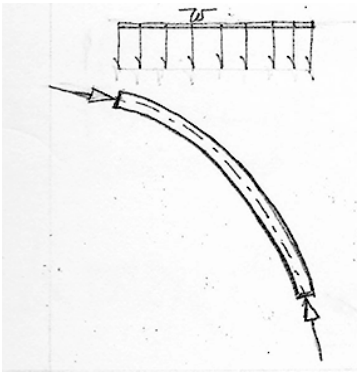

Figure 26: Gridshell lath modeled as simply-supported bi-axial member

Though the first gridshell is considered to be a steel rib elliptic paraboloid roof, designed in 1897 by Russian engineer Vladimir Shukhov (English 2005), German architect Frei Otto was the first to implement the concept in timber (Happold & Liddell 1975) for the Mannheim Multihalle in Germany (1975). At full-scale, design loads would cause a single lattice to fail, yet timber laths deep enough for sufficient stiffness would rupture before achieving the desired curve. Consequently, Arup, the structural engineer for the Mannheim Multihalle, proposed a double lattice of thin laths, overlaid over one another, with slotted, spring-loaded bolts at their intersecting nodes. This general approach was also used for contemporary lattice timber gridshell construction, such as the Downland Gridshell (2002) and the Savill Garden Gridshell (2008), albeit with adjustments made to the node connection design and then erection process (Harris et al. 2004; Harris 2011; Harris & Roynon 2008; Pone et al. 2013).

In an era without 3D modelling software, the process of translating the architectural geometry to numerical values for analysis involved iterations of physical and analytical models and innovative techniques to measure them (Happold & Liddell 1975; Williams 2014). Otto's form-finding process consisted of hanging chain models or soap bubbles sealed in vacuums, which were overlaid with shadow-cast gridlines and stereo-photographed (Otto et al. 1973). Points were hand-plotted and then due to imperfections in the physical model, such as friction between the strings, had to be computationally adjusted before analysis could begin, using one of the first nonlinear computational models. Otto's Essen Pavilion (1957) was also used as a scale model for physical testing. Latter examples of timber gridshells were designed with comparative ease through the use of 3D parametric Grasshopper models.

In contrast, other contemporary timber gridshell examples consist of discretized individual members whose initial curved state is unstrained (Adriaenssens, Barnes, et al. 2014), whose fabrication consists of thin laths are bent over formwork and glued to produce curved, rigid timber composite members. This method in conjunction with parametric modeling permits more freeform geometry, but requires advanced calculation, machining, and proprietary connection detailing not possible without 3D parametric models or CNC fabrication (Jeska & Pascha 2014).

Collaborations between Frei Otto with Japanese architect Shigeru Ban in the 2000s illustrate evolution of the active-bent gridshell type to this discretized type. The lattice of the Metz Pompidou in Paris (2010) consists of an interwoven tri-axial GLT lattice. The GLT chords, too deep to be laid flat and form-found were fabricated with curves and twists, yet relied on LVL spacers fastened between the chords to provide a composite section and served as guides during

construction. The parametric model used to design the Metz Pompidou structure began with a pre-determined global geometry. Structural design, including member dimensions, the curve and twist of each glulam, and the boundary conditions, were manipulated to suit this geometry (Jeska & Pascha 2014).

The parametric model of Nine Bridges Golf Club in South Korea (2010) calculated the minimum surface geometry based on membrane theory with given boundary conditions, projected a grid onto the surface, and then performed dynamic relaxation to locate nodes. This resulted in a roof which sinks into basket-like, hollow, hyperbolic paraboloid columns, consisting of radially woven glulam chords. Local fire code did not allow exposed steel connections. As such, each glulam chord therefore consisted of two halved beams, resulting in member-integral nodal connections, achieved by means of interlocking scarf and halving joints at the beam intersections.

Significantly, a similar approach of forming composite sections from layered members was used for the Elefantenhaus (2014) in Zurich using CLT panels. Like parametric modelling, CNC fabrication was essential to the project, not only in the production of the glulam curves and their joint geometries, but also the assembly templates, which were cut from CLT and used to ensure precision prefabrication of the structure's 32 sections (Jeska & Pascha 2014). The parametric model, using a dynamically-relaxed funicular form, generated the global geometry as well as the scaffolding and fabrication templates, for an 80m diameter and 18m high dome with an off-centre. An irregular network was projected over the surface to define the outlines of 271 polygonal apertures. The shell consists of three layers of 3-ply CLT, with each layer turned 60°

with respect to the next (Kuebler 2014). Each panel was fabricated with single curvature and then routed at its narrow ends with half-recessed tenon connections to form continuous strips. Though the final design was to have considerable number of apertures cut into the shell, the bottom layers of CLT were assembled blind to ensure geometry and stability during construction. To form a composite section, panel layers were secured together with crossed pairs of 850 mm long, 13 mm diameter STS, inserted at 45° to the normal surface. However, the mechanically connected composite sections are only 30% as stiff as same section with rigid connections, ie adhesive (Jeska & Pascha 2014).

2.8 Discussion

It is evident that advances in fabrication technologies, research on CLT, proprietary connections, within the realm of timber engineering, and computational modeling in the fields of architecture and design, can be combined through collaboration to produce timber structures with unprecedented geometry and innovation. Such periodic alignments are rare, but integrated models can provide the means to fostering more such design relationships and propel timber structures even further.

The design and structural behaviour of these example plate and shell structures provide insight to how similar forms can be attained with CLT panels. Precedent folded timber panel structures, though made of plywood, address similar design concerns which would arise when using full-scale CLT panels. As CLT panel design methods can address both transverse and longitudinal loading capacities, and recalling the structural behaviour of folded plates, such folded plate

forms are possible in CLT so long as the edge connections properly transfer shear to adjacent plates: here STS provide a strong yet versatile solution. Meanwhile, progression in gridshell design points towards the potential of a doubly curved CLT panel whose surface continuity would provide its own shear resistance without additional diagonal bracing or clamping connections to form composite sections.

Folded CLT and doubly curved CLT panels are without precedent, however, and hence their behaviour in these configurations is not understood. Digitally integrated models allow structural engineers to engage more easily with these types of complex geometries, yet implementation requires known values of material properties and behaviours to inform the process. Developing definitions for CLT panels and STS connections within the parametric model is therefore an important first step towards wider implementation and of great concern for this research. In all the example structures the key to their design has been detailing, to the extent that the connections should perhaps be considered before while the form is still being determined in the preliminary design stage. Embedding connection design considerations into the generative architectural scripts is thus also approached in this research. All the more reason for architects and engineers to collaborate early and adopt integrated models. Chapter 3 details introductory understanding of the software involved for its setup, operation, and the tools it provides to proceed forward in this manner.

Chapter 3: Developing Integrated Parametric Models

3.1 Software Concept

No ‘generic’ process to develop an integrated parametric model exists and specific forms and/or projects have applied different processes. Figure 27 and Figure 28 illustrate the software and the steps associated with each in an integrated modelling process as it was applied within this thesis research. Each will be described in more detail in the subsequent sub-chapters, but their relationship is broadly sketched here for conceptual reference.

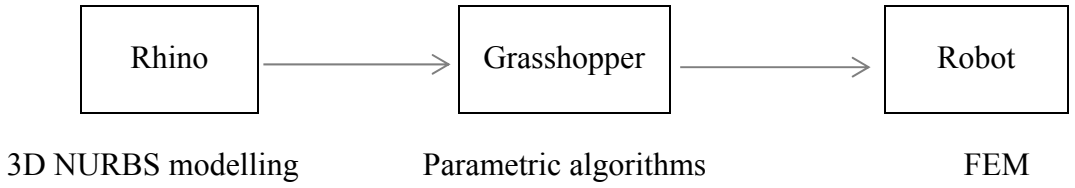

Figure 27: Primary software for integrated models

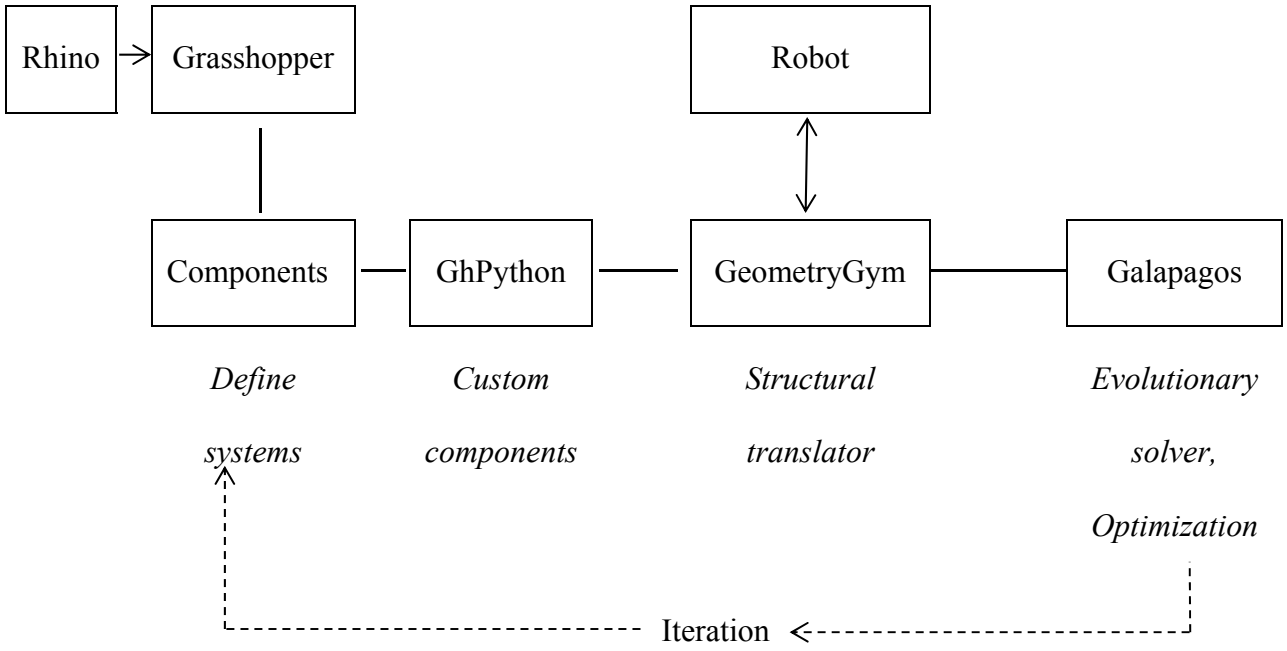

Figure 28: Flowchart showing software hierarchy and corresponding operations

Grasshopper reproduces Rhino operations as algorithms in a visual programming interface. GeometryGym and Galapagos are types of third-party plugins nested within Grasshopper. The former translates the Grasshopper geometry into structural elements for analysis by exterior FEM software, and then re-interprets the results back into Grasshopper data. Galapagos is a genetic evolutionary solver which can adjust input parameters for a target output: for example, changing a parametric beam depth to meet deflection criteria. The analysis and model adjustment repeat iteratively until the difference between the result and the target value is deemed sufficiently negligible.

3.2 Rhinoceros and Grasshopper

Rhinoceros3D ("Rhino") (Robert McNeel & Associates 2014b) is a 3D modeling software well suited for complex geometry and serves as the primary modeling platform. It operates using is effective on its own and originated as an industrial design software in 1994. Users can exploit the NURBS curve algorithms by means of the Rhino plugin Grasshopper (Robert McNeel & Associates 2015). What distinguishes Rhino and Grasshopper from other parametric software platforms is its visual programming interface and large library of free plug-ins.

Grasshopper's user interface presents scripting operations visually as "components". Like functions, the majority of components take one or more inputs (left side of the component), performs an operation with them, and delivers one or more outputs (right side of the component). A Grasshopper script consists of a network of components connected by their inputs and outputs.

A cylinder whose height and radius are equal provides a good example of how geometry is generated in Grasshopper. First, abstracting the algorithm for generating a cylinder might go like this: A cylinder has a circle section along a linear axis. The circle has a centre and a radius, and the axis line is a vector normal to the centre point with the same magnitude of the radius. Here the numerical values of point coordinates and the radius are geometric elements whose values cannot be broken into other operations and are therefore called the parameters, or inputs. All else is generated in relation to these values.

Hence, like the parametric apple drawing, composing a parametric Grasshopper script that defines a cylinder (Figure 29) begins with inputs which define the centre point and the radius

magnitude and produces resultant geometry (Figure 30). By observation, the sequence of operations in the Grasshopper script itself, like individual components, can be classified as inputs, outputs, and operations.

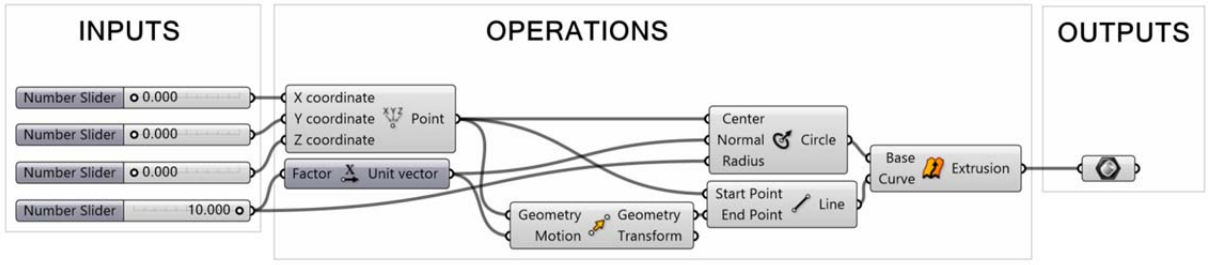

Figure 29: Grasshopper script for a parametric cylinder

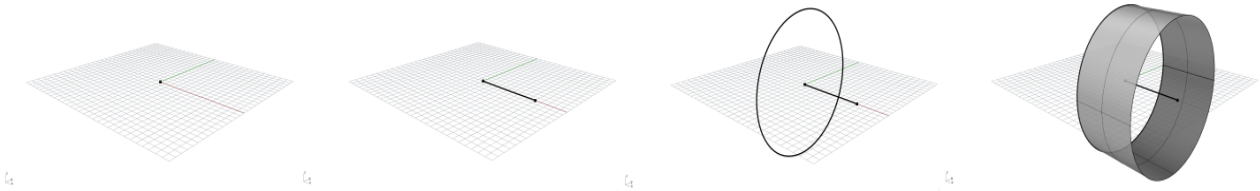

Figure 30: Rhino display progression of Grasshopper script

3.3 Third-Party Plugins

As-built, Rhino and Grasshopper simply manipulate numbers, generating geometry, and have a finite set of built-in default operations for doing so. Third-party plugins provide a broad range of additional versatility and flexibility which, in attrition to the visual programming interface, distinguish Grasshopper from other parametric software.

Key to Grasshopper's power is the manner in which its platform software Rhino was built. Robert McNeel and Associates constructed the program with Microsoft's DotNET software framework, which provides language interoperability, a large framework class library, and

importantly, is partially open-source. To encourage third-party customization of both Rhino and Grasshopper, its Software Development Kit (SDK), which included the Application Programming Interface (API) necessary for third-party component development, was made freely available as RhinoCommon DotNET SDK. As a result, plugins from multiple disciplines have proliferated. There are more than 200 available at present, which can be classified into functional types. Table 2 shows some common examples, while only those plug-ins listed in Table 3 were used for this research.

3.3.1 Python-scripted Customized Components

GhPython (Robert McNeel & Associates 2014a) allows a user to define their own component using the scripting language Python. On its own GhPython does nothing, but it can be valuable for defining a characteristic for which no available component can describe. Similar plugins exist for C# and Visual Basic, but as only Python is free to use and compile, GhPython was selected for this research.

Table 2: Types of Grasshopper plugins

Type	Function	Examples
Programmable	allow user to code custom components within Grasshopper	GhPython
Manipulator	creation and manipulation of data or geometry	Weaverbird (weave patterns); lunchbox (general); elk (GIS Topology); SmartForm (form-finding and rationalization)
Simulators:	either of natural phenomena, energy usage, or the fabrication process using animation	kangaroo (physics); ladybug+honeybee (environmental); RhinoVAULT (funicular form finding)
Interpreter	allow Grasshopper to interact with other proprietary software	GeometryGym (Revit, FEM software, IFC); Grevit (Revit); beaver (Hundegger); woodpecker (Kuka robots); firefly (Arduino); quokka (Kinect); 3DPrintButton
Solver	runs complex algorithms and calculations	Octopus (genetic solver), kangaroo (dynamic relaxation); goat (genetic solver)

Table 3: Grasshopper plugins used to created integrated models

Plug-In	Description
GhPython	Codes custom components with Python
Weaverbird	Data management and manipulation to generate geometry
GeometryGym	Interoperability with FEM software
Galapagos	Parametric optimization using genetic algorithms

3.4 Integration with FEM Analysis

In 2005, Australian civil engineer Jon Mirtschin was introduced to Rhino and saw a need to facilitate communication within this digital workflow (Mirtschin 2011). Mirtschin has since developed his custom code for interoperability into GeometryGym, a suite of Grasshopper plug-ins (Mirtschin 2015); some sets are directed towards BIM platforms, while others sets are

specific to different FEM programs (Table 4). The "ggRobot" suite provides the live information exchange with Robot from within Grasshopper.

Table 4: Software supported by GeometryGym

Model Type	Interoperable Software
BIM	Revit, Navisworks, Archicad
FEM Structural Analysis	SAP, ETABS, Robot, GSA Oasys, Tekla, Sofistik, Strand, Spaceglass, gbXML

No other openly-available plugins are available which will provide the same interoperability with FEM software, though a component creator like GhPython could be used to create something similar. Autodesk has recently released a version of its own visual parametric interface not unlike Grasshopper called Dynamo, which communicates directly with Revit. As integration with FEM structural analysis, rather than BIM model generation, is the objective, Dynamo was not considered in this research, though future versions of Dynamo may communicate directly with Robot in the future.

GeometryGym functions using a combination of syntax parsing and API interaction to exchange models. In the case of Robot, GeometryGym generates an .rtd file by converting the data in Grasshopper to .rtd script format and uses the API to initialize or modify Robot from within Grasshopper. Prior familiarity with direct usage of the FEM software on the engineer's part is still necessary, as a suite of GeometryGym components follow the same terminology and modelling procedure as the FE software it communicates with.

The approach for generating a structure with ggRobot is as follows: Recalling that a Grasshopper model script can be organized into Inputs, Operations, and Outputs, GeometryGym provides both Operations-type and Output-type components. Operations-type components interpret the reference geometry into the text of a Robot structural file; this includes defining materials, sections, and load cases. The fully defined model is given to another ggRobot component which initializes Robot and returns the analysis results. Output-type components re-interpret the Robot results back into Grasshopper script data for further interpretation. Figure 31 illustrates the progression of the parametric concept to full script for a simply supported beam with a point load at mid-span.

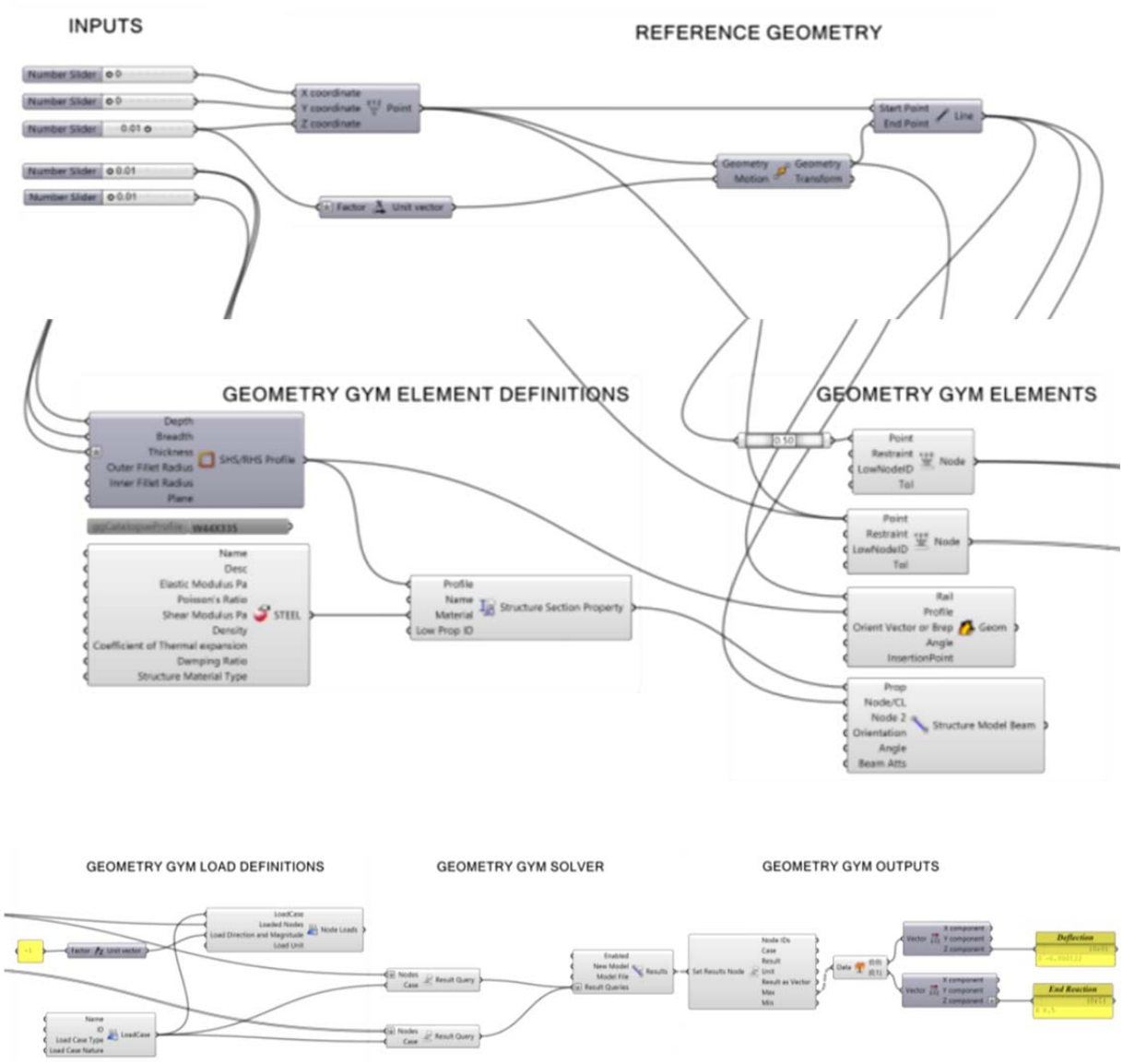

Figure 31: Grasshopper script defining a simply supported beam using GeometryGym

3.5 Genetic Algorithm Evolutionary Solvers for Optimization

Genetic Algorithms (GA) are a subset search algorithms, used both in computational and natural sciences, which use Darwinian evolutionary mechanics of natural selection and evolution,

applied to a mathematic problem space (Williams 2014). These algorithms are valuable for solving complex, non-differential problems with interconnected sub systems and multiple potential solutions, whose parameters are continuous, discrete, and/or categorical (ie, sizing members in a multi-member structure to satisfy structural and cost criteria). A detailed extrapolation of the relevant formulae is beyond the scope of this research, but their general operation is as follows. Given a system, the parameters, target performance criteria, and tolerance (how closely a solution needs to match a target value) must be identified.

- Initialization: By assigning input parameter values randomly the algorithm produces an initial set of candidate potential solutions.
- Operation: Each candidate is run through the defined system and scored based on the proximity of their results to the target criteria.
- Selection: A best fit selection operation orders the candidates by score and discard the lower half. The remaining candidates are cross-propagated to produce the next set of potential candidates.
- Iteration: Operation and selection are repeated until the target criteria values are met within the threshold of the tolerance value.
- Termination: Notably, these algorithms do not produce a unique solution but a set of satisfactory candidates (Coelho et al 2014).

Grasshopper has a built-in Genetic Solver Optimization (GSO) component called Galapagos, though other third-party GSO components are available which can handle larger sets of parameters and provide different levels of user-interaction with the process.

Chapter 4: Integrated Parametric Modelling of Folded CLT Plates

4.1 Approach

The integrated model as described in chapter 3 was first applied to the conceptual design of a folded CLT panel wall. For a folded panel wall, the architects required geometric bounds for initial compositions, but had no reference guide for permissible dimensions. The dimensions of building elements and fabrication machines dictate what geometry is feasible and need to be observed at the outset.

To inform the architectural design process, the structural objective was to determine the material, joint, and fabrication requirements which would restrain the model dimensions, specifically by investigating: i) the maximum allowable spans for a range of fold angles in relation to material deflection behaviour, ii) the minimum allowable lengths through a study of the connection spacing requirements of self-tapping screws, and iii) evaluating the performance of triangular CLT panels by modeling the material properties of cross-grain CLT panels. These bounds were then introduced to the shared Grasshopper model as scripted definitions.

Afterwards, though not indicative of the behaviour of a full-scale CLT structure, a small-scale plywood prototype required applying the same integrated structural Grasshopper definition that would be applied to a full-scale CLT structure. Prototype fabrication also introduced a fourth constraint based on available CNC machining tolerances that dictated the range of allowable fold angles. In doing so the prototype would not only help identify fabrication limitations not evident

when using digital design software, but also serve to test the logic of the integrated structural scripts.

4.2 Possible Spans and Fold Angles

CLT is a composite anisotropic material, with different flexural behaviour from a uniform anisotropic material which was discussed in Chapter 2. The procedure to determine the maximum permissible span of a folded CLT beam with varying fold angle consisted of three steps:

- 1) Scripting Shear Analogy using Python as a GhPython component
- 2) Modeling a loaded CLT panel in Grasshopper using the Shear Analogy component
- 3) Model a folded panel as two hinged CLT panels, allowing fold angle and span to vary

4.2.1 Scripting Shear Analogy into a GhPython Component

The material properties of a CLT panel had to be defined for the Grasshopper model. GeometryGym provides an orthotropic material definition component for modeling timber in Robot (Figure 32) which requires inputs for homogenized orthotropic moduli values, and implies that Robot assumes a uniform timber section: there is no composite material definition component. Input elastic and shear moduli would need to be derived from effective elastic and shear stiffness values for CLT using one of the analytical methods described in Chapter 2.1.3.

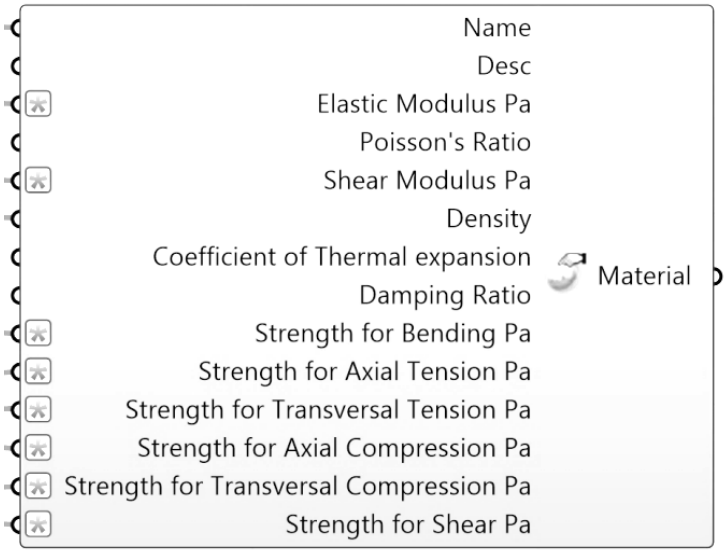

Figure 32: Timber material definition component in ggRobot

Shear analogy was selected to model the CLT material properties, as the method permits the easiest manipulation of material angles within the composite layup. The model was initially scripted in Python and assumed CLT panels with the following characteristics:

- Individual laths have zero cross-grain, $\alpha = 0°$
- Each lamination is layered orthogonally with respect to adjacent lamination. The lamina angle of rotation, $\beta = 90°$, is constant.
- Panels have odd-numbered layups of lamina, with symmetric layering about the middle layer.

The Python script allows a panel to be defined by the number of lamina, n, and the cross-grain angle, α, of the exterior face laminations of a CLT panel, with the implication that alternating laminations would have cross-grain angles of $\alpha + \beta$.

In the analytical procedures for designing CLT, the effective moment of inertia, I_{eff}, of a CLT panel is simply the reduction of $\frac{(EI)_{eff}}{E}$. This implies that effective stiffness values can be

manipulated into equivalent effective bending moduli E_{eff} and effective shear moduli G_{eff} by dividing the effective stiffness values by the appropriate geometric property.

$$E_{eff} = \frac{(EI)_{eff}}{I} \tag{14}$$

$$G_{eff} = \frac{(GA)_{eff}}{A} \tag{15}$$

The Python code for the shear analogy was augmented accordingly to return E_{eff} and G_{eff} values and then placed into a custom Grasshopper component (Figure 33) using the GhPython plug-in. Figure 33 shows that inputs such as elastic modulus, shear modulus, lamina thickness, total number of lamina, and the reference face angle, were up to the user to define. In this research, material properties were taken from the CSA O86 (2009) Wood Properties Table for No. 2 Douglas Fir-Larch.

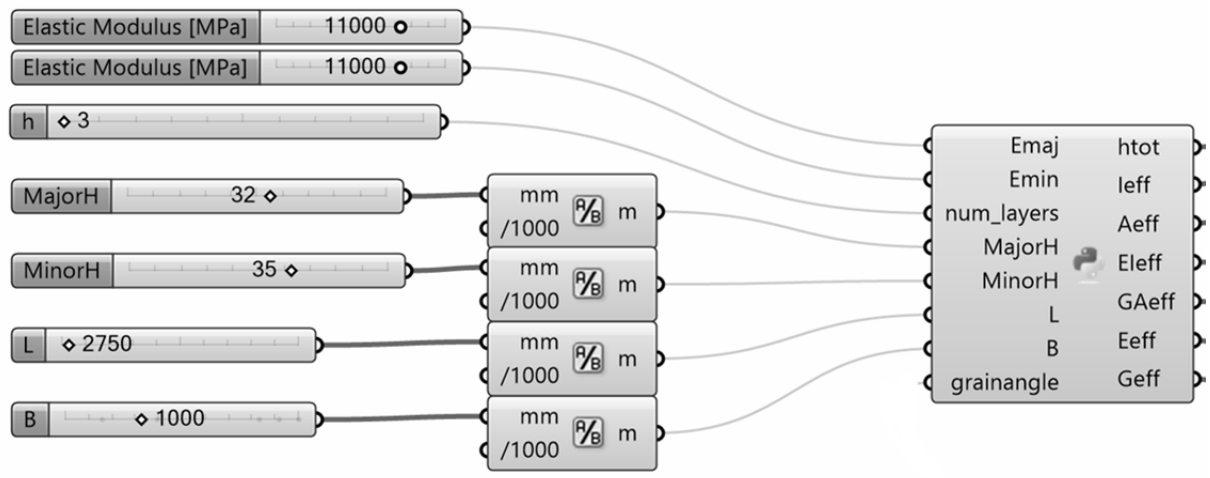

Figure 33: Shear Analogy material definition component

4.2.2 Modeling a CLT Panel Defined with Shear Analogy in Grasshopper

Once the CLT material component was completed, a 1 m x 2.75 m 3-ply CLT panel was modeled in Grasshopper and integrated with Robot using GeometryGym. This panel was assigned simple supports and a cross-grain angle $\alpha = 0°$, ie, aligning the longitudinal axis of the exterior laminations with the span. For the uniformly distributed loads defined in Table 5, the integrated model predicted deflections which agreed with predictions given by the shear analogy method.

Table 5: Generic area loads

Self-Weight	Misc. Dead	Live Load	Serviceability Load Case
0.51 kN/m^2	0.5 kN/m^2	1.0 kN/m^2	2.01 kN/m^2

4.2.3 Varying Fold Angle to Determine Maximum Span

At this point, the panel was tilted about its long edge and mirrored, producing a folded CLT beam. The seam of the fold was modeled as a continuous hinge connection. Fold angle θ_{fold} ranged between 0° to 180° in 15° increments. For each fold angle increment, under the same uniformly distributed area loads, the panel lengths were allowed to vary parametrically in order to determine the maximum possible span for each fold which would satisfy L/300 serviceability criteria. Based on the model predictions, Figure 34 shows the maximum spans possible if CLT panels could be laminated continuously in the longitudinal direction, as glulam can be. Table 6 gives numerical values.

Figure 34: Relationship between fold angle and beam span

Table 6: Maximum permissible span for a folded CLT panel by fold angle

Fold Angle θ_f	0°	15°	30°	45°	60°	75°	90°	105°	120°	135°	150°	165°	180°
Max Span [m]	49.0	40.7	40.2	38.8	36.1	33.0	29.7	28.0	24.5	22.0	15.4	10.1	4.4

4.3 Minimum Panel Dimensions and Connection Design

Having defined a material definition component for CLT and determined a Grasshopper script to model span as a function of deflection due to material behaviour, the Grasshopper model needed to be constrained from producing panel geometries which would be too small to contain a sufficient number of connections to other panels. In addition, fastener spacing requirements vary by connection system and loading direction, with parallel-to-grain tensile loading being the least

desirable. Subsequently, a Grasshopper script definition for minimum panel dimensions could be based on spacing requirements for tensile loading for a given connection system.

The geometry of joining edges dictates which connection systems can be applied to them. Sharp knife-edges of the folds could only be accomplished with mitred edges. The sloping surfaces of the mitred edges rendered interlocking clip connectors incompatible. Either the screws would protrude from the panel surfaces or the clips would not intersect. Alternatively, STS provide a high-capacity connection which can also be modified to accommodate angled panels, so long as screws are not inserted into the end grain of a lamination. Crossed pairs of screws provide higher resistance and can accommodate reverse loading. In this manner, the connection system was rationalized around the geometric limitations imposed by the geometry and STS were selected as the reference connection system for determining minimum panel dimensions. The generic rationalized parametric STS schedule is shown in Figure 35; it was derived as follows:

Spacing requirements for STS, as detailed in the product Approval CCMC 13677 R and described in Chapter 2.3, are given in multiples of screw diameter d, and vary with type of STS and type of wood product, but can be generalized. Panel thickness, h, is used to dictate the maximum allowable screw diameter unit as not more than $h/10$: conversely, for a range of available screw sizes, a CLT panel must have a minimum screw penetration, $l_p = 10\ d$, and so must be at least $10\ d$ thick.

Concerning panels with unknown orientations or loading, an edge distance $e_{1t,}$ for worst-case tensile loading is required at the terminus of all edges. Thereafter minimum row spacing, $e_{1,}$ is needed between screws in a line, with an additional gap, $e_{x,}$ to separate the shafts of crossed

screw pairs. According to the product Approval, all connections using fully threaded STS need a minimum of 2 screws, while all connections with partially-threaded screws need a minimum of 3. Complying with the latter requirement, this equates to a minimum edge length d_{min} of $2e_{1t} + 2e_1$. STS passing through the mitered edge must navigate both panel face (p) and panel edge (e) spacing requirements, which are synthetized together in Figure 35 and whose values are given in in units of d.

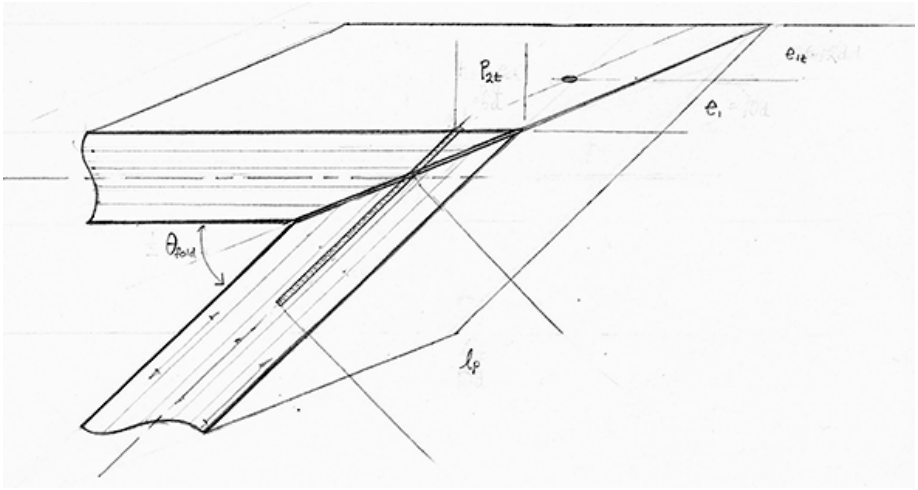

p_{2t}	l_f	e_{1t}	e_1	e_x	d_{min}
6 d	10 d	12 d	10 d	1.5 d	$= 2e_{1t} + 2e_1 + 3e_x = 48.5$ d

Figure 35: STS spacing requirements for CLT with mitered edges

The geometry of triangular panels presents two additional spacing conflicts which need to be addressed. First, the tapering faces may cause screws to protrude from the opposite side, (the problem is shown in Figure 36).

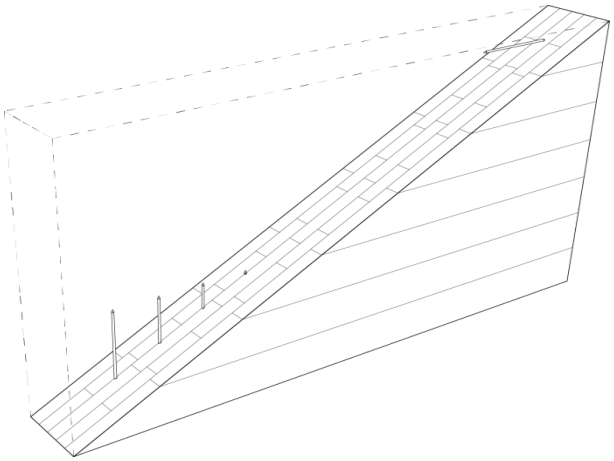

Figure 36: Standard STS spacing requirements do not anticipate acutely angled panels

As such, the tension-loaded edge distance e_{1t} is replaced with *e*' (Figure 37), which is the larger of e_{1t} and the length of the screw l_s. Similarly, the tension-loaded edge distance for the panel face, p_{1t}, is replaced with *p'*, the larger of p_{it} and l_s. These *p* values ensure that any apertures cut into a panel will be set deep enough into the panel to prevent a screw tear-out failure.

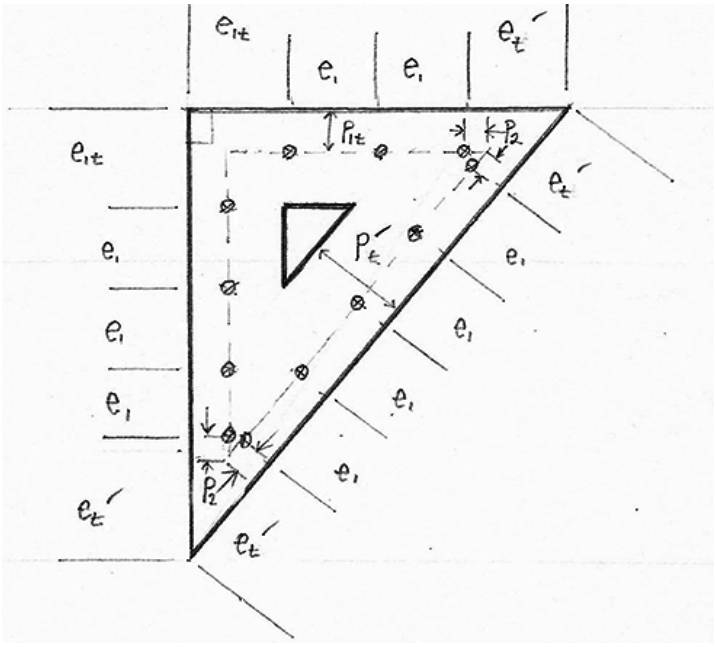

Figure 37: Parametric connection-spacing rationale

Additionally, based on the geometric principles of a triangle, the acuteness of the interior angles, ϑ, influences the length of adjacent edges. Therefore ϑ also needed to be constrained in relation to d_{min}, such that minimum allowable triangle angle, ϑ_{min}, can be governed by Equation (16.

$$\theta_{min} = \tan^{-1}\frac{2l_s}{d_{min}} \tag{16}$$

For triangular panels which satisfy these minimum dimension constraints, connections can be located parametrically as follows: triangle edges are first offset into the face of the panel by *e'* (Figure 38). If a circle is circumscribed about the apex points at the corners of the offset lines, then the points of tangency with the panel edges are the first and final connection points along each edge. The remaining edge distance between them is dissected by the row spacing distance *s* into potential connection point locations (Figure 37). From this list any set could be isolated according to a variable frequency. By calculating the unit capacity for a pair of crossed screw connections, the frequency of connections along each panel edge is then adjusted in response to static analysis performed in Robot. When this process is reversed within Grasshopper, the spacing requirements for any connection type can be used as the basis for propagating the geometry of the whole.

4.4 Effective Stiffness of CLT Panels with Cross-Grain

Another consequence of triangular panels is the effect of cross-grain angle on the material behaviour, in which all lamina would experience the mixture of bending and shear described in Chapter 2.1.4. In a multi-way spanning slab, the one-way behaviour of the weakest loading

direction will control the panel design (Gagnon & Pirvu 2011). Present design guidelines assume that this is at a face angle $\theta = 90°$ (Gagnon & Pirvu 2011; Structurlam 2014) yet prior research on in-plane loading of cross grain CLT (Pearson et al. 2012; Nakashima et al. 2012) suggests that intermediate cross grain angles will affect stiffness properties and should be considered for out-of-plane flexural response. To identify the critical angle which would produce the largest out-of-plane deflection, this research combines Hankinson's Equation with the Shear Analogy method to determine the stiffness properties of CLT at any cross-grain angle.

4.4.1 Comparing Analytical Methods

First an analytical study was needed to develop a baseline model for the one-way behaviour of a rectangular CLT panel with cross-grain. The largest available Structurlam® 3-ply CLT panel is 3 m by 12.2 m and therefore may be inscribed with a 3 m circle: within this circle a smaller 1 m by 2.75 m panel can be cut with any cross-angle orientation (Figure 38).

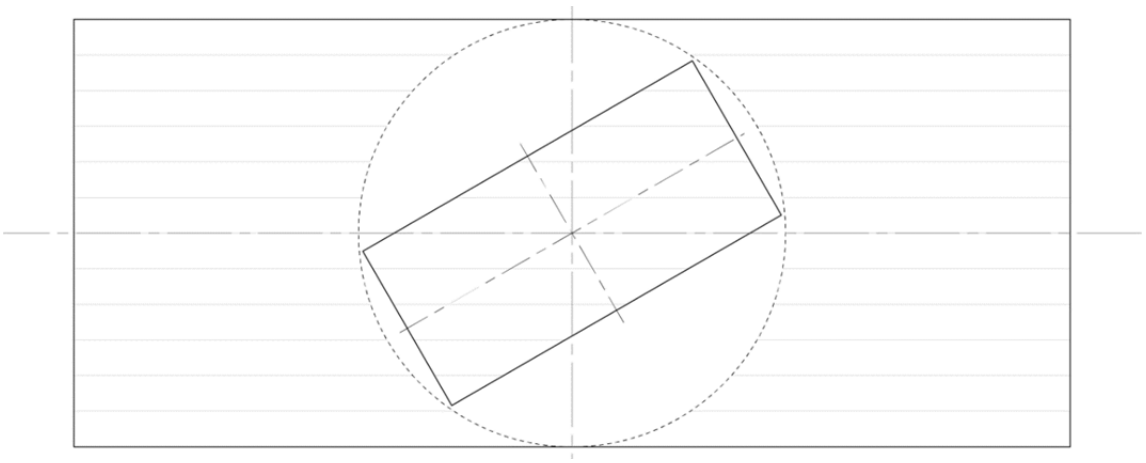

Figure 38: Diagram of CLT panel with inscribed, rotated sample panel

For this analytical study and comparison, the panel was assumed simply supported on its shorter ends, given the uniformly distributed area loads from Table 7, and then assigned cross-grain angle values $0° \leq \alpha \leq 90°$ in 15° increments.

Figure 39 compares predicted stiffness values for a 3-ply CLT panel made the proposed hybridized Hankinson-Shear Analogy model and Hankinson's equation alone where Shear Analogy has been used to provide only the parallel and perpendicular reference stiffness values. If shear analogy is taken as an accurate predictor of panel flexure and deformation at 0° and 90° cross-grain angle orientations (Gagnon & Pirvu 2011), then results produced Hankinson's equation alone are un-conservative at those angles, and so questionable across the intermediate angles. The modified Hankinson-Shear Analogy method reproduces expected 0° and 90° stiffness values for 3-ply CLT and shows increasing stiffness from a mid 60° angle and higher. The effect of this increased stiffness is a corresponding increase in flexural response across the intermediate angles. The combined Hankinson-Shear Analogy model was then also applied to 5 and 7-layer CLT panels, see Figure 40.

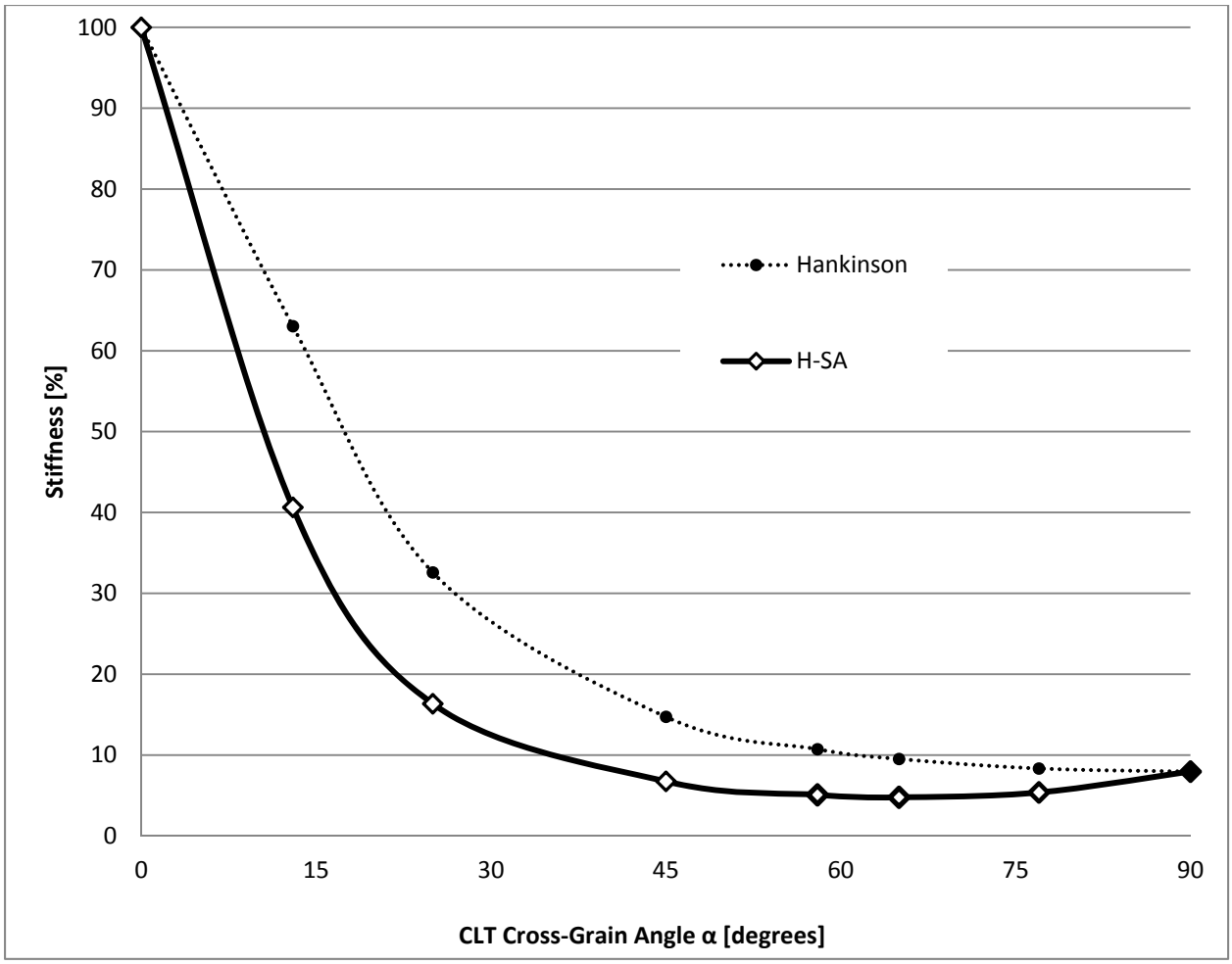

Figure 39: Comparison of Analytical Methods for Cross-Grain 3-ply CLT, Normalized for Shear Analogy Stiffness at α = 0°

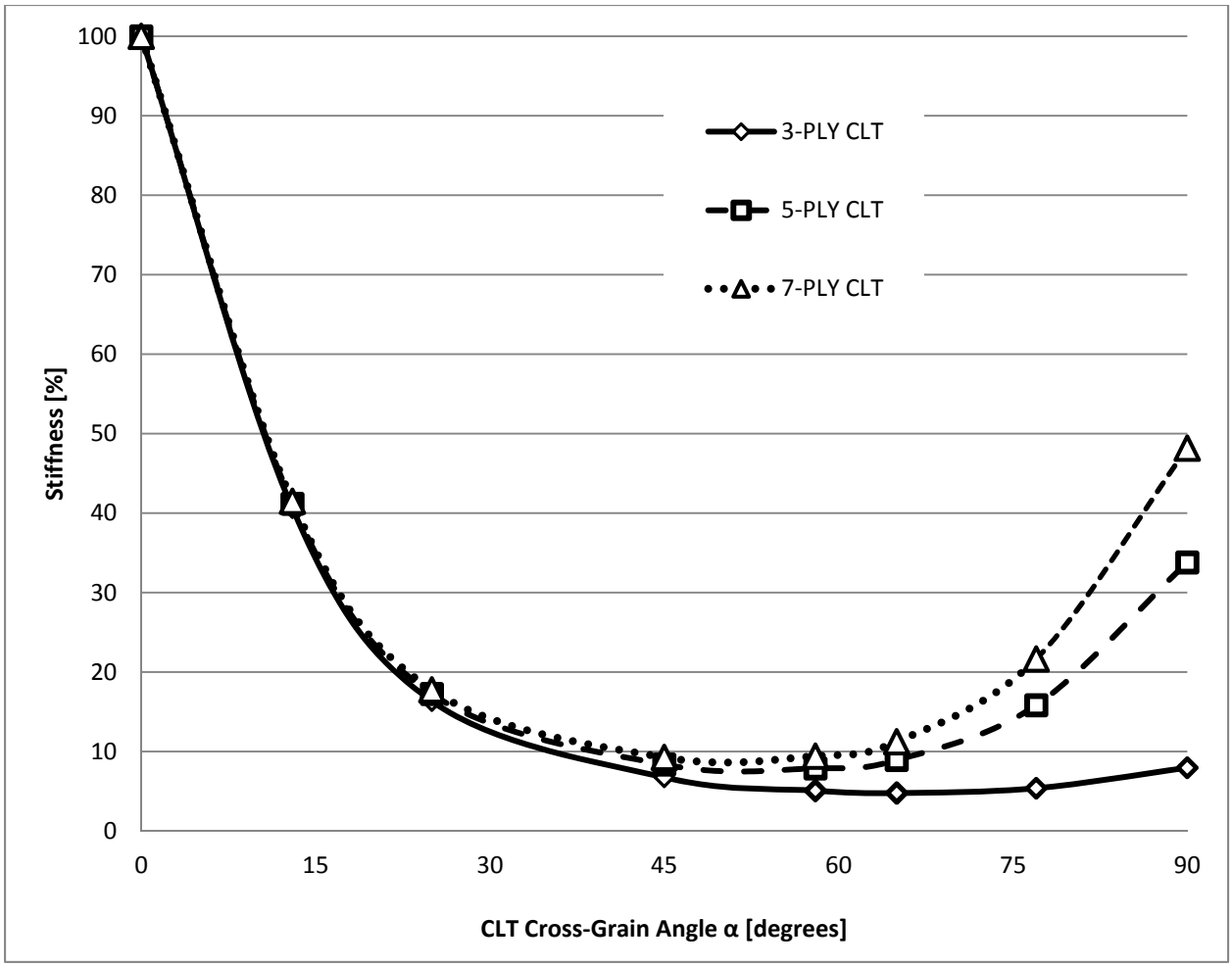

Figure 40: Normalized Cross-Grain Deflection of 3, 5, and 7-layer CLT per Hankinson-Shear Analogy

Figure 40 shows the panel stiffness values normalized for their respective maximum stiffness values at $\alpha = 0°$. The effect of cross-grain effect is that the thicker 5 and 7-layer panels loose less stiffness over the interim cross-grain angles than the 3-layer CLT, and see a greater increase in stiffness between 60° and 90°. However, as shown in Figure 41, the actual cross-grain stiffness values of the thicker panels are much higher than the 3-layer CLT panel. Stiffness being inversely related to deflection, the 5 and 7-layer CLT panels have higher stiffness values and so

exhibit a more muted flexural response (Figure 42) than the 3-layer CLT panels over the cross-grain angles, when 1 x 2.75 m panels are subjected to a 1 kN mid-span point load.

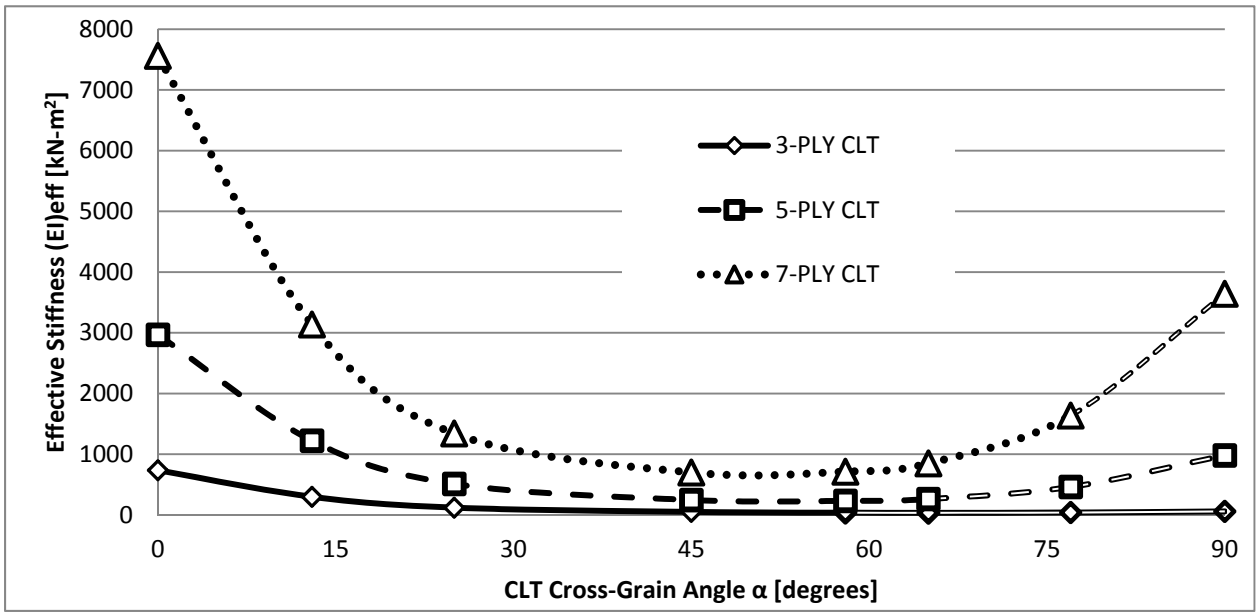

Figure 41: Calculated Cross-Grain Effective Stiffness Values for 3, 5, and 7-Layer CLT per Hankinson-Shear Analogy

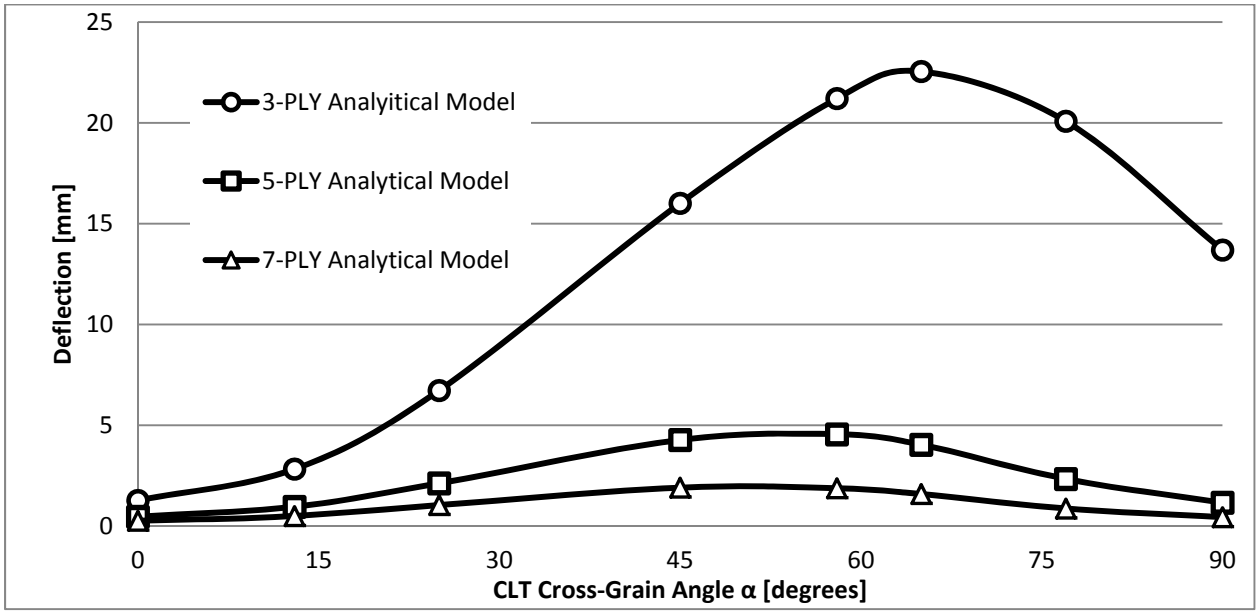

Figure 42: Comparing Analytical and Integrated Model Cross-Grain Mid-Span Deflections

4.4.2 Implementation in Grasshopper

The combined Hankinson-Shear Analogy method was coded into the custom GhPython material definition component (Figure 43).

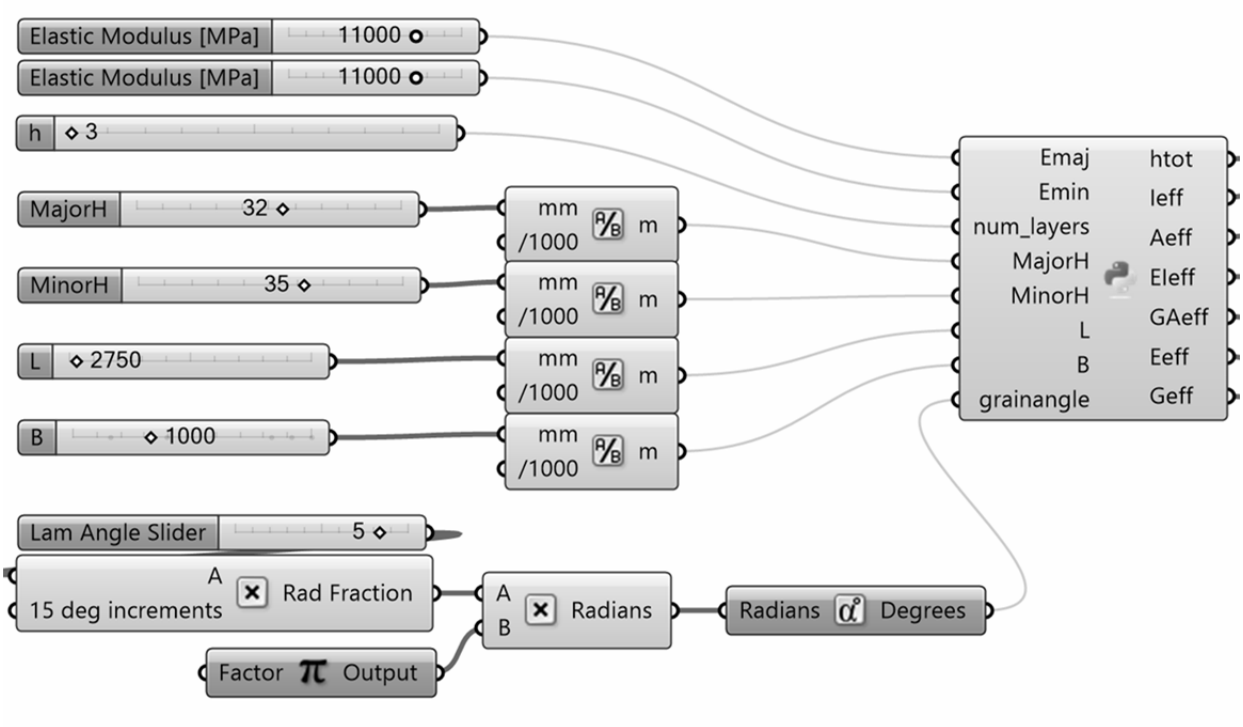

Figure 43: Hankinson-Shear Analogy material definition component with user-defined cross-grain angle input

Within Grasshopper, the same 1 m x 2.75 m 3-layer CLT panel was set on simple supports, given the same loading, and again assigned cross-grain angle values $0° \leq \alpha \leq 90°$ in 15° increments. The stiffness results calculated from Robot are plotted and compared to the analytical predictions in Figure 44 and for 5 and 7-layer CLT panels as well in Figure 45, which shows minor disagreement between the two, but good congruency.

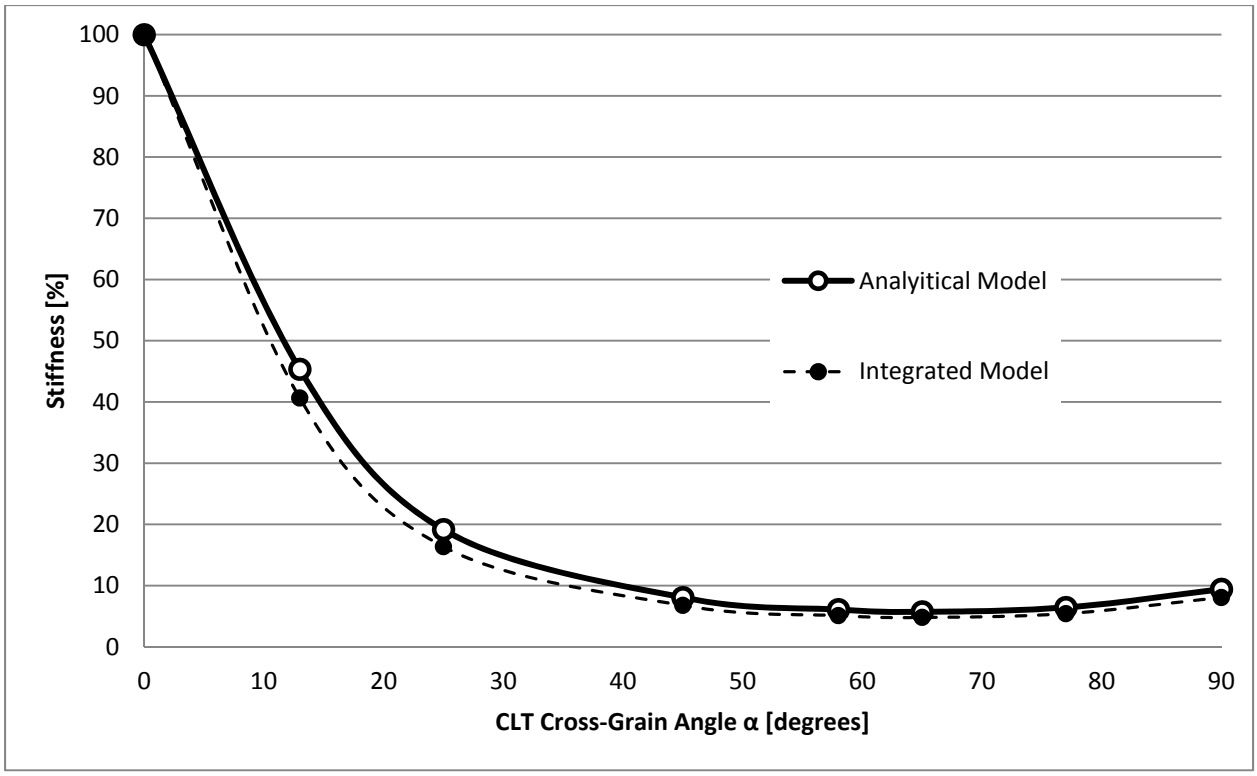

Figure 44: Comparison of Analytical and Computational Modelling of Cross-Grain CLT Stiffness

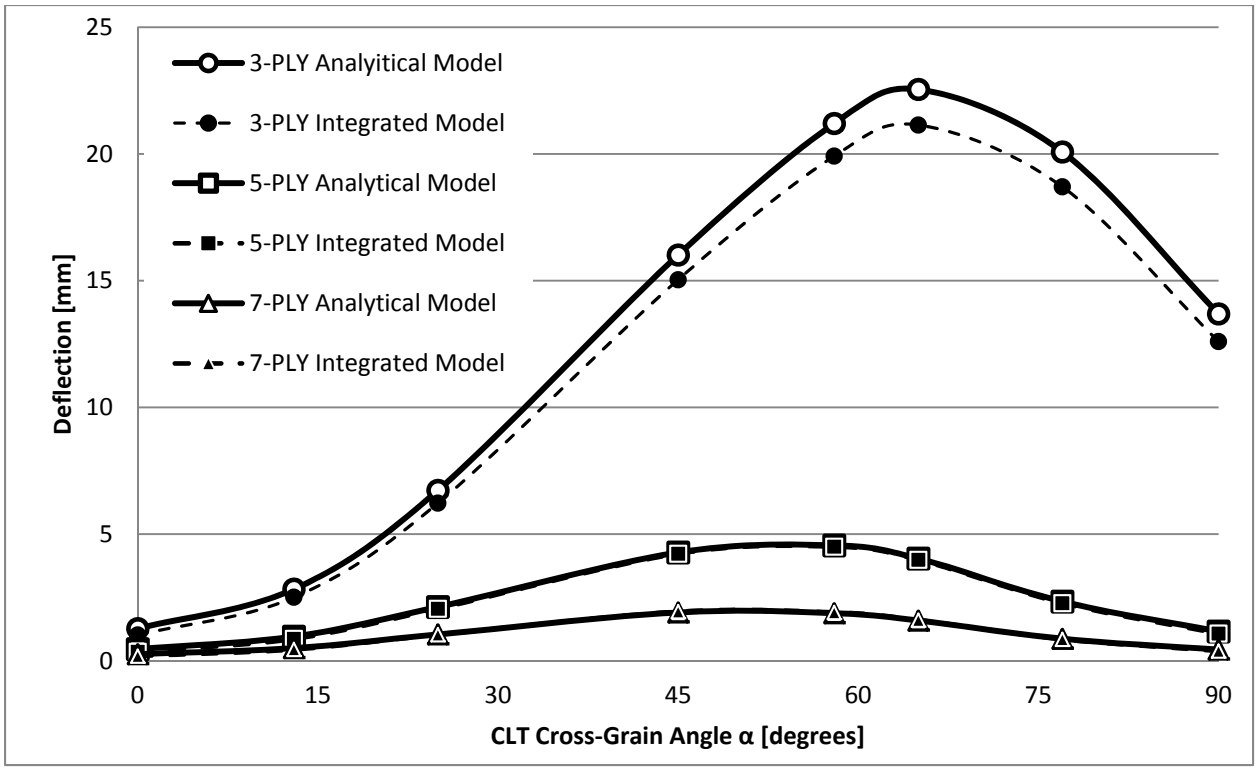

Figure 45: Comparison of Analytical and Computational Modelling of Cross-Grain CLT Deflection

Initially, the evolutionary solver Galapagos was used in an attempt to reverse-calculate homogeneous moduli. By setting the analytical prediction deflection value as a target and the elastic modulus as a parameter, the component was instructed to iteratively back-calculate corresponding equivalent elastic moduli which would produce the desired response. Doing so underscored the material modeling limitations of GeometryGym's orthotropic material definition component. The bell-shaped deflection plot is only reproducible for individually defined panels with their own specified cross-angle.

GeometryGym does not provide a composite material definition component, but even within Robot the cross-grain effect in a composite panel cannot be assigned as a characteristic which would change automatically with respect to geometry and orientation. If defined reference

architectural geometry were available, the Grasshopper model could be directed to rationalize CLT panel cuts to associate favourable cross-grain values according to shape, orientation, or loading. In cases where reference geometry is not available, and recalling that the weakest loading direction will govern the panel behaviour, these findings suggest that the ggRobot material definition component should be assigned those properties associated with the cross-grain angle which produces the highest deflection response. Figure 46 shows the deflection of a triangular (1 m x 2.75 m x 2.93 m) 3-layer CLT panel defined with the custom Hankinson-Shear Analogy material component under the uniformly distributed area loads and simply supported on all sides. The resulting 15.6 mm deflection is in violation of the L/300 deflection limit (9.77 mm), meaning that subsequent optimization using Galapagos would need to shorten the panel dimensions to meet this deflection criteria.

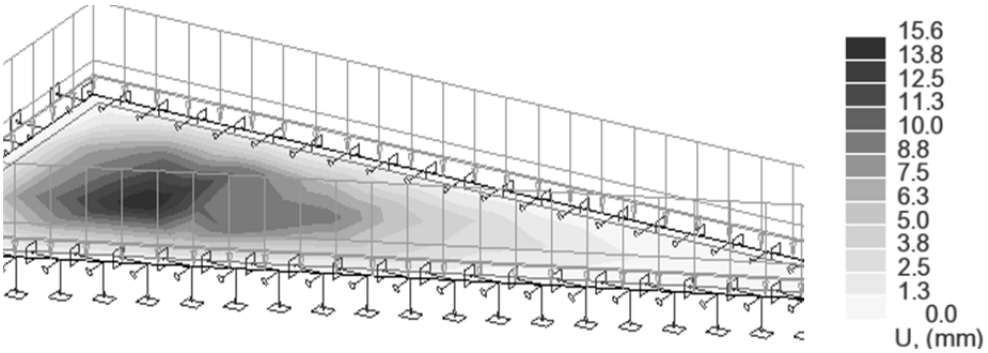

Figure 46 Deflection of a triangular CLT panel assigned material with 68° cross-grain properties

4.5 Prototyping and Assembly

Based on material availability and time constraints, the design team elected to construct a scaled prototype and selected a short, upright wall as the prototype geometry (Figure 47). As a scaled model, instead of CLT panels, high quality, grade “BB” Baltic Birch (*Betula pendula*) plywood

panels, 1½" thick were used. The function of the scaled prototype was mainly illustrative, but useful as a means to evaluate the fabrication process and the underlying structurally and materially-informed design logic. In this manner it served as nevertheless to proof that CLT can be used in the same application.

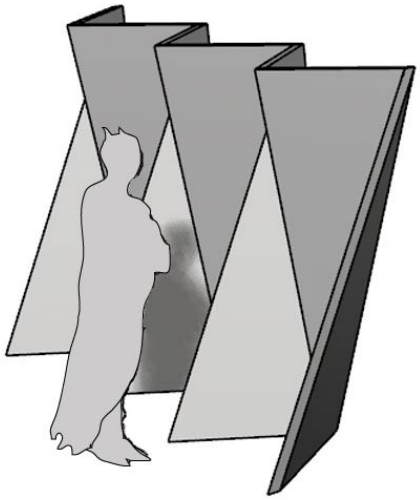

Figure 47: Folded wall model with figure for scale

As would occur with a full-scale folded CLT panel wall design, a series of rationalizations took place which considered the following 3 constraints:

1) Available panel sizes
2) Machining limitations
3) Available fastener sizes

4.5.1 Available Panel Sizes

Stock birch plywood panels were not available in the requested 1½” (35 mm) thickness, so two ¾” (19 mm) panels were glue-laminated together to form one 1½” (38 mm) thick panel. To minimize waste, the model’s triangular panel dimensions should maximize each panel. The largest available panel dimensions which could accommodate the wall height were 4’ x 8’ (1219 mm x 2438 mm): hence diagonally halving each panel would limit the height of the prototype wall to slightly less than 7’. Taking material losses due to milling, finishing, and the smaller size of the upper fold triangular panels into account, the architects selected a final vertical height of 6’-11” (2108 mm) and adjusted the Grasshopper model accordingly. The final dimensions of the upper and lower triangular panels are shown in Figure 48.

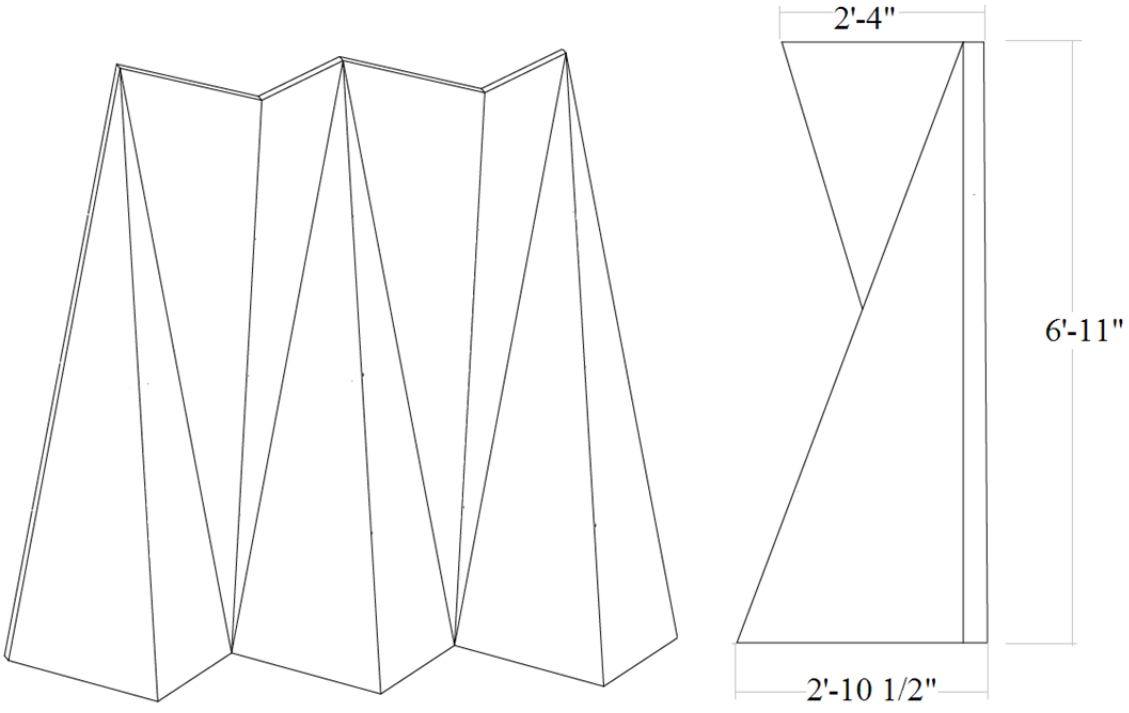

Figure 48: Rationalized wall height and length

4.5.2 Machining Limitations

The machining and fabrication of the folded wall would take place at CAWP. An SCM Record 110 AL TVN Prisma, 5-axis CNC machine would perform the cutting and mitring. This machine had a maximum drill bit size ¾" (19 mm) diameter, 1½" (38 mm) long, which limited the length of the mitre cut to a maximum of 3" (76 mm), and hence the angle between joining plates to 60°. A more acute fold would have been possible with a longer bit, yet mitred edges thinner than this are more difficult to align; any thinner and edges would become so thin self-weight alone would force the fasteners to tear-out.

4.5.3 Available Fasteners

The narrow thickness of the panels meant that the majority of structural STS were oversized. Furthermore, plywood design with STS is not presently addressed by the Canadian Approval CCMC 13677-R. However, the design guidelines in ETA-11/0190, on which CCMC 13677-R was partially based, permits plywood panels $h = 4\ d$ thick for screws $d < 8$ mm. Considering that the midpoint of the mitred edge where the screws are inserted is 19 mm deep, effectively half the original panel thickness, the screws would need to be 4.75 mm d or smaller. Partially-threaded SWG ASSY 3.0 CSK STS were selected for the design, being the smallest available which would meet thickness criteria. Each screw is 4.0mm d, with a 8.0 mm wide head and is 60 mm long ($l_s = 60$ mm), of which 34 mm is threaded. Recalling the mitred edge connection spacing rationalization described in section 5.3, the spacing values in units of d for ASSY 3.0 CSK STS are given in Table 8.

Table 8: Determination of panel dimensions based on STS spacing requirements

	Spacing for connections with ASSY 3.0 CSK STS and Plywood
p_{2t}	5 *d*
e_{1t}	12 *d*
e_1	1.0 *d*
e_x	1.5 *d*
l_f	10 *d*

The spacings between screws are shown in Figure 49. Heads were placed 35 mm from the edge, satisfying the minimum 5 *d* loaded edge distance requirement for ASSY 3.0 CSK screws and increasing the side panel embedment length from 19 mm to 22 mm. Screws were angled 60° to the face of each side member panel in order to penetrate the main member directly.

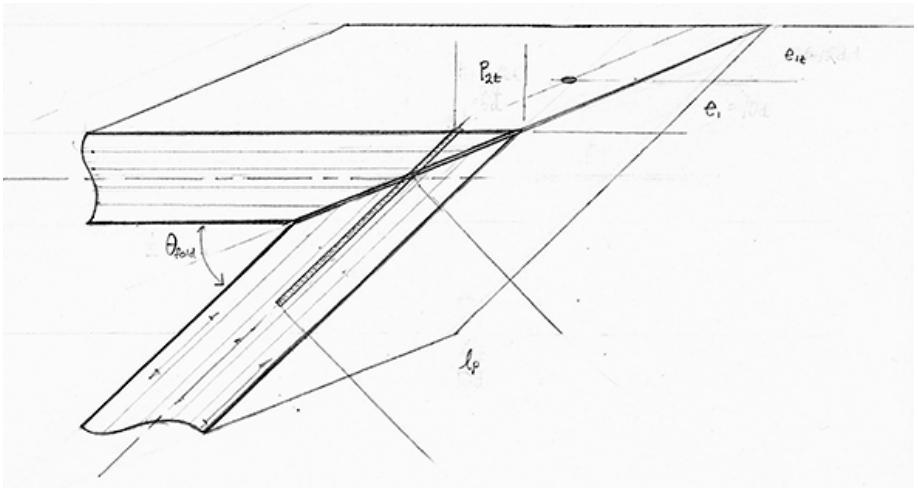

d	l_f	P_{2t}	e_{1t}	e_1	e_x	d_{min}
4.0 mm	60 mm	35 mm (20 mm minimum)	24 mm or greater	60 mm or greater	6 mm or greater	186 mm or greater

Figure 49: Minimum spacing values for SWG ASSY 3.0 CSK STS

CCMC 13677 R provide 1.53 kN/screw of factored withdrawal resistance and requires lateral resistance calculated according to Canadian lag screw design procedures in CSA O86-09, Section 10.6.6, resulting in 0.72 kN/screw of factored shear resistance. The head pull-through resistance of screws these small is not listed in CCMC 13677-R, so the characteristic pull-through resistance of 13.0 N/mm^2 from ETA-11/0190 was used instead: for a 4.0 mm diameter screw with 22 mm side panel embedment length, this equates to 0.88 kN/screw.

Table 9: Calculated STS unit connection resistance

	Factored resistance per pair of crossed screws	Reference for calculation
Withdrawal	3.01 kN/screw	CCMC 13677-R
Lateral	1.43 kN/screw	CSA O86-2009
Head pull-through	0.67 kN/screw	ETA-11/0190, EN 1995 1.1

The prototype structure would be displayed indoors and would not expect serious forces in its service. Design loads therefore considered only self-weight (density ρ_k = 690 kg/m^3, 0.33 kN/panel) and modest lateral live loads (0.5 kPa). Through the integrated model of the wall, the parametric connection location script was used to determine load demands at different potential connection points, shown in Figure 50: Robot model showing demand loads at connection points for loaded assembly. Only three crossed pairs of crossed STS were necessary along each folded seam, spaced 550 mm apart on centre along the vertical seams and 612 mm apart on centre along the folded seams, as shown in Figure 51.

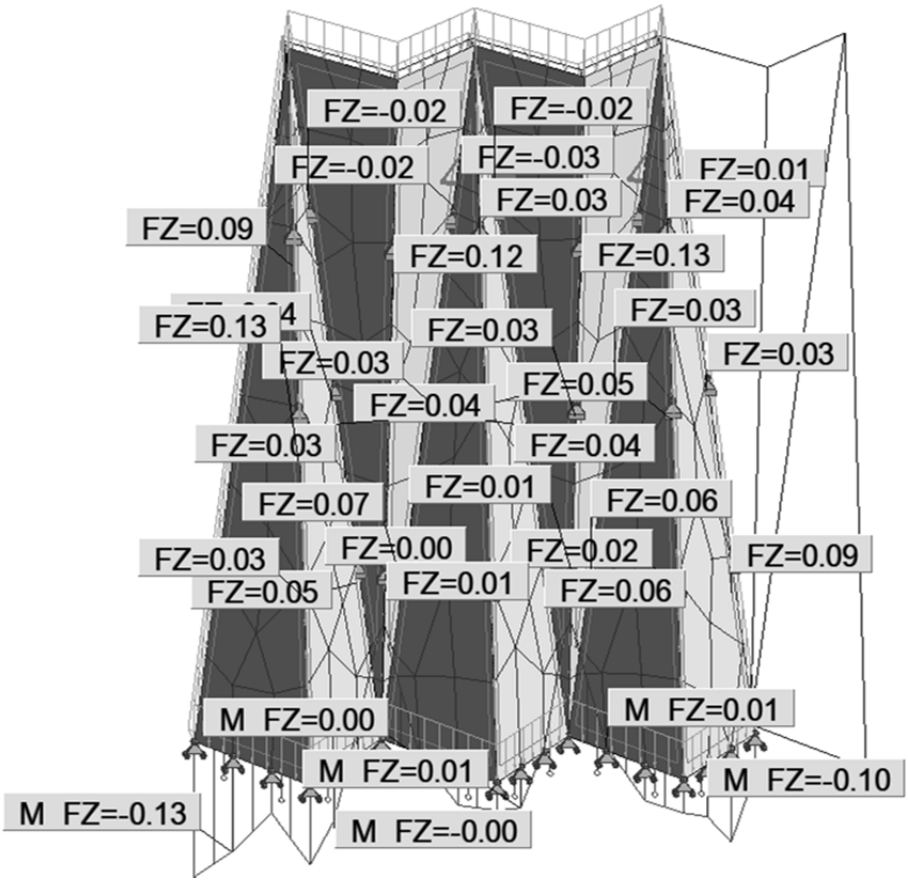

Figure 50: Robot model showing demand loads at connection points for loaded assembly

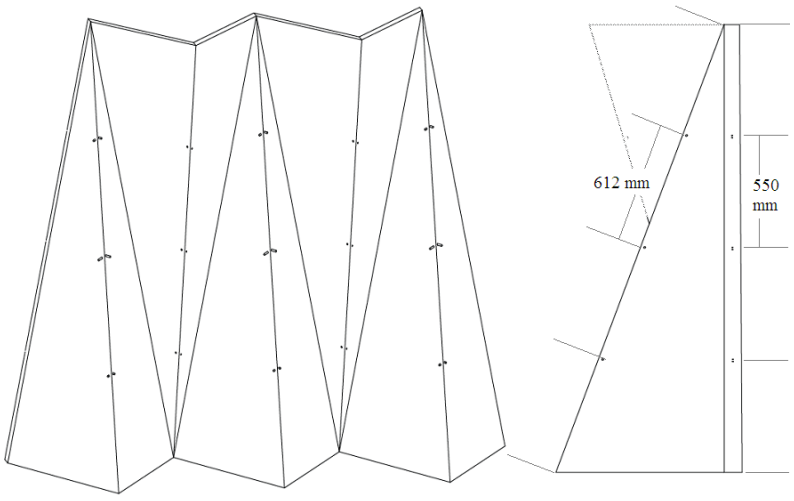

Figure 51: STS schedule for folded plate wall assembly

4.6 Prototype Fabrication

Once the constraints of the prototype and the connection detailing were established, the resulting folded plate model geometry was executed in Grasshopper, saved as a Rhino model, then exported as G-code for machining on the 5-axis CNC. Small drilled dots were added to each panel to facilitate the assembly process (see diagram, Figure 52).

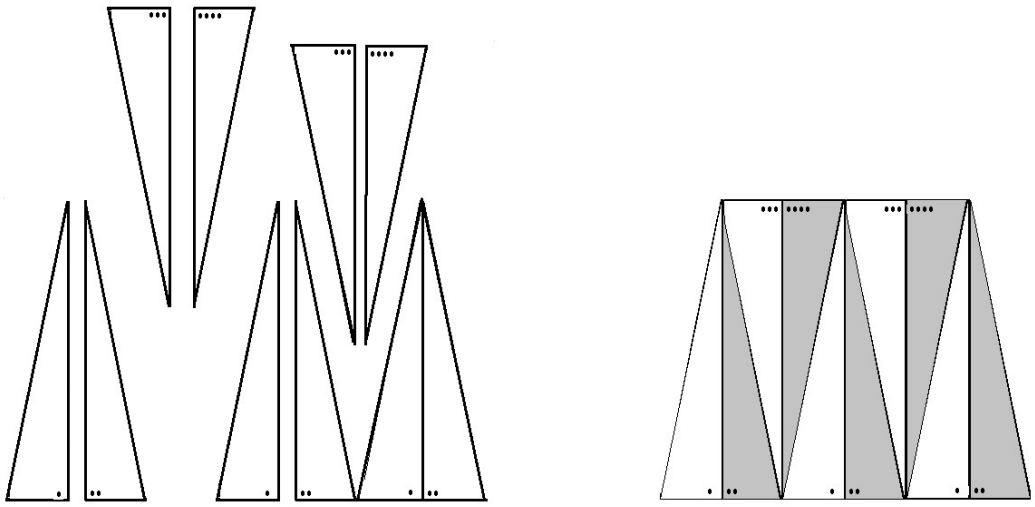

Figure 52: Wall assembly using markers. One and two-dot edges meet to form supporting base fold pairs. Three and four-dot edges form upper fold pairs.

Surfaces were finished with an orbital sander. Base pairs were assembled first as they were self-supporting, while upper panels were attached individually to the edges of the base pairs and were held in place while their mating seams were screwed together. The finished wall (Figure 53) took four hours to assemble, though the process would have benefitted from simple supporting scaffolding, which could have been made from off-cuts of the panels.

Figure 53: Finished folded CLT panel wall

4.7 Discussion

The process described for the design and fabrication of a folded timber wall allowed the underlying rationale and integrated model framework to be evaluated for geometric validity. It should be next applied to full-scale CLT assemblies by changing the input parameters accordingly, at which point further modelling is needed to test robustness of the generative constraints presented here. Determining which structural arrangements are controlled by fastener spacing, panel geometry, or another property not considered here, should be evaluated. This could be done by conducting a series of morphogenetic modeling trials: for instance, an origami tessellation scheme could be applied to a form-found surface, in which the size and distribution of the scheme could be varied over grid whose gradient is manipulated by an evolutionary solver primed to identify those arrangements which report satisfactory outcomes in Robot. Of the

potential solutions selected by the evolutionary solver, a few could be selected for fabrication and testing.

Other fabrication methods of simple yet versatile prefabrication and assembly should also be explored as generative constraints. STS are individually versatile, but the use of construction frames or jigs would be necessary for higher accuracy. Leitner (2004) proposed textile joints sandwiched between flat plywood plates. Solid wood edge ridges and blocking with countersunk STS connections could be used to determine and secure the angle.

Ideally such future research should consider full-scale models with CLT. Though scaled plywood models provide a means of evaluating the logic and assumptions of the design, implementing a folded structure in CLT is the next step if these modeling and fabrication methods are to become demonstrably valid for application to mass-timber structures.

Chapter 5: Integrated Parametric Modelling of Double-Curvature CLT

5.1 Approach

Through the use of integrated models, the objective of this portion of the research was to determine a means of fabricating doubly-curved CLT panels using integrated digital models and robotic fabrication technology. Single-curvature CLT panels are available in Europe, albeit rarely, and are formed by fitting lath layers across curving formwork, a process not dissimilar from curved glulam fabrication. The Elefantenhaus in Zurich stands as an example of a doubly-curved surface, but it was composed of layers of singly-curved CLT panels and relied upon their inherent flexibility and screwed connections between the layers to form the less severe secondary curvature on-site. Doubly-curved CLT, in which the panel itself is fabricated with curvature in each in-plane axis, are without precedent. As with the study of folded CLT panel walls, the main challenge was identifying the material and fabrication constraints with which the integrated parametric model could be rationalized further.

5.2 Geometry of Doubly-Curved CLT Panels

A layer of parallel lathes, forced into bending along their longitudinal axes, would produce a shell with single-curvature. Introducing a second curvature, however, will cause the laths to splay at their edges. The problem is shown in Figure 54.

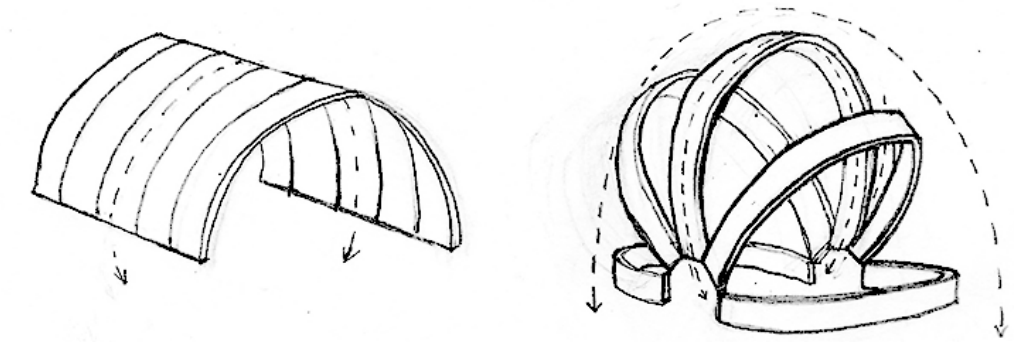

Figure 54: Introducing single (left) and double (right) curvature to an array of laths

Historic precedents for curving timber shells can be found in early 19th and 20th century water main and sewer designs. These pipes were built with laths, arrayed about their transverse axis, and tightly butt-jointed at their ends (Redwood Manufacturer Company 1911; Herzog et al. 2004). To prevent gaps at their sides, each lath was dressed on its wide faces to curve with the pipes circular profile, and cut inward along its edges to match radial lines. Transverse bands of steel cables hooped around the staves and were passed through iron shoes and tightened by means of nuts on their threaded ends. The concept itself descended from older shipbuilding and barrel-making trades, which used tapered laths called staves to produce double-curvature. This barrel geometry provided the baseline geometric logic for double curved CLT panels (Figure 55).

The method of modelling a barrel-like CLT panel within Grasshopper follows five steps: i) Each lath layer was described with an axial curvature and transverse curvature, both of which were modeled as arcs which ii) formed the plane of the lamination surface. The curvature arcs of uniformly curved surfaces share a centre point. These points bifurcate in the case of doubly-curved surfaces with different curvature radii. iii) Radial lath profiles were produced by rotating the arc of one curvature about the centre point of the other. iv) The tapering profiles which result

from the sweep produce the transverse curve. v) The same process is repeated for each lamination layer, resulting in a “layered-barrel”.

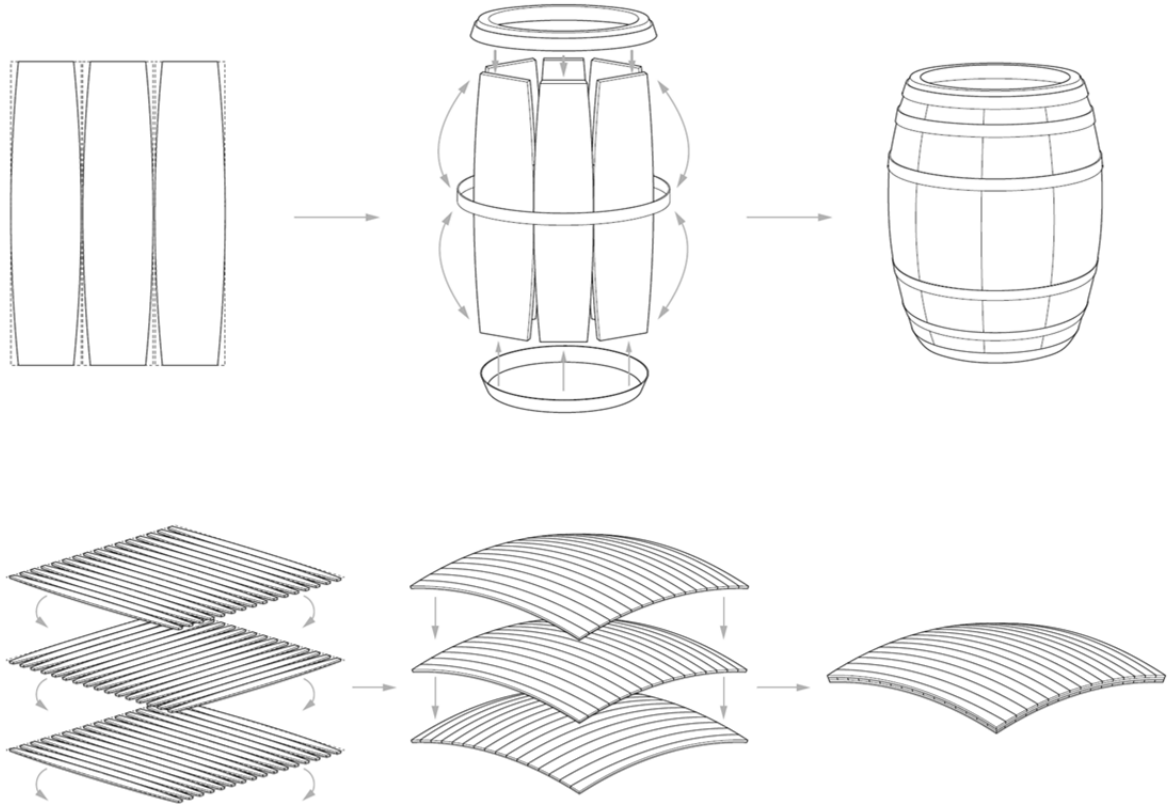

Figure 55: Top: barrel fabrication. Bottom: barrel analogy applied to CLT fabrication (Gaudin 2014)

As GLT and CLT are both fabricated by bending sawn lumber, the same curvature guidelines for GLT (CSA O86-09) were used to define the allowable curvature for CLT panels. These guidelines are based on the thickness of the innermost board, which undergoes the tightest curvature: the thinner the board, the more curvature it can tolerate without rupturing. Values from these guidelines are partially repeated in Table 10.

Table 10: Curvature limitations

h Smallest Lam Thickness [mm]	$R_{c,min}$ smallest allowable radius measured to innermost lam [mm]
6	800
10	1400
13	2200
16	3000
19	3800
25	6200
29	7300
32	8500
35	9500
38	10800

Given these constraints, and following their own preliminary study of the special consequences of thicknesses and their associated curvatures, the architecture students 13 mm thick laths were selected for a 2500 mm radius of curvature, R_c. With these values and grasshopper models was programmed to generate a panel B x L x H 1200 mm x 1200 mm x 39 mm. Figure 56 shows the resulting Rhino model. While the thickness of individual laths was based on glulam curvature limits for softwood, the number of laminations, and thus total panel thickness, was rationalized to accommodate potential panel-to-panel connections for the same SWG ASSY 3.0 CSK STS which were used in the folded panel wall assembly.

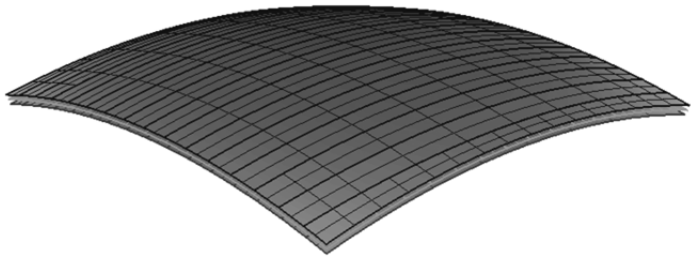

Figure 56: Rhino model for doubly-curved CLT panel

5.3 Preliminary Integrated Model of a Doubly-Curve d CLT Panel

Since the material behaviour of doubly-curved CLT is not well-understood, the first prototype was intended primarily to determine whether the digital panel geometry could be physically possible to fabricate, and if so, then secondarily as a means of evaluating the behaviour first-hand. Therefore, the integration of the Grasshopper model with Robot was kept very simple.

GeometryGym permits three different methods for defining panel elements from Grasshopper geometry. The most straightforward is i) the ggRobotCreatePanel component, which defines the perimeter of a panel with a polyline. Unfortunately, it is not applicable to curved panels because it can only form panels with planar surfaces. To generate panels with curved surfaces, the 3D surface geometry must be converted into a quadrangular mesh first. The mesh is then transformed into a panel using either ii) ggRobotMeshConvertPanel, or iii) translating the mesh directly to finite elements using ggRobotMeshConvertFiniteElements. The integrated model was constructed with this latter method.

The mesh generated from the reference Grasshopper surface was used to describe the FE mesh and assigned the material properties of a planar 3-layer CLT panel with 90° cross-grain (Figure

57). With this material definition, the stresses reported by Robot (Figure 58: Integrated model of doubly-curved CLT panel) indicated the panel would be capable of supporting a 1.0 kN point load at its centre.

Figure 57: Grasshopper reference surface geometry for doubly-curved CLT panels

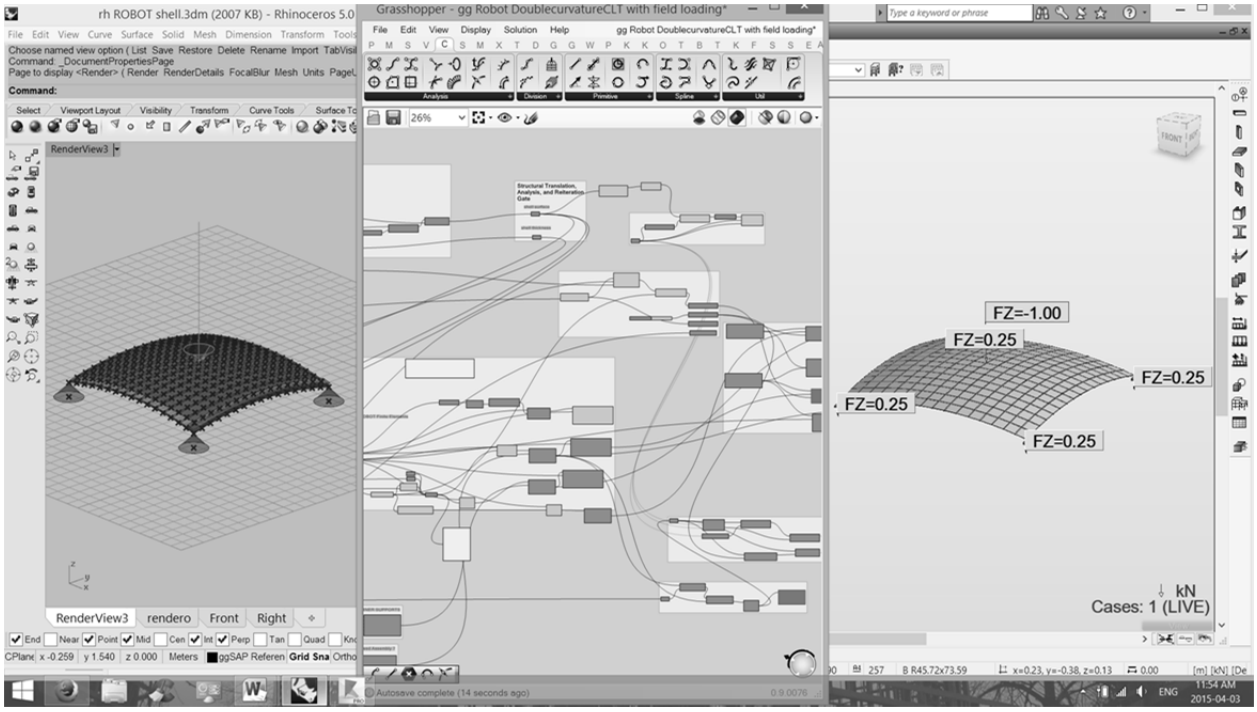

Figure 58: Integrated model of doubly-curved CLT panel

5.4 Fabrication of Doubly-Curved CLT Panels

5.4.1 Preparation

The purpose of the prototypes was to evaluate whether our digital geometric hypothesis could be manifested in the physical world. The process began by exporting the Rhino model as CNC machining files for both the fabrication form made of Medium-Density-Fibreboard (MDF) (Figure 59) and the tapered laths. These panels were fabricated in succession over the same MDF form, the first assembled with screws and the second with wood glue. The digital machining files were sent to CAWP, where an SCM Record 110 AL TVN Prisma 5-axis CNC machine performed the milling for the MDF form and the tapered laths.

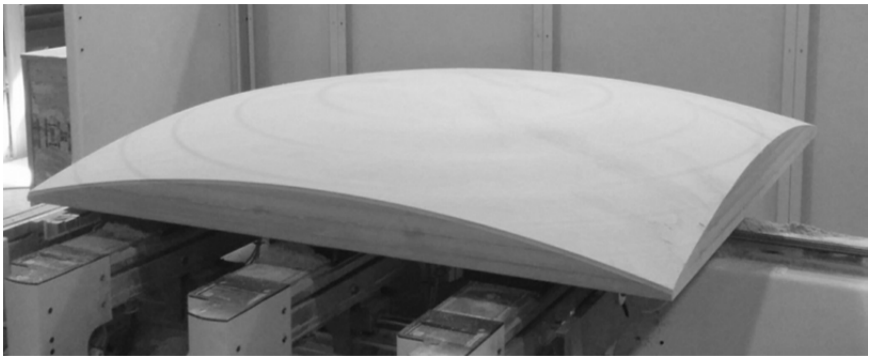

Figure 59: MDF Form for Doubly-Curved CLT

Each lath began as an 8 ft long (2,438 mm) 1 ft x2 ft (36 mm x 89 mm) architectural grade Douglas Fir board. These were cut into 1,250 mm long laths and milled down from 36 mm thick to 13 mm. To taper the sides, each lath was fixed at their ends with screws to plywood boards for stability before being placed on the CNC machine. For the laths the laths which would form the bottom (first) laminations, tabs of wood were left on the ends where the securing screws were

located (Figure 60). These tabs were used to secure the first lamination against the form by screwing them to edge boards which framed the MDF form. Second and third lath laminations had no end tabs and were instead temporarily fixed at ends with clamps.

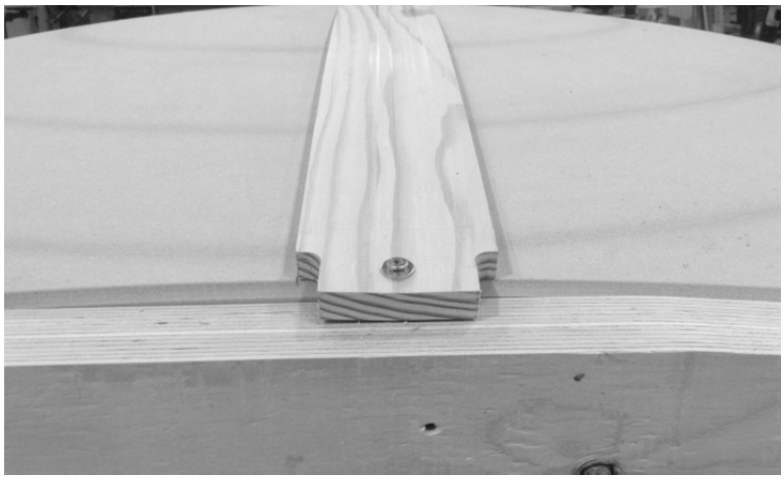

Figure 60: Tabs for Securing Laths During Fabrication

5.4.2 Screw-Fastened Doubly-Curved CLT Panel

The middle (second) and top (third) laminations of the first doubly-curved CLT panel were fastened-together with screws. Screwed layer connections consisted of #6 steel screws, 1-1/2" (38 mm) long, inserted at 45° to the normal plane (Figure 61) and staggered over each lath as shown in Figure 62.

Figure 61: Inclination and location of a screw with respect to a lath

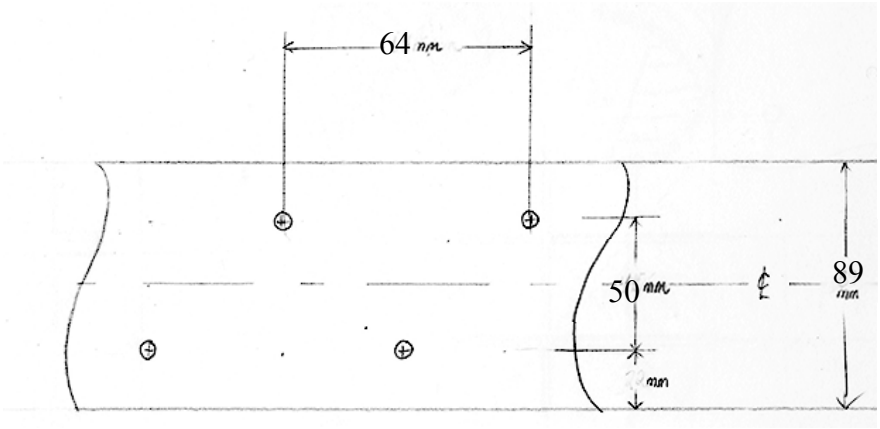

Figure 62: Lamination screw schedule

Once finished, the securing screws in the end tabs of the bottom layer were removed. The freed panel exhibited visible springback deformation; that is, a flattening-out from the original curve of the form (Figure 63). The screw-fastened prototype proved that manufacturing doubly-curved CLT panels was possible. At this point the design team debated whether a glued panel would hold its form better and elected to fabricate the second curved panel with adhesively-bonded laminations in order to observe the difference in behaviour between the two.

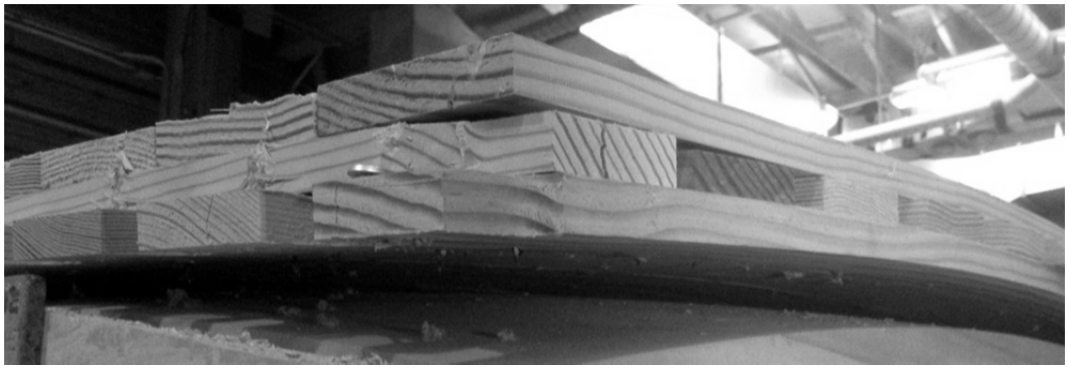

Figure 63: Springback Deflection of the Screw-Fastened Doubly-Curved CLT Panel

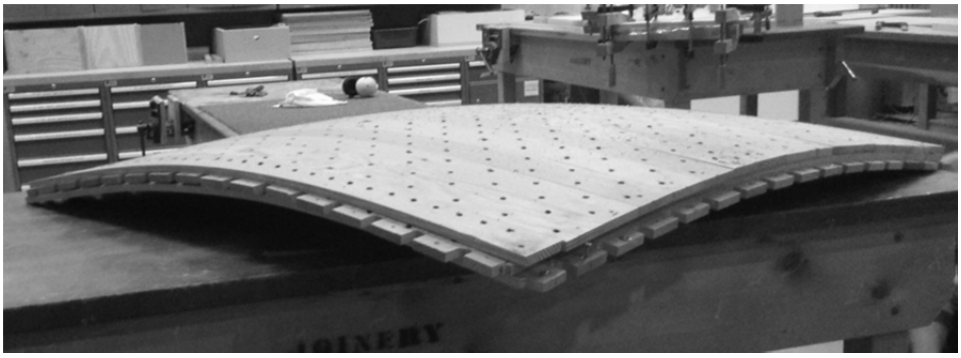

Figure 64: Finished Screw-Fastened Doubly-Curved CLT Panel

5.4.3 Adhesively-Bonded Doubly-Curved CLT Panel

To prevent adhesive from bonding the finished panel to MDF form, the form was wrapped in a plastic sheet. Thereafter the base layer assembly of the glued panel was identical to that of the screwed panel (Figure 65).

Figure 65: First Layer of the Adhesively-Bonded Doubly-Curved CLT Panel

Each subsequent layer of laths was individually glued with wood glue (*polyvinyl acetate aliphatic resin*), secured at their ends with clamps, and then allowed to dry for 7 days before unclamping and applying the next layer. The interior layer of laths was also staggered, with the intention of creating slots for future jointing with other curved panels (Figure 66), via either complimentary finger joints or interior splines, fixed with STS.

Figure 66: Glued Fabrication Process, Showing Interior Layer Staggered Edge

Figure 67 shows the finished adhesively-bonded doubly-curved CLT panel. When its clamps were removed, the panel was slightly offset from centre. Thus, though the apparent gap between the released panel and the MDF form were smaller, it was not known if they were the result of springback or simply due to translation of the assembly.

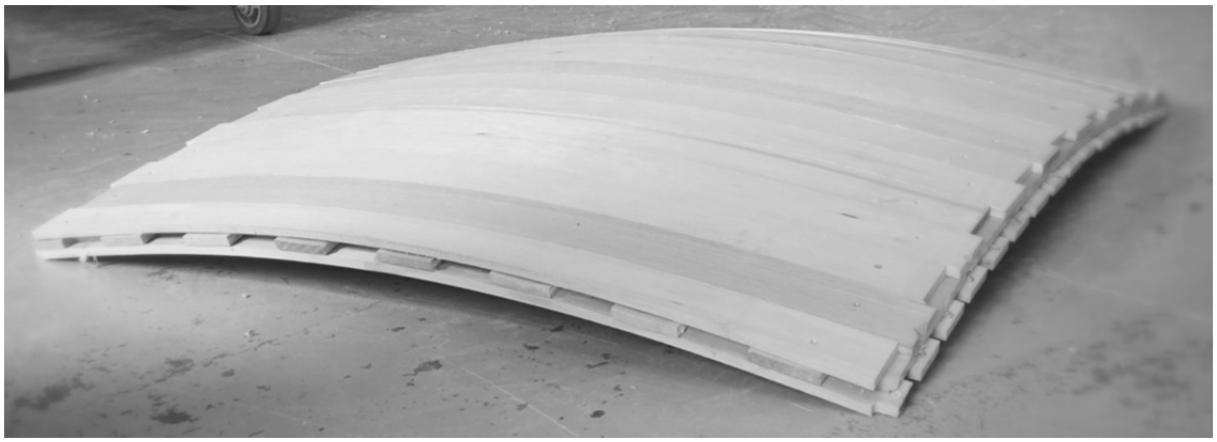

Figure 67: Finished adhesively-bonded doubly-curved CLT panel

5.5 Prototype Evaluation

Figure 68 shows both panels side by side for comparison, where higher deformation is clearly present in the screwed assembly.

Figure 68: Adhesively-bonded panel (left) and screw-fastened panel (right)

The amount of deflection in each panel was measured by comparing the final dimensions of the panel edges to the dimensions of the MDF form. Table 11 displays the final lateral and vertical dimensions which were measured from the fabricated panels.

Table 11: Differences in curved geometry of the screw-fastened and adhesively-bonded panels.

Edge		Original form	Screw-fastened	Adhesively-bonded
A	Span [mm]	1200	1225	1217
	Camber [mm]	73	39	61
	R_c [mm]	2500	4829	3066
B	Span [mm]	1200	1215	1207
	Camber [mm]	73	50	62
	R_c [mm]	2500	3716	2968
C	Span [mm]	1200	1211	1212
	Camber [mm]	73	53	59
	R_c [mm]	2500	3485	3142
D	Span [mm]	1200	1227	1218
	Camber [mm]	73	38	63
	R_c [mm]	2500	4971	2975

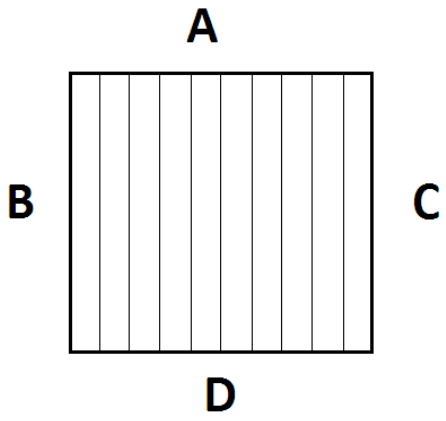

Notably, higher deformations in the screw-fastened panel correspond to the number of laminations running parallel to that axis. Given the near perfect rigidity of adhesive connections and the expected slip between mechanical fasteners in a composite beam, the higher springback deformation in the screw-fastened panel is not surprising but provides an important insight into the panel structure. Recalling the barrel analogy, the method of fabrication resembles force-formed gridshell construction in miniature. Each lath is individually bent into a curve, clamped at their ends, and then bonded to an adjacent lath layer to form a composite section, just as a lattice

net is pushed into form, secured at the base, and fixed at the nodes to form a composite section. Resulting lateral and vertical deflection then depends on the level of composite action between layers in the panels, and similarly the number of parallel layers in section.

Without further tests, it is difficult to assess the structural properties of these panels, but based on this proposed mechanism, the following discussion describes a theoretical model for predicting the panel properties using the springback deflection measurements. A brief analytical exercise was performed considering a one lath (89 mm) wide unit strip of panel, shown in Figure 69, using the γ-method described in Chapter 2.1.3.2, as this method permits easy comparison between screwed versus glued connections in the same assembly. If the layers in the panel are of uniform section dimensions and material properties (ie, $A_1 = A_2$; $E_1 = E_{23}$; $I_1 = I_2$), then the area A = 1,157 mm^2 and the moment of inertia $I = 16{,}294$ mm^4 for both panels, and Equation (6 for the effective bending stiffness $(EI)_{eff}$ can be simplified to Equation (17:

$$(EI)_{eff} = 2E(I + \gamma A a^2) \qquad (17)$$

Where a is the distance from the centroid of the outer layers to the centroid of the panel, a = 6.5 mm in the A-D direction, but a = 0 in the B-C direction.

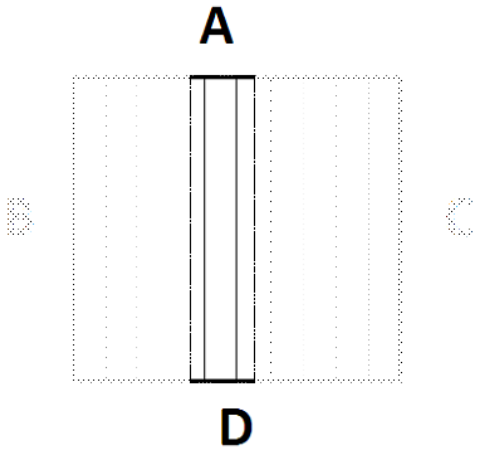

Figure 69: Panel strip analyzed for deflection due to slip

Connection stiffness was calculated assuming that the staggered screw schedule could be modeled as a single line of screws spaced only 25 mm apart, so that γ_{SCR} was calculated as 0.25. The adhesive-bond stiffness was calculated with an 89 mm unit width, such that γ_{GLU}, was calculated as 0.92 in the A-B direction and 0.85 in the D-C direction. The effective bending stiffness of the screwed panel assembly, $(EI)_{effSCR}$, the glued panel assembly, $(EI)_{effGLU}$, are shown in Table 12:

Table 12: Effective stiffness of screw-fastened and adhesively-bonded panels in parallel (||) and transverse (_|_) directions

$(EI)_{effSCR\|\|} =$	$6.24x10^8\ Nmm^2$
$(EI)_{effSCR\perp} =$	$3.85x10^8\ Nmm^2$
$(EI)_{effGLU\|\|} =$	$1.34x10^9\ Nmm^2$
$(EI)_{effGLU\perp} =$	$1.27x10^9\ Nmm^2$

Since γ-method is based on simple beam theory and the rolling shear deflection is captured by the imaginary fastener slip, the equation for live load deflection Δ_L remains valid. When

rearranged and solved for a single 13 mm x 89 mm lath, ω_L represents the uniformly distributed line load (UDL) required during fabrication to bend each lath over the surface of the mold and clamp it in place.

$$\omega_L = \Delta_L \frac{384(EI)_{eff}}{5L^4} \tag{18}$$

$$\omega_L = 73.068mm \frac{384 \times 1.79.x10^8\ Nmm^2}{5(1212.57mm)^4} = 0.465 \frac{N}{mm}$$

In these equations, Δ_L and ω_L are linearly related. If the same load ω_L is applied to a CLT section defined by $(EI)_{effSCR}$, or $(EI)_{effGLU}$ then the resulting deflections are equivalent to the springback. Since strip A-D defines the curvature over B-C and vice-versa, the calculated springback for the panels is summarized in Table 13 and compared to the measured values in Figure 70.

Table 13: Comparing springback deflection of the prototype with its analytical model

		Screw-fastened		Adhesively-bonded	
		Measured Average [mm]	Modeled [mm]	Measured Average [mm]	Modeled [mm]
Edges A, D	Springback	34.0	36.5	12.0	10.3
	Residual Camber [mm]	39.0	36.5	61.0	62.7
Edges B, C	Springback	23.0	21.0	11.0	9.7
	Residual Camber [mm]	50.0	52.0	62.0	63.3

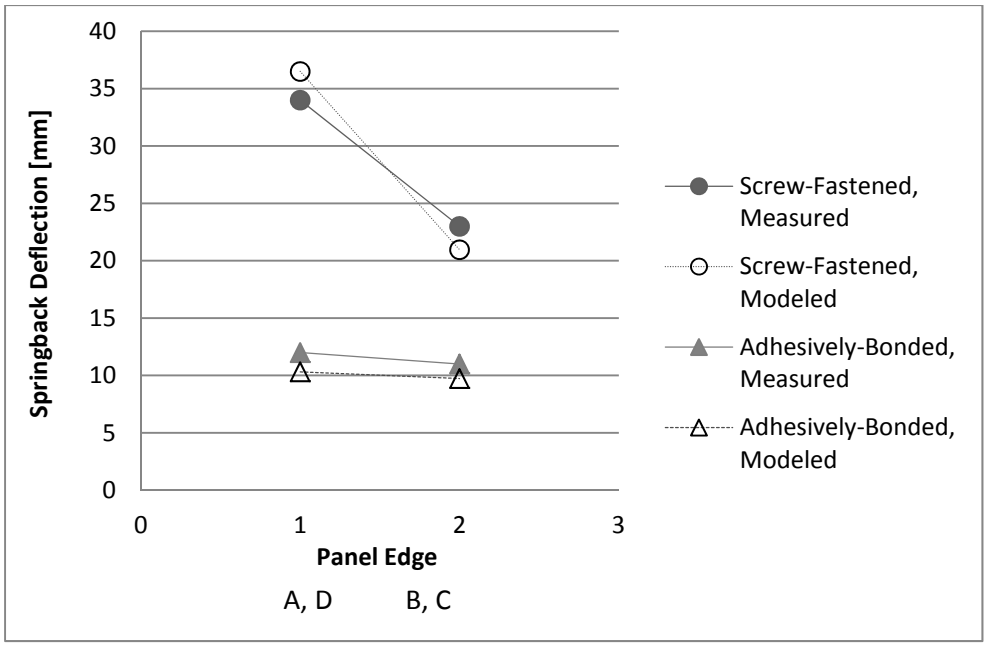

Figure 70: Comparison of analytically modelled springback deflection model to measured values

The proposed analytical model was applied to a full gridshell as an integrated model with Grasshopper. The same Grasshopper geometric reference surface was used to produce a grid, in which each gridline represented the lath layers running in that direction. Each set could be assigned the respective A-D or B-C direction stiffness value as determined from γ-method for either screw-fastened or adhesively bonded assemblies. Results from the integrated model, however, reported edge deflections of only 2.7 mm in the A-D direction and 6.2 mm in the B-C direction, see Figure 71.

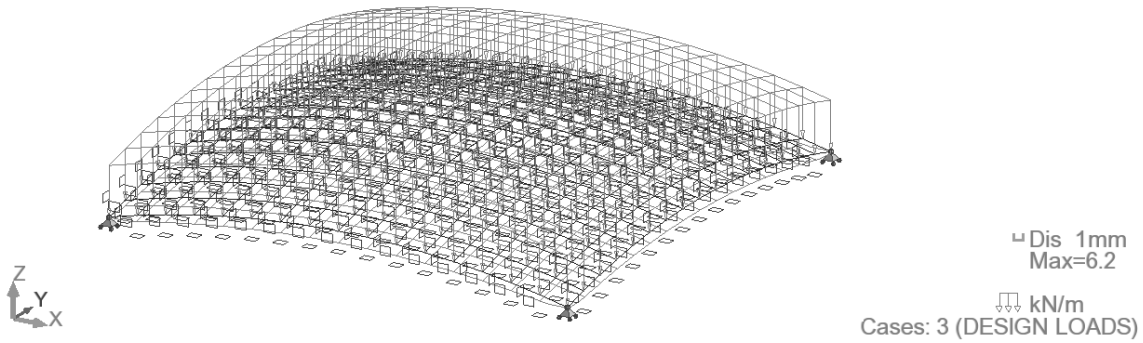

Figure 71: Modeling doubly-curved CLT panel as a gridshell

5.6 Discussion

The discrepancy in physical response of the panels between with the analytical and computational predictions illustrates the limitations of the ggRobot interface, which does not permit dynamic analysis necessary for modeling bucking and deflection over time. Notably, both modal and nonlinear analysis options are available in GeometryGym suites for interfacing with other FEM software, while other Grasshopper plugins offer dynamic relaxation of a membrane form.

Given the extremely small tolerance level required of complex timber structures, the ability to design doubly-curved CLT for desired levels of final curvature requires a method for anticipating residual springback. Though the proposed static deflect model is promising for preliminary conceptual design estimates, future pursuit of dynamic analysis modelling options would be the logical next step for future research. Additional fabrication and testing would also be needed to refine the design and material behaviour of doubly-curved CLT panels further. Even so, the production of prototype doubly-curved CLT panels proves that such geometry is physically feasible, greatly aided by the use of integrated digital modeling.

Chapter 6: Conclusions

6.1 Summary of Work

This thesis presents an example of "co-rationalized" architectural and structural collaboration, using a mixture of digitally-integrated and analog models, for the design and construction of solid timber shell structures using CLT panels. Through a co-rationalized design process timber engineering details are identified and integrated into the architectural model and the structural engineer takes an active rather than reactionary role in the preliminary design stages. The result of this process was the design, fabrication, and assembly of a folded plate wall prototype and two CLT panels with double curvature, demonstrating how integrated parametric models and digital fabrication enables the realization of the great architectural versatility that mass-timber has to offer.

6.2 Future Research

Areas of future research include both architectural and structural topics. The design and manufacture of innovative connections between panels, specifically those combining adhesive with traditional joinery techniques, warrant investigation. Developing more detailed integrated models which anticipate rebound deflections are needed to produce more predictable global geometries. As has been described and demonstrated in this thesis, material properties play an essential role in both structural design and morphogenetic architectural theory. Further, thorough testing needs to be conducted in order to evaluate the analytical models proposed here and to gain better understanding of the effect of cross-grain angle and springback on the material

properties of both angle-cut and doubly-curved CLT panels. Other proprietary connection systems could also be investigated and extrapolated into their own generative, integrated models.

Unfamiliarity or misunderstanding of mass-timber, as well a lack of design tools which incorporate modelling with mass-timber design criteria, are some of the hurdles to the implementation of mass-timber to large construction in general, a condition highlighted in the case of designing timber shell structures.

6.3 Conclusion

Parametric models and digital fabrication allow for increasingly complex architectural geometries which present new challenges for structural engineers. Integrating FEM software into this design chain grants structural engineers the same geometric versatility. Through integrated models structural engineers may not only easily adapt and respond to rapid model variations and unusual assemblies, but also inform the building design from inception.

This project is set within the larger discussion on the structural design challenges associated with mass-timber structures with complex geometry. It provides an example to architects and engineers; and in this state it began with concepts, rather than defined geometry or materials. As such it focuses on identifying design challenges and how to approach them rather than providing explicit solutions, in which the design and fabrication of folded CLT plates and double-curvature CLT panels serve as examples for future extrapolation and exploration. This co-rationalized research refutes misconceptions of timber as a limited material and challenges architects,

engineers, and researcher alike to experiment further with this sustainable material and new design tools.

Bibliography

Adriaenssens, S., Barnes, M., et al., 2014. Dynamic relaxation: design of a strained timber gridshell. In S. Adriaenssens et al., eds. *Shell Structures for Architecture: Form Finding and Optimization*. Birkhäuser, p. 340.

Adriaenssens, S., Brown, N., et al., 2014. Structural Analysis of Reinforced Concrete Folded Hyperbolic Parabolid: A Case Study of the Modern Miami Marine Stadium. *International Journal of Architectural Heritage*, 8, pp.498–516. Available at: http://www.tandfonline.com/doi/pdf/10.1080/15583058.2012.694967 [Accessed August 28, 2015].

Blass, H.J. & Fellmoser, P., 2004. Design of Solid Wood Panels with Cross Layers. In *Proceedings for the 8th World Conference on Timber Engineering*. Lahti, Finland, pp. 543–548. Available at: http://holz.vaka.kit.edu/public/36.pdf [Accessed August 26, 2015].

Bodig, J. & Jayne, B.A., 1982. *Mechanics of wood and wood composites*, Van Nostrand Reinhold. Available at: https://books.google.ca/books/about/Mechanics_of_wood_and_wood_composites.html?id=GsFRAAAAMAAJ&pgis=1 [Accessed August 26, 2015].

Boeykens, S., 2012. Bridging building information modeling and parametric design. In Gudnason & Scherer, eds. *eWork and eBusiness in Architecture, Engineering, and Construction*. London: Taylor & Francis Group, pp. 453–458.

Brandner, R., 2013. Production and Technology of Cross Laminated Timber (CLT): A state-of-the-art Report. In *COST Action FP1004, Focus STS-European Conference on Cross-Laminated Timber (CLT)*. Gratz, pp. 2–36.

Buri, H., Stotz, I. & Weinand, Y., 2011. *Curved Folded Plate Timber Structures*, Lausanne.

Buri, H. & Weinand, Y., 2011. *ORIGAMI – Folded Plate Structures , Architecture*, Lausanne.

Buri, H.U., 2010. *Origami - Folded Plate Structures*. Ecole Polytechnique Federale de Lausanne.

Buri, H.U. & Weinand, Y., 2010. Origami aus Brettsperrholz. *Detail*, (10), pp.2–4.

Canadian Construction Materials Centre, 2014. *Evaluation Report CCMC 13677-R: SWG ASSY*

VG Plus and SWG ASSY 3.0 Self-Tapping Wood Screws, Canada: National Research Council Canadian Construction Materials Centre.

Closen, M., 2012. *Self-Tapping Screw Assemblies Under Monotonic Loading*. University of British Columbaia.

CORE studio, 2014. *CORE studio | Thornton Tomasetti*, New York. Available at: https://s3.amazonaws.com/corewebsite-media-uploads/CoreStudioBrochure/COREstudio.pdf [Accessed August 26, 2015].

D'Amico, B., Kermani, a. & Zhang, H., 2014. Form finding and structural analysis of actively bent timber grid shells. *Engineering Structures*, 81, pp.195–207. Available at: http://linkinghub.elsevier.com/retrieve/pii/S014102961400580X [Accessed November 27, 2014].

Deutsch, R., 2011. *BIM and Integrated Design: Strategies for Architectural Practice*, John Wiley & Sons. Available at: https://books.google.ca/books/about/BIM_and_Integrated_Design.html?id=pYtxLE5ivlsC&pgis=1 [Accessed August 26, 2015].

English, E.C., 2005. Vladimir Shukhov and the Invention of Hyperboloid Structures. In *ASCE Structures Congress 2005*. p. 9.

European Organisation for Technical Approvals, 2013. *European Technical Approval ETA-11 / 0190 Wuerth self-tapping screws*,

Farnsworth Jr, D.B., 1999. *Behaviour of Shell Structures*. Massachusetts Institute of Technology.

Farshad, M., 1992. *Design and Analysis of Shell Structures*, Springer Netherlands. Available at: https://books.google.ca/books/about/Design_and_Analysis_of_Shell_Structures.html?id=X66ZWY7oUdEC&pgis=1 [Accessed August 26, 2015].

Gagnon, S. & Pirvu, C. eds., 2011. *CLT Handbook : Cross-Laminated Timber* Canadian E., Quebec City: FPInnovations.

Gaudin, R.T., 2014. Barrel Analogy.

Government of British Columbia, 2009. Wood First Act. *B. C. Government Website*. Available at: http://www.bclaws.ca/Recon/document/ID/freeside/00_09018_01 [Accessed October 18,

2015].

Haasis, M. & Weinand, Y., 2014. *ORIGAMI - Folded Plate Structures , Engineering, Preliminary Study, and Numerical Pre-Dimensioning*.

Happold, E. & Liddell, W.I., 1975. Timber Lattice Roof for the Mannheim Bundesgartenschau. *Structural Engineer*, 53(3), pp.99–135.

Harris, R. et al., 2003. Design and Construction of the Downland Gridshell. *Building Research & Information*, 31(November-December), pp.427–454. Available at: http://dx.doi.org/10.1080/0961321032000088007.

Harris, R., 2011. Design of timber gridded shell structures. *Proceedings of the ICE - Structures and Buildings*, 164(2), pp.105–116. Available at: http://www.icevirtuallibrary.com/content/article/10.1680/stbu.9.00088 [Accessed September 16, 2014].

Harris, R., Dickson, M. & Kelly, O., 2004. *The Use of Timber Gridshells for Long Span Structures*,

Harris, R. & Roynon, J., 2008. The Savill Garden gridshell: Design and construction. *Structural Engineer*.

Hauschild, M. & Karzel, R., 2011. *Digital Processes: Planning, Designing, Production*, Birkhäuser. Available at: https://books.google.com/books?id=OdDTAAAAQBAJ&pgis=1 [Accessed August 26, 2015].

Hensel, M. & Menges, A., 2006. *Morpho-ecologies*, Architectural Association. Available at: https://books.google.ca/books/about/Morpho_ecologies.html?id=W7RxQgAACAAJ&pgis=1 [Accessed August 26, 2015].

Hensel, M., Menges, A. & Weinstock, M., 2010. *Emergent Technologies and Design: Towards a Biological Paradigm for Architecture*, Routledge. Available at: http://www.amazon.com/Emergent-Technologies-Design-Biological-Architecture/dp/0415493447/ref=pd_bxgy_14_text_y [Accessed August 26, 2015].

Hensel, M., Menges, A. & Weinstock, M., 2006. Towards self-organisational and multiple-performance capacity in architecture. *Architectural Design*, 76(2), pp.5–11. Available at: http://doi.wiley.com/10.1002/ad.234 [Accessed August 15, 2015].

Herzog, T. et al., 2004. *Timber Construction Manual*, Birkhäuser Architecture. Available at: http://www.amazon.com/Timber-Construction-Manual-Manuals-englisch/dp/3764370254/ref=sr_1_1?ie=UTF8&qid=1440611913&sr=8-1&keywords=timber+construction+herzog [Accessed August 26, 2015].

Heyman, J., 1995. *The Stone Skeleton: Structural Engineering of Masonry Architecture*, Cambridge University Press. Available at: http://www.amazon.com/Folding-Techniques-Designers-From-Sheet/dp/1856697215/ref=pd_sim_14_7?ie=UTF8&refRID=0R6KX9AGSTR2SKSEVTVF [Accessed August 26, 2015].

Jeska, S. & Pascha, K.S., 2014. *Emergent Timber Technologies: : 9783038215028: Amazon.com: Books*, Birkhäuser. Available at: http://www.amazon.com/Emergent-Timber-Technologies-Simone-Jeska/dp/3038215023/ref=sr_1_1?ie=UTF8&qid=1440611630&sr=8-1&keywords=Emergent+timber [Accessed August 26, 2015].

Jöbstl, R.A., Borgensperger, T. & Schickhofer, G., 2008. In-Plane Shear Stiffness of CLT. In *41st CIB Meeting, St. Andrews, Canada*.

Jokerst, R.W., 1982. The effect of geometry on the performance of structural finger-joints. In C. F. L. Prins, ed. *Production, Marketing and Use of Finger-Jointed Sawnwood*. New York: The United Nations, pp. 169–180.

Kahaner, L., 2014. Working from the Cloud: New Solutions, Interoperability and Mobile Apps Pushing Constructions Technology. *Structure Magazine*, (August), pp.45–58.

Kara, H. ed., 2008. *Design Engineering: Adams Kara Taylor*, Actar. Available at: http://www.amazon.com/Design-Engineering-Adams-Kara-Taylor/dp/8496540669/ref=sr_1_2?ie=UTF8&qid=1440616247&sr=8-2&keywords=hanif+architecture [Accessed August 26, 2015].

Kara, H. & Georgoulias, A., 2012. *Interdisciplinary Design: New Lessons from Architecture and Engineering*, ACTAR Publishers. Available at: https://books.google.com/books?id=oNQsXtPz6CcC&pgis=1 [Accessed August 30, 2015].

Kloft, H., 2003. Engineering of Freeform Architecture. In M. Bechthold et al., eds. *New Technologies in ArchitectureII & III: Digital Design and Manufacturing Techniques*.

Cambridge, MA: Harvard University Graduate School of Design, pp. 110–127. Available at: https://books.google.com/books?id=kJEMWde-REYC&pgis=1.

Krieg, O.D. & Correa, D., 2014. *Machinic Morphospaces in Timber Construction*,

Kuebler, W., 2014. Das neue Elefantenhaus im Zoo Zürich. *Bautechnik*, 91, pp.51–57.

Kuebler, W., 2013. Freiformschale Elefantenpark Zoo Zürich : Statische Formfindung und Konstruktion. *Holzbautag Biel*, pp.115–126.

Larsen, K.E., 2007. Ten Timber Software Solutions. *Innovasjon Norge*, p.31.

Leitner, K., 2004. *Tragkonstruktionen aus plattenförmigen Holzwerkstoffen mit der textilen Fuge*. Technische Hochschule, Aachen.

La Magna, R. et al., 2013. From Nature to Fabrication : Biomimetic Design Principles for the Production of Complex Spatial Structures. *International Journal of Space Structures*, 28, pp.27–39.

Maher, A. & Burry, J., 2006. The Re-Engineering Project. *ACADIA 06 Synthetic Landscapes*, pp.200 – 2012.

Manglesdorf, W., 2010. Structuring Strategies for Complex Geometries. In R. Oxman & R. Oxman, eds. *Architectural Design: The New Structuralism: Design, Engineering and Architectural Technologies*. Wiley, pp. 40–45. Available at: http://doi.wiley.com/10.1002/ad.1101.

Mark, R., 1990. *Light, Wind, and Structure: The Mystery of the Master Builders*, The MIT Press. Available at: http://www.amazon.com/Light-Wind-Structure-Mystery-Builders/dp/026263158X/ref=sr_1_1?s=books&ie=UTF8&qid=1440613960&sr=1-1&keywords=wind+and+light+structures [Accessed August 26, 2015].

McKalip, D., 2014. Announcing the U.S. Tall Wood Building Prize Competition to Innovate Building Construction. *whitehouse.gov*. Available at: https://www.whitehouse.gov/blog/2014/10/10/announcing-us-tall-wood-building-prize-competition [Accessed August 26, 2015].

Menges, A. ed., 2012. *Material Computation: Higher Integration in Morphogenetic Design*, Academy Press. Available at: http://www.amazon.com/Material-Computation-Higher-

Integration-Morphogenetic/dp/0470973307/ref=pd_sim_14_25?ie=UTF8&refRID=0W8N9GFT1WN0J2ZM2DX7 [Accessed August 26, 2015].

Menges, A. & Ahlquist, S., 2011. *Computational Design Thinking: Computation Design Thinking*, Wiley. Available at: http://www.amazon.com/Computational-Design-Thinking-Computation/dp/0470665653/ref=pd_sim_14_20?ie=UTF8&refRID=0AD4SGC2MVG7SK775RQQ [Accessed August 26, 2015].

Mestek, P. & Kreuzinger, H., 2008. Design of Cross Laminated Timber (CLT). Available at: http://www.researchgate.net/publication/267555559_Design_of_Cross_Laminated_Timber_(CLT) [Accessed August 26, 2015].

Mirtschin, J., 2011. Engaging Generative BIM Workflows. In *Collaborative Design of Lightweight Structures - LSAA 2011*. p. 8. Available at: http://www.lsaa.org/index.php?option=com_content&view=article&id=256:lsaa-2011-links&catid=45:past-events&Itemid=52.

Mirtschin, J., 2014. Generative BIM using IFC4. In *Revit Technology Conference Australasia*. pp. 1–19.

Mirtschin, J., 2015. GeometryGym.

Mohammad, M., 2010. Connections in CLT Assemblies. *City*.

Mohammad, M., 2011. Connections in CLT Assemblies.

Naicu, D., Harris, R. & Williams, C., 2014. Timber Gridshells: Design methods and their application to a temporary pavilion. In *Proceedings of the World Conference on Timber Engineering, Quebec City*. Quebec City, p. 10.

Nakashima, S. et al., 2012. Evaluation of tensile performance of drift pin joint of cross laminated timber with steel inserted plate. *World Conference on Timber Engineering*, 7(July), pp.417–424.

Olsen, C. & Mac Namara, S., 2014. *Collaborations in Architecture and Engineering: Clare Olsen, Sinead Mac Namara: 9780415840620: Amazon.com: Books*, Routledge. Available at: http://www.amazon.com/Collaborations-Architecture-Engineering-Clare-Olsen/dp/0415840627/ref=pd_sim_14_16?ie=UTF8&refRID=0W8N9GFT1WN0J2ZM2D

X7 [Accessed August 26, 2015].

Otto, F., Trostel, R. & Schleyer, F.K., 1973. *Tensile structures; design, structure, and calculation of buildings of cables, nets, and membranes, Volumes 1-2*, The MIT Press. Available at: https://books.google.com/books?id=tOxSAAAAMAAJ&pgis=1 [Accessed August 26, 2015].

Parliament of British Columbia, 2009. *Wood First Act*, Available at: https://www.leg.bc.ca/39th1st/1st_read/gov09-1.htm [Accessed August 26, 2015].

Pearson, H., Evernden, M. & Harris, R., 2012. Anaysis of Engineered Timber Panels using a Strut and Tie Model for use in Folded Plate Structures and Deep Beams. *Proceedings of the World Conference on Timber Engineering, Auckland*.

Pone, S. et al., 2013. Timber Post-formed Gridshell : Digital Form-finding / drawing and building tool. In *Proceedings of the International Association for Shell and Spatial Structures (IASS) Symposium 2013*. pp. 1–8.

Pottmann, H. et al., 2007. *Architectural Geometry* D. Bentley, ed., Bentley Institute Press. Available at: http://www.amazon.com/Architectural-Geometry-Helmut-Pottmann/dp/193449304X/ref=pd_sim_14_4?ie=UTF8&refRID=1HKKMCM1W1021XNEYA5Q [Accessed August 26, 2015].

Ramage, M.H. et al., 2009. Advanced Geometry , Rudimentary Construction : Structural form fi nding for unreinforced thin-shell masonry vaults. , p.29.

Redwood Manufacturer Company, 1911. *Wooden Stave Pipe*,

Rippmann, M., Lachauer, L. & Block, P., 2012. Interactive Vault Design. *International Journal of Space Structures*, 27(4), pp.219–230. Available at: http://multi-science.metapress.com/openurl.asp?genre=article&id=doi:10.1260/0266-3511.27.4.219.

Robeller, C., Nabaei, S.S. & Weinand, Y., 2014. Robotic Fabrication in Architecture, Art and Design 2014 W. McGee & M. Ponce de Leon, eds. , pp.67–81. Available at: http://link.springer.com/10.1007/978-3-319-04663-1 [Accessed July 17, 2014].

Robeller, M., 2015. *Integral Mechanical Attachment for Timber Folded Plate Structures PAR*. Ecole Polytechnique Federale de Lausanne.

Robert McNeel & Associates, 2014a. GhPython.

Robert McNeel & Associates, 2015. Grasshopper 3D: Algorithmic Modeling for Rhino.

Robert McNeel & Associates, 2014b. Rhinoceros 5.0: NURBS Modeling for Windows.

Scheurer, F., 2012. Digital Craftmanship: From Thinking to Modeling to Building. In S. Marble, ed. *Digital Workflows in Architecture*. Birkhäuser, p. 280. Available at: http://www.amazon.com/Digital-Workflows-Architecture-Scott-Marble/dp/3034607997/ref=pd_sim_14_31?ie=UTF8&refRID=04828HXCM7159PFSQCMN.

Schimek, H. et al., 2012. Sewing Timber Panels. , pp.213–222.

Schineis, R., 2004. Gefalteter Klangkörper Musikprobensaal Thannhausen Thannhausen Rehearsal Room Sala di musica Thannhausen. *Internationales Holzbau Forum*, pp.1–9.

Schwitter, C. & Keough, I., 2012. Continuous Integration. In S. Marble, ed. *Digital Workflows in Architecture*. Birkhäuser, p. 280.

Staub-French, S. & Khanzode, A., 2007. 3D and 4D modeling for design and construction coordination: issues and lessons learned. *ITcon*, 12, pp.381–407. Available at: http://www.itcon.org/cgi-bin/works/Show?2007_26 [Accessed September 14, 2015].

Structurlam, 2014. *Cross Laminated Timber Design Guide*,

Tas, L.M., 2013. *Curved Folded Timber Plate Structures*.

Taylor, L., 2013. Parametric Tools & The Evolving Design Process.

Tessmann, O., 2013. Computation in Design. In C. Schittich & P. C. Schmal, eds. *DETAIL engineering 3: Bollinger + Grohmann*. p. 144. Available at: http://www.amazon.com/DETAIL-engineering-3-Bollinger-Grohmann/dp/3920034880/ref=sr_1_1?ie=UTF8&qid=1440808038&sr=8-1&keywords=detail+bollinger%2Bgrohmann [Accessed August 29, 2015].

Thornton Tomasetti, 2014. CORE studio.

Timoshenko, S. & Woinowsky-Krieger, S., 1987. *Theory of Plates and Shells*,

Weinand, Y., 2009. A New Generation of Structures. In *Proceedings of the International Association for Shell and Spatial Structures (IASS) Symposium 2009*. Valencia, p. 8.

Weinstock, M., 2010. *The Architecture of Emergence: The Evolution of Form in Nature and Civilisation*, Wiley. Available at: http://www.amazon.com/The-Architecture-Emergence-Evolution-Civilisation/dp/0470066334/ref=pd_rhf_dp_s_cp_19?ie=UTF8&refRID=1AYCKBE22BB69Z4KBJ48 [Accessed August 26, 2015].

Wien, S. & York, N., 2014. *Robotic Fabrication in Architecture, Art, and Design* S. Brell-Cockan & J. Braumann, eds.,

Wieser, C., 2012. Art and Science. In A. Flury, ed. *Cooperation: The Engineer and the Architect*. Birkhäuser, pp. 249–257. Available at: https://books.google.com/books?id=Q2R-8XdtrzAC&pgis=1 [Accessed August 29, 2015].

Wikipedia Commons, 2009. Her Secret Is Patience. Available at: https://upload.wikimedia.org/wikipedia/commons/4/4b/HerSecretIsPatiencePhoenix.png.

Williams, C., 2014. What is a shell? In S. Adriaenssens et al., eds. *Shell Structures for Architecture: Form Finding and Optimization*. Routledge, p. 340. Available at: http://www.amazon.com/Shell-Structures-Architecture-Finding-Optimization/dp/0415840600/ref=sr_1_1?ie=UTF8&qid=1440612106&sr=8-1&keywords=shell+structures+for+architecture [Accessed August 26, 2015].

Woodbury, R., 2010. *Elements of Parametric Design*, Routledge. Available at: http://www.amazon.com/Elements-Parametric-Design-Robert-Woodbury/dp/0415779871/ref=pd_sim_14_1?ie=UTF8&refRID=17N084C709JBPZSS7M8P [Accessed August 26, 2015].

Zhong, T., 2002. The Generative Method of Multi-storey Chinese Pagodas. *Generative Art*, pp.1–12.

Zwerger, K., 2012. *Wood and Wood Joints: Building Traditions of Europe, Japan and China*, Walter de Gruyter. Available at: https://books.google.ca/books/about/Wood_and_Wood_Joints.html?id=yPoEBDZSUyoC&pgis=1 [Accessed August 26, 2015].

Appendix A **Joining Options for CLT Panels**

A.1 Overview

Timber connections can be grouped into two generic types. Mechanical joints rely on physical interlock and friction between components and include carpentry and dowel-type joints, while adhesively-bonded joints are made by means of a glue bond between elements. Of these connector types, (14 lists the proprietary connection systems which were identified as potential candidate solutions for this project. Figure 72 shows their potential application to folded and curved CLT assemblies. Each branches out into subtypes and other smaller design variations, which will be explained in more detail:

Table 14 Connection design matrix

Connector	Mechanical				Adhesive	
Type	Screws Only		With KNAPP Hangers		Finger Joints	Tongue-and-Groove
	90°	45°	Walco V60	Ricon S 80/40		
Application	Half-Lapped Lapped Top Spline Tongue-and-Groove	Butted Half Lapped Lapped Alternating Fingers	Dropped-in Panels	Slotted-in Panels or Modular Panel Assemblies	Co-planar Panel assemblies "Folded" Panel Assemblies	Co-planar Panel Assemblies

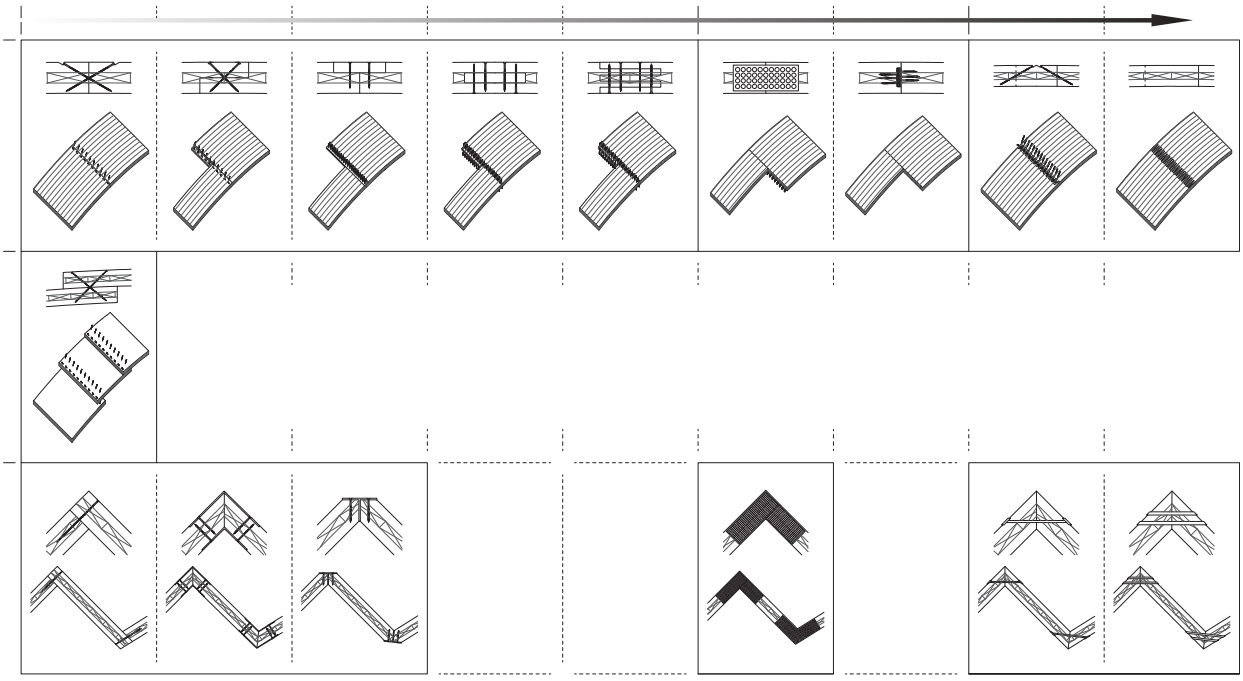

Figure 72: Matrix of connection design options. Vertical axis: Plate arrangements. Horizontal axis: gradient from industry-ready to experimental connection systems

Connection design controls how and where loads are transferred from one structural element to another. Usually this is a process which begins by adjusting external load values to the dimensions of a predetermined form. Design loads are estimated for temporary structures, as follows:

Table 15: Loads for preliminary connection design

Loads	Curved Prototype	Structurlam Panel
Dead	5.2 kN/m^3 for Douglas Fir; 0.5 kPa for roofing	4.4 kN/m^3 for SPF 0.5 kPa for roofing
Live	1.0 kPa	1.9 kPa
Snow	1.0 kPa	1.0 kPa

In a parametric design study, explicit geometric values or member configurations are not available. It is not unreasonable, however, to expect plates to occasionally form roof or wall-like assemblies. Therefore, though the final structure is expected to have more complex geometry and excised apertures, a simplified configuration can be considered for preliminary connection designs. Two panels were assumed to be horizontally oriented between simple supports. Therefore, for the two panel types under consideration, the connection design data is as follows:

Table 16: Design data for doubly-curved and standard CLT panels under preliminary loading

Panel Type	Prototype Double Curvature Panel	Standard Structurlam Panel
Thickness	13 mm layers; 39 mm total	32 mm, 35 mm, 32 mm layers; 99 mm total
Length x Breadth	1,200 mm x 1,200 mm	3,000 mm x 3,000 mm
Wood Species and Density	Douglas Fir, 5.2 kN/m3	SPF, 4.4 kN/m3
Uniformly Distributed Load, ω	2.733 kN/m	13.564 kN/m
End Reactions, V	6.28 kN	6.69 kN

A.2 Assemblies with Self-Tapping Wood Screws

Direct Panel-to-Panel Screwed Assemblies

Self-tapping screws (STS) are the industry standard connector in Europe for CLT panel assemblies (Mohammad 2011). These screws are made from high capacity steel, need no pre-drilling, and are easy install. Properly designed STS connections are highly efficient, practical, and easy to hide by countersinking screw heads into the panels and filling the holes with wood inserts. Though not a rigid connection and designed as simple supports, pairs of crossed screws are used to provide moment resistance. Only the threaded section embedded in the main member, termed the effective length (l_{ef}), provides withdrawal resistance for the connection. These connections function best when screws are loaded in withdrawal and inserted at an angle to the grain direction of the outer layer to maximize l_{ef}; 90° insertions may be favourable for ease of assembly.

Eurocode 1995, in conjunction with the ETA and the CCMC approval for Würth ASSY STS, approaches the design of STS by considering screw lateral and axial capacities under shear and tensile loads, respectively. Shear demand is calculated according to Johansson yield equations, while screws loaded predominantly in tensions or compression are designed according to their withdrawal resistance.

The thickness of the CLT panel limits the maximum allowable diameter of the fastener, upon which related spacing requirements and minimum panel breadths are based. According to the CCMC approval for Würth ASSY STS, the maximum screw diameter d is $1/10^{th}$ of the panel

thickness. Additionally, the total length of the screw must not allow it to protrude from the panel assembly. Providing a minimum 6 *d* edge distance "margin" at the perimeter of all STS connections accommodates any of the proposed the connection configurations, whether loaded in tension, compression, or bending. Arrays of screws, either perpendicular or angled, must have a separation of at least 4 *d*, though the shafts in a pair of crossed screws may be as close as 2 *d*. Full calculations for panel-to-panel assemblies with Würth ASSY VG fully threaded self-tapping screws are summarized in Table 17 by joint and panel type.

Table 17: Detailing for Würth ASSY VG fully threaded STS connections

Joint Type	39 mm Prototype Panels	99 mm Structurlam Panels
Lapped	(4) φ3 mm x 50 mm STS (2 pairs) inserted at 90° spaced at 400 mm o. c. Or (4) φ3 mm x 70 mm STS (2 pairs) inserted at 45° spaced at 400 mm o. c.	(8) φ 6 mm x 180 mm STS (4 pairs) inserted at 90° spaced at 600 mm o. c. Or (6) φ 6 mm x 260 mm STS (3 pairs) inserted at 45° spaced at 750 mm o. c.
Half-Lapped	(5) φ3 mm x 30 mm STS inserted at 90° spaced at 300 mm o. c. Or (4) φ3 mm x 50 mm STS (2 pairs) inserted at 45° spaced at 400 mm o. c.	(11) φ6 mm x 90 mm STS inserted at 90° spaced at 250 mm o. c. Or (16) φ5 mm x 120 mm STS (8 pairs) inserted at 45° spaced at 300 mm o. c.
Butted	(4) φ3 mm x 50 mm STS (2 pairs) inserted at 45° spaced at 400 mm o. c.	(16) φ5 mm x 120 mm STS (8 pairs) inserted at 45° spaced at 300 mm o. c.
Top Spline	(2) φ3 mm x 35 mm STS inserted at 90° spaced at 400 mm o. c.	(3) φ6 mm x 90 mm Würth ASSY self-tapping screws inserted at 90° spaced at 750 mm o. c.
Interior Spline	(4) φ3 mm x 50 mm STS (2 pairs) inserted at 45° spaced at 400 mm o. c.	(12) φ6 mm x 90 mm STS (6 pairs) inserted at 90° spaced at 23 0 mm o. c.
Tongue-and-Groove	(5) φ3 mm x 35 mm STS inserted at 90° spaced at 200 mm o. c.	(11) φ6 mm x 90 mm STS inserted at 90° spaced at 250 mm o. c.
Steel Plate for a 30° Corner	(4) φ3 mm x 30 mm STS (2 pairs) inserted normal to plate top spaced at 400 mm o. c.	(12) φ6 mm x 90 mm STS (6 pairs) inserted normal to plate top spaced at 230 mm o. c.